NOTICE

The quality of this microform is heavily dependent upon the quality of the original thesis submitted for microfilming. Every effort has been made to ensure the highest quality of reproduction possible.

If pages are missing, contact the university which granted the degree.

Some pages may have indistinct print especially if the original pages were typed with a poor typewriter ribbon or if the university sent us an inferior photocopy.

Reproduction in full or in part of this microform is governed by the Canadian Copyright Act, R.S.C. 1970, c. C-30, and subsequent amendments.

AVIS

La qualité de cette microforme dépend grandement de la qualité de la thèse soumise au microfilmage. Nous avons tout fait pour assurer une qualité supérieure de reproduction.

S'il manque des pages, veuillez communiquer avec l'université qui a conféré le grade.

La qualité d'impression de certaines pages peut laisser à désirer, surtout si les pages originales ont été dactylographiées à l'aide d'un ruban usé ou si l'université nous a fait parvenir une photocopie de qualité inférieure.

La reproduction, même partielle, de cette microforme est soumise à la Loi canadienne sur le droit d'auteur, SRC 1970, c. C-30, et ses amendements subséquents.

CALCITE CEMENTS IN CARBONATES OF THE SVERDRUP BASIN, CANADIAN ARCTIC ARCHIPELAGO

by

MARTINE SAVARD

A thesis submitted to the School of Graduate Studies

in partial fulfilment of the requirements for the Degree of

Doctor of Philosophy in Geology

OTTAWA-CARLETON GEOSCIENCE CENTRE

UNIVERSITY OF OTTAWA

DEPARTMENT OF GEOLOGY

OTTAWA, ONTARIO

ISBN 0-315-70529-9

UNIVERSITÉ D'OTTAWA
UNIVERSITY OF OTTAWA

ABSTRACT

Calcite cements from the Upper Paleozoic sequences 2, 3 and 4 of the Sverdrup Basin (Canadian Arctic Archipelago) are the subject of this study. On a micro-scale, petrography with light microscopy, cathodoluminescence (CL), scanning electron microscopy (SEM) and staining helped to identify two main textural groups of cements, neomorphic and primary. Both are, in turn, subdivided into two categories: *calcitized aragonite and recrystallized high-magnesium calcite* for the former, and *meteoric calcite* and *burial (late) calcite*, for the latter. In neomorphic cements, eleven micro-scale CL eleven patterns can be recognized. The combination of relationships of these patterns suggests that stabilization operated via numerous diagenetic systems and involved more than one dissolution-reprecipitation step.

In an associated trace element study, application of Secondary Ion Mass Spectrometry (SIMS) enabled direct measurements of chemical composition in thin sections, constituting a precedent. The precisions obtained were 12, 6, 6 and 6% for Mg, Fe, Mn and Sr, respectively.

Petrographic observations guided the micro-sampling for geochemical studies, including $\delta^{13}C$, $\delta^{18}O$, $^{87}Sr/^{86}Sr$, Sr, Mg, Fe and Mn. For marine neomorphic cements, the CL patterns - or stages of textural preservation - do not correlate with preservation of the isotopic signal. Many texturally well preserved cements show clearly altered isotopic signatures and *vice versa*. Moreover, a detailed trace element study of uniform

cathodoluminescence zones revealed that cements with less than about 1000 ppm of Fe and 225 ppm of Mn may be luminescent, nonluminescent or dull. The existence of this "undifferentiated" domain implies that the redox sensitive Fe-Mn pair is not the sole control of cathodoluminescence zoning. These results for trace elements in CL zones and for isotopes in patterns of neomorphic cements signify that, at this stage, it is better to avoid interpretation of CL in terms of chemistry. Nevertheless, the luminoscope remains a useful petrographic tool.

The above cited four petrographic categories of cements have distinctive, although overlapping, geochemical attributes. Stabilized aragonite-precursors have Sr contents in excess of 1000 ppm, whereas the remaining cements have mean contents of about 250 ppm. The most notable features are, however, the conspicuous depletion in ^{18}O and ^{13}C, and the significant enrichment in ^{87}Sr, from early marine to late and to meteoric cements.

On a regional scale, analysis of the stratigraphic distribution of cements, and of their geochemical attributes, suggests the following main diagenetic trends in the three carbonate sequences. The general succession consists of (1) early marine cementation, (2) recrystallization of marine cements concurrent with late cementation during shallow burial, mostly in a marine environment, and (3) continuing burial cementation at greater depths. However, interesting exceptions to this general model do exist. In sequence 2, the western region of the Moscovian Sverdrup Basin was affected by upward migration

of oxygenated hot waters. This hydrothermal activity apparently ceased prior to burial. In contrast, the eastern early cements were possibly recrystallized first by cold marine waters following drowning, and subsequently by saline waters during shallow burial. In sequence 3, precipitation of early marine cements has been followed by partial exposure of the sequence to meteoric diagenetic realm that resulted, at least partly, in their dissolution and recrystallization. The late cements appear to have multiple origins. The diagenetic systems probably alternated between phreatic meteoric and phreatic saline end-members. These alternations were probably forced by frequent fourth- to fifth-order fluctuations of sea level during the Permian. Overall, it seems that the precipitation of the classical dull late cements took place in phreatic and shallow burial environments (with a maximum depth of burial of about 1 km).

Through the studied time span, the best $\delta^{18}O$ and $\delta^{13}C$ estimates indicate that the Sverdrup Sea composition remained relatively constant. The data fall at the heavy end of the previously published range for coeval basins. On the other hand, the $^{87}Sr/^{86}Sr$ ratios are more radiogenic than published values obtained from brachiopods. These higher ratios may signify that the studied marine components were somewhat affected by saline (?) ^{87}Sr-rich waters. Nevertheless, the overall trend agrees with the previously advocated trend in Sr isotopic composition of sea water, declining from more radiogenic values in the Moscovian to less radiogenic ones in the Artinskian.

RÉSUMÉ

Cette étude traite des ciments calcitiques provenant des séquences paléozoïques supérieures 2, 3 et 4 du Bassin de Sverdrup (Archipel de l'Arctique canadien), et ce, à deux échelles. À l'échelle microscopique, la pétrographie par microscopie optique, cathodoluminescence (CL), microscopie électronique à balayage et tests de coloration, permet l'identification de deux principaux groupes texturaux, ciments néomorphiques et ciments primaires, eux-mêmes respectivement subdivisés en deux catégories: *aragonite calcitisée et calcite magnésienne recristallisée*, et, *calcite météorique et calcite d'enfouissement (tardive)*. En CL, l'étude détaillée des ciments néomorphiques permet de reconnaître onze patrons dont les relations texturales suggèrent que la stabilisation s'est accomplie par plusieurs systèmes diagénétiques et a probablement comporté plus d'une étape de dissolution-reprécipitation.

Cette étude crée un précédent en géochimie des ciments calcitiques car elle présente les premiers résultats d'analyses ponctuelles en lames minces des éléments traces par SIMS (faisceau d'ions secondaires en spectrométrie de masse). Les précisions obtenues pour Mg, Fe, Mn et Sr sont respectivement de 12, 6, 6 et 6%.

Les observations pétrographiques ont gouverné le micro-échantillonnage lors de l'étude géochimique qui comprenait $\delta^{13}C$, $\delta^{18}O$, $^{87}Sr/^{86}Sr$, Sr, Mg, Fe et Mn. Dans les ciments marins néomorphiques, les patrons en CL - degrés de conservation texturale - ne correspondent pas aux degrés de conservation des signaux isotopiques. Plusieurs ciments à texture bien conservée ont des bagages isotopiques indéniablement altérés, et *vice versa*. De plus, l'étude détaillée des zones uniformes de luminescence montre que

des ciments contenant moins de 1000 ppm de Fe et 225 ppm de Mn peuvent être luminescents, non luminescents ou ternes. Ce domaine "non-différencié" implique que la paire Fe-Mn n'est pas l'unique contrôle de la zonation en CL. La composition chimique des zones de luminescence et les signaux isotopiques des divers patrons dans les ciments néomorphiques impliquent qu'à ce stade-ci, il vaut mieux éviter d'interpréter la CL en termes géochimiques. Le luminoscope n'en demeure pas moins un outil pétrographique fort utile.

Les quatre grandes catégories pétrographiques de ciments ont des attributs géochimiques qui se chevauchent mais qui sont tout de même distincts. Les précurseurs aragonitiques stabilisés ont des contenus en Sr très élevés, excédant 1000 ppm, alors que les autres groupes de ciments n'ont en moyenne que 250 ppm. Toutefois, en passant des ciments marins, aux ciments tardifs (d'enfouissement) et aux météoriques, les traits les plus frappants sont le remarquable appauvrissement en ^{18}O et ^{13}C et l'enrichissement significatif en ^{87}Sr.

À l'échelle régionale, l'analyse de la distribution stratigraphique des ciments et de leurs attributs géochimiques montre la succession générale suivante dans les trois séquences étudiées: (1) cimentation marine précoce, (2) recristallisation des phases marines simultanément avec une cimentation d'enfouissement peu profond, et finalement, (3) cimentation continue en milieu plus profond. Néanmoins, il existe d'intéressantes exceptions à ce modèle général. Dans la séquence 2, au Moscovien, la région ouest du bassin a été affectée par des eaux ascendantes, chaudes et oxygénées. Cette activité hydrothermale aurait cessé avant l'enfouissement de la séquence. D'autre

part, dans la région est, des ciments marins précoces ont possiblement été recristallisés d'abord par des eaux marines froides après l'inondation de la plate-forme et puis par des eaux salines au début de l'enfouissement. Dans la séquence 3, la cimentation marine a été suivie par une dissolution et une recristallisation, au moins partielle, d'origine météorique. Pour ce qui est des ciments tardifs, leurs sources semblent multiples. Les systèmes diagénétiques auraient alterné de météorique-marine mixte à saline. Ces alternances ont probablement été provoquées, au Permien, par les fréquentes fluctuations marines du quatrième ou cinquième ordre. De façon générale, il semble que la précipitation des classiques ciments ternes et tardifs se soit accomplie en milieux phréatique et d'enfouissement à une profondeur maximale de 1 km.

Les estimés des valeurs de $\delta^{18}O$ et $\delta^{13}C$ indiquent que pendant l'intervalle temporel étudié, la Mer de Sverdrup avait un signal constant. Il correspond aux signaux les plus lourds de résultats antérieurement publiés pour des bassins du même âge. D'autre part, les rapports $^{87}Sr/^{86}Sr$ sont plus radiogéniques que ceux d'autres études publiées, obtenus pour des brachiopodes. Ces rapports plus élevés suggèrent que les ciments marins utilisés ont été quelque peu affectés par des eaux salines (?) riches en ^{87}Sr. Néanmoins, les résultats suivent le profil mondial qui va de plus radiogénique au Moscovien à moins radiogénique à l'Artinskien.

REMERCIEMENTS

Je remercie sincèrement le Dr Benoît Beauchamp de la Commission géologique du Canada (Institut de géologie sédimentaire et pétrolière de Calgary) pour son support et ses commentaires stimulants. Je remercie Jan Veizer pour m'avoir laissé entière liberté lors de mes travaux de recherche; je tiens de plus à souligner la grande patience de ce dernier qui a méticuleusement corrigé le texte anglais de ce manuscrit et qui l'a édité.

Je veux exprimer ma gratitude aux docteurs R. Hinton et J. Craven qui m'ont accueillie au Grant Institute de l'Université d'Édimbourg et qui m'ont aidée lors de mes travaux à la sonde ionique. Je lance mille mercis à toutes ces personnes qui m'ont épaulée et/ou qui ont contribué à mes travaux: A. Desrochers, L. Dubé, A. Hébert, R. Hébert, Y. Houde, A. Lalonde, L. Michard, P. Middlestead, M. McLaren, G. Mrazek, M. Parent, J.-P. Ricbourg, J. Rublee, M. J. Savard, G. St-Jean, J.-F. Tardif, H. Tremblay et M. Turner. J'apprécie grandement le travail effectué par les examinateurs de la thèse: les docteurs A. Desrochers, J.A. Donaldson, K. Hattori et K.C. Lohmann (Université du Michigan à Ann Arbor).

Pendant mes études doctorales, j'ai bénéficié de bourses d'études supérieures offertes par le CRSNG (Conseil de recherches en sciences naturelles et en génie du Canada), les Fonds FCAR (Fonds pour la formation de chercheurs et l'aide à la recherche du Québec) et par l'École des études supérieures et de la recherche de l'Université d'Ottawa. Mes travaux de terrain ont été entièrement financés par l'IGSP. Les travaux en laboratoire ont été subventionnés par le CRSNG (subvention de chercheur au Dr. Jan Veizer).

TABLE OF CONTENTS

LIST OF TABLES

LIST OF FIGURES

1. INTRODUCTION

Carbonate cements, ubiquitous products of diagenesis, are of interest to geology because of both economic and scientific significance. From an economic point of view, cements affect the permeability - and hence reservoir potential - of sedimentary rocks. From a scientific perspective, the successive generations of cements contain encoded information on the nature of parental fluids, which, in turn, enables reconstruction of the lithification history of the sediments, evolution of diagenetic environments and, ultimately, of basin history. The study of cements has two complementary dimensions: the minute scale of crystal precipitation, and the grand scale of basin porosity evolution. During the last two decades, studies of calcite cements have involved sophisticated petrographic and geochemical tools, yet many features of ancient cements are still enigmatic.

The Upper Paleozoic sequence of the Canadian Arctic contains spectacular examples of massive cementation of carbonate build-ups (Davies *et al.*, 1978; Davies and Nassichuk, 1990) and therefore provide an excellent geological setting for the study of ancient cements. In their reconnaissance studies, the above authors demonstrated that cements of Moscovian age are neomorphic products after aragonite and high-Mg calcite, and they also pointed out that marine cementation is "a common and often critical stage in the development of many reefal and shelf-margin to slope carbonates". This study was designed to expand and complement their initial reconnaissance results in a systematic fashion. The specific aims are:

A) a petrographic inventory of cements, utilizing light microscopy, staining tests, SEM and cathodoluminoscopy;

B) assignment of petrographic cement types to specific diagenetic environments;

C) documentation and quantification of processes involved in the stabilization of early marine cements through a combination of petrographic observations and geochemical data (Sr, Mg, Fe, Mn, $\delta^{18}O$, $\delta^{13}C$ and $^{87}Sr/^{86}Sr$);

D) estimation of the isotopic composition of the early Carboniferous to early Permian Sverdrup seawater (marine calcite composition);

E) collation of the diagenetic histories of the studied carbonate sequences in the context of their regional stratigraphic framework; and

F) development and utilization of the ion microprobe technique for the study of diagenetic cements as well as for quantification of relationships, if any, between trace element chemistry and cathodoluminescence zones of cements on a microscopic scale.

2. GEOLOGICAL SETTING

The Sverdrup Basin is located in the Canadian Arctic Archipelago. It follows the northeast/southwest axis of a former rift, from northern Ellesmere Island to northern Melville Island, and covers an area of about 300 000 sq. kilometres (fig. 2-1). The basin originated by rifting of the folded and faulted Lower Paleozoic rocks of the Franklinian Geosyncline. Many Paleozoic tectonic events deformed the Precambrian to Devonian basement rocks, the latest being the Ellesmerian Orogeny that started in middle Devonian and ended in early Carboniferous. The Early Carboniferous to Early Triassic Sverdrup Basin fill comprises thirteen kilometres of sedimentary and minor volcanic strata (locally intruded by minor plutonic rocks) that lie with an angular unconformity over the Lower Paleozoic basement. The strata have been divided into eight transgressive-regressive sequences (Beauchamp, 1989 a, b). These are marked by major unconformities at the basin margins, but are conformable in the centre of the basin due to continuous sedimentation.

Long term stratigraphic, sedimentologic and structural studies have recently led to a comprehensive summary of the Upper Paleozoic history of the basin (Beauchamp *et al.*, 1989 b, c; Beauchamp and Henderson, 1991). The chronostratigraphy is based on biozones of ammonoids, brachiopods, conodonts, corals, small foraminiferans, fusulinaceans and palynomorphs. Conodonts, the most precise biostratigraphic tool, define 23 zones that can be correlated at stage and sub-stage levels with stratotypes in

North America and Europe. Seven transgressive-regressive sequences were deposited during four phases of tectonic evolution (fig. 2-2).

Sequence 1, the Emma Fiord Formation, consists of nonmarine fine to coarse clastic sediments that were deposited in lakes formed at the time of initial thermal uplift or incipient rifting. Sequences 2, 3 and 4 were products of prolonged marine cycles during the rifting stage of the basin. They contain alluvial, shallow platform and deep water clastic rocks. The platform sediments encompass thick successions of carbonates of diverse facies, from calcrete, to shallow shelf, to deeper water marine mud mounds. Sequence 5 comprises deltaic clastic sediments that were deposited in response to the Melvillian Disturbance that affected Upper Carboniferous to Early Permian rocks and created local uplifts and unconformities. Sequences 6 and 7 are composed mainly of clastic marine sediments deposited during a stage of passive subsidence. During the entire evolution of the Basin, carbonate units formed a peripheral platform around three central basins that were depositional sites for evaporites and deeper water clastic units (fig. 2-1).

Based on paleomagnetic reconstruction, the Sverdrup Basin drifted from 20 °N in the Early Carboniferous to more than 50 °N in the Late Permian and subsequently to its present position at 80°N (Beauchamp, 1987). This northern drift, from tropical warm and arid climate into the temperate humid and finally the polar zone, must have resulted

in significant changes in populations of marine organisms, and possibly also in the nature of early marine diagenetic processes (Beauchamp, 1987 and 1989).

2.1 CARBONATE SEQUENCES OF THE SVERDRUP BASIN

The present study concentrates on sequences 2 and 3 ("reconnaissance" in 4) (fig. 2-3) which are described in some detail below. Previous reconnaissance studies of Davies *et al.* (1978) and Davies and Nassichuk (1990) were based on samples from sequence 2, and dealt solely with the geochemistry and light microscope petrography of the early marine cements.

2.1.1 Sequence 2 - Serpukhovian to Lower Asselian

The carbonate-containing formations of Canyon Fiord, Otto Fiord, Antoinette, Nansen and Hare Fiord (fig. 2-2) comprise sequence 2. This sequence has a maximum thickness of 1800 metres and represents a record of up to 50 Ma of depositional history. The descriptions below are based mostly on the summary of Beauchamp *et al.* (1988 b).

Canyon Fiord Formation

This Formation rests on the Franklinian Basement and is characterized by red weathering units grouped into 3 members: the lower clastic member composed of basal conglomerate and subordinate sandstone and limestone (10 to 600 metres), the middle

limestone member composed of recessive-resistant couplets of variably fossiliferous bedded limestone with subordinate sandstone (140 to 845 metres), and the upper clastic member composed of sandstone with minor limestone (0 to 860 metres). Along the eastern side of the basin, the Canyon Fiord Formation constitutes a part of the Marginal Clastic Belt. The Lower Clastic Member of this formation has been interpreted as an alluvial fan to braided river system that was active during the synsedimentary rifting of the basement. The intermediate Middle Limestone Member represents marine inner shelf cycles, whereas the Upper Clastic Member has been interpreted as a coastal plain to fluvial system (Thériault and Beauchamp, 1991). The latter marks the boundary between the Canadian Shield and the Sverdrup Basin.

Otto Fiord Formation

This evaporitic formation overlies the Borup Fiord Formation, the latter a basinward equivalent of the Canyon Fiord Formation. It is, in turn, overlain by the Hare Fiord Formation. The Otto Fiord Formation is composed mainly of anhydrite beds that are rhythmically interlayered with limestones, the latter containing minor shale and sandstone intercalations. The limestone units consist of highly bioturbated shaly wackestone, bioclastic packstone and algal boundstone mounds. The mounds usually show a vertical succession that initiates with crinoidal wackestone at the base and grades upwards into a cap of branching tubular algae. A tectonically active ridge periodically restricted marine circulation between the ocean and the basin. As a result, the Otto Fiord Formation is restricted to the central part of the basin, where the evolution from

subaqueous evaporites to limestones represents hypersaline to normal marine transition (Davies and Nassichuk, 1988).

Hare Fiord Formation

This Formation marks the return to permanent normal marine conditions in the central area of the basin. Its shelf equivalent, the Nansen Formation, is a limestone that overlies the Canyon Fiord Formation. The Hare Fiord Formation consists of two broad subdivisions. The lower subdivision comprises cherty bedded limestone (fine and shaly to coarse and bioclastic) and massive bryozoan reef-mounds. In contrast, the upper subdivision consists of noncalcareous siltstone and shale. The limestone, generally topped by mud mounds, was deposited during a widespread marine transgressive event that may have caused cessation in growth of the mounds (Davies *et al.*, 1988). Subsequent deposition of fine clastic units likely proceeded in a stagnant deep-water marine environment (Thorsteinsson, 1974).

Nansen Formation

This Formation both surrounds and overlies the Hare Fiord Formation and is, in turn, overlain by the Trappers Cove Formation. The Nansen Formation consists predominantly of carbonate rocks. Mixed clastic-carbonate and clastic facies are subordinate. The characteristic feature of the formation is the alternation of recessive and resistant units that form couplets of variable thicknesses. Well developed *Paleoaplysina* and phylloid algal mound complexes locally appear in resistant units.

Equivalent facies stratigraphically under the Mount Bailey Formation belong to the Antoinette Formation.

2.1.2 Sequence 3 - Early Asselian to Late Sakmarian

Fifteen million years of depositional history recorded in sequence 3 reaches a maximum thickness of 800 metres. Its carbonate units are distributed among the Belcher Channel, the top of the Antoinette, the Tanquary, and the top of the Nansen Formations.

Belcher Channel Formation

By definition, this formation overlies the Canyon Fiord Formation. In terms of cyclicity and distribution of facies, the Belcher Channel Formation resembles the Nansen Formation. The cyclical alternations that characterize the Belcher Channel Formation consist of siltstone, shale and subordinate sandstone as the main component in the recessive units, and of purer carbonates in the resistant units. Again, well developed *Paleoaplysina* and phylloid algal mound complexes locally appear in the resistant outer shelf units.

Nansen and Tanquary Formations

The Nansen Formation of sequence 3 is essentially identical to that described in sequence 2. Facies equivalent units, where stratigraphically above Mount Bailey Formation, are included in the Tanquary Formation.

Cycles and shelf anatomy

All formations of sequences 2 and 3 that contain carbonate units (Canyon Fiord, Belcher Channel, Antoinette, Tanquary, and Nansen) are characterized by thin, sharp-based, shallowing-upward sequences. Each consists of a couplet of fine clastic-rich recessive and of carbonate-rich resistant units. The couplets are interpreted as being the result of rapid transgressions and subsequent shallowings, the latter a consequence of re-establishment and expansion of biogenic carbonate production (Beauchamp, 1987). Although they are characterized by complex vertical and lateral variations in the couplets, Beauchamp (1987) has been able to recognize a repeating pattern of an upward increase in the abundance and diversity of biotic components, increase in the bed thickness, decrease in the proportion of clastics, and shallowing-upward depositional trends. He integrated all these observations into an interpretative sedimentological model of shelf anatomy that evolved in response to oscillating sea level stands (fourth- to fifth-order cycles as defined by Kendall and Schlager, 1981). Based on their paleogeographic setting along the inner (high-energy) or the outer (low-energy) shelf, the couplets were classified into six types. According to this interpretation, section 28 and the top of section 2 represent deposits of the basin margin and basin centre respectively (fig. 2-3).

Results from recent investigations on the fourth- to fifth-order cycles will eventually help to better define the factors controlling the cyclicity (Morin, M.Sc thesis in progress; Morin *et al.*, 1991).

2.1.3 Sequence 4 - Late Sakmarian to Early Kungurian

The top of the Canyon Fiord, the Raanes and the base of the Trappers Cove Formations constitute the transgressive portion of sequence 4. The regressive phase is represented by the Great Bear Cape and the top of the Trappers Cove Formations (Beauchamp and Henderson, in press; Scott *et al.*, 1991).

The ***Raanes Formation*** is a platform unit made of 4 to 6 deepening-upward, inner to outer shelf cycles composed of mixed clastic-carbonate fine sediments. Each cycle coarsen upward and grades vertically from thinly bedded, unfossiliferous shales, that form a thick recessive succession, to thickly bedded, more resistant carbonate-rich fossiliferous shale to mudstone. Reefs sporadically occur in the Raanes Formation.

The ***Great Bear Cape Formation*** consists of a single, shallowing-upward, progradational sequence composed of highly fossiliferous, variably cherty, cliff-forming limestones. Locally present are bryozoan-sponge reef mounds, representing the youngest buildups of the Sverdrup Basin (Beauchamp, 1988).

The ***Trappers Cove Formation*** is a basinal unit composed of a dark siliceous shale at the base, and an overlying spiculitic chert that contains sparse carbonate lenses.

2.1.4 Reef mounds

In contrast to most of the Phanerozoic, with its high-standing reefs of framestone, the Upper Paleozoic is typified by lens-like mounds and banks that are accumulations of mudstone, bindstone and bafflestone (Wilson, 1975). The Sverdrup Basin, in the time span from the early Bashkirian to late Artinskian, contains numerous mud mounds that fringe the periphery of the carbonate platform (Geldsetzer *et al.*, 1989). These mounds can be subdivided into three morphological types, small patch reefs, wide tabular banks and large reef-mounds. Their characteristic biogenic components are calcareous algae, bryozoans-algae and bryozoans, respectively. According to Beauchamp (in prep.), the morphology of these three mound types reflects the space available for their growth within the inner-shelf, outer-shelf and slope environments, respectively.

The buildups sampled selectively for this study were Early Moscovian algal patch reefs (section 10; Davies and Nassichuk, 1980), Moscovian bryozoan-algae reef-mounds (section 9.5, 11, 37), Sakmarian algal reef-mounds (sections 2, 3; Beauchamp, 1987), Sakmarian bryozoan-*Tubiphytes* patch reefs (section 2; Beauchamp, 1989 b), Sakmarian algal patch reefs (section 35) and the Artinskian bryozoan-sponge reef-mounds (Beauchamp, 1989 a) and patch reefs (sections 17, 18 and 27). These mounds are characterized by abundant early marine cements that fill the fenestral pores. These marine cements may have recorded the geochemical evolution of the partially enclosed "Sverdrup Sea".

2.1.5 Sampling sites

The study area corresponds to the northern half of the Sverdrup Basin where the carbonate sequences can be sampled in outcrops. In the southern portion of the Basin, these sequences are known only from cores and their stratigraphy has not yet been resolved. During the 1987 and 1988 field seasons, the author concentrated on selective sampling of cements from as diverse as possible depositional environments and on covering the largest possible spatial and temporal range. The existing ISPG collection (gathered by Davies, Nassichuk and Beauchamp) provided additional samples from the few areas that were not visited by the author. Sixteen measured sections from Ellesmere, Devon and Axel-Heiberg Islands were sampled. The resulting spatial and temporal distribution of macrosamples is illustrated in figure 2-3. In terms of depositional environments, the samples cover the following facies: calcrete, inner shelf, outer shelf and mud mounds, the latter from the entire inner shelf to slope profile.

LATE PALEOZOIC PALEOGEOGRAPHY OF THE SVERDRUP BASIN

Figure 2-1

Three central depocenters are encircled by a carbonate platform. From Beauchamp and Henderson (in press).

SVERDRUP BASIN

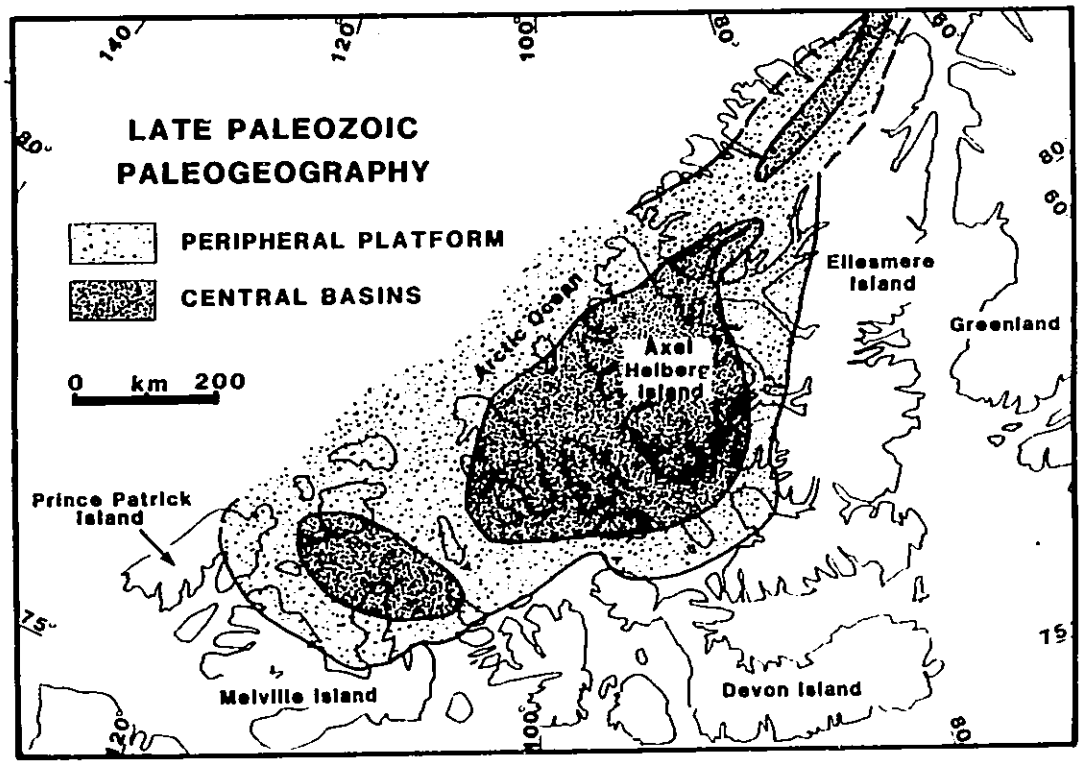

SEQUENCES OF THE SVERDRUP BASIN

Figure 2-2

Schematic description of the Lower Carboniferous to Lower Triassic lithology and stratigraphy for the Sverdrup Basin (after Beauchamp, 1989a). Major transgressive-regressive fluctuations generated the numbered sedimentary sequences that are shown in relation to tectonic evolution. Carbonates of sequences 2, 3 and 4 were the subject of this study. The profile would theoretically pass from the southeast (left) to the centre of the Basin in the north.

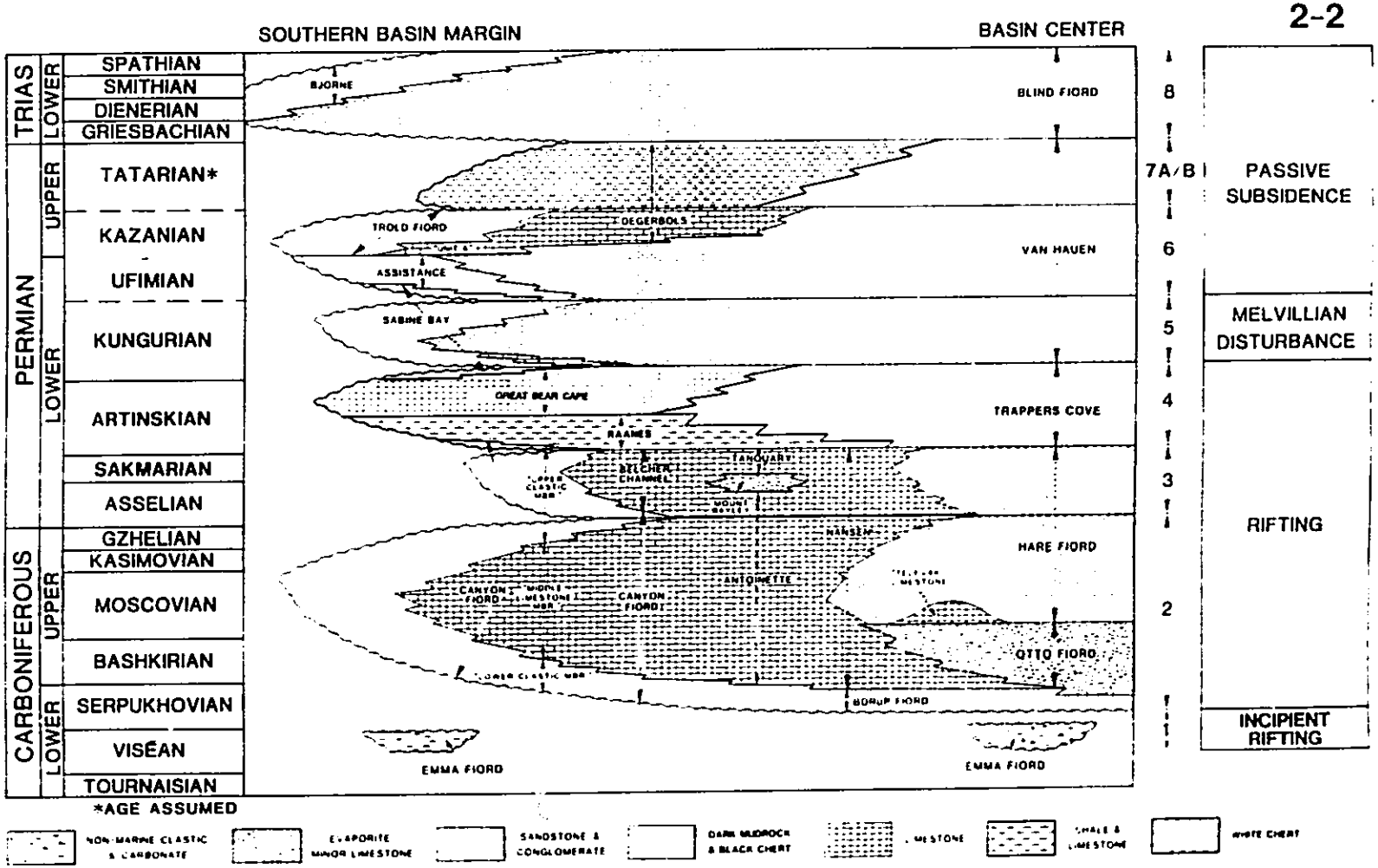
SOUTHERN BASIN MARGIN
BASIN CENTER
TRIAS
PERMIAN
CARBONIFEROUS
LOWER
UPPER
SPATHIAN
SMITHIAN
DIENERIAN
GRIESBACHIAN
TATARIAN*
KAZANIAN
UFIMIAN
KUNGURIAN
ARTINSKIAN
SAKMARIAN
ASSELIAN
GZHELIAN
KASIMOVIAN
MOSCOVIAN
BASHKIRIAN
SERPUKHOVIAN
VISEAN
TOURNAISIAN
*AGE ASSUMED
BJORNE
BLIND FIORD
TROLD FIORD
DEGERBOLS
VAN HAUEN
ASSISTANCE
SABINE BAY
GREAT BEAR CAPE
TRAPPERS COVE
RAANES
BELCHER CHANNEL
FANQUART
HARE FIORD
ANTOINETTE
CANYON FIORD
OTTO FIORD
BORUP FIORD
EMMA FIORD
EMMA FIORD
8
7A/B
6
5
4
3
2
1
PASSIVE SUBSIDENCE
MELVILLIAN DISTURBANCE
RIFTING
INCIPIENT RIFTING
NON-MARINE CLASTIC & CARBONATE
EVAPORITE MINOR LIMESTONE
SANDSTONE & CONGLOMERATE
DARK MUDROCK & BLACK CHERT
SHALE & LIMESTONE
WHITE CHERT

LOCATION OF THE STUDIED SECTIONS

Figure 2-3

a) Distribution of sampled sections across the Late Paleozoic carbonate platform of the Sverdrup Basin. The studied area is restricted to the northern half of the Basin (cf. fig. 2-1).

b) Idealized paleoenvironmental and stratigraphic distribution of the sampled sections. The stratigraphic sections are shown as *time* units and not as thicknesses. Sections 35 and 37 are transposed into a north-south profile.

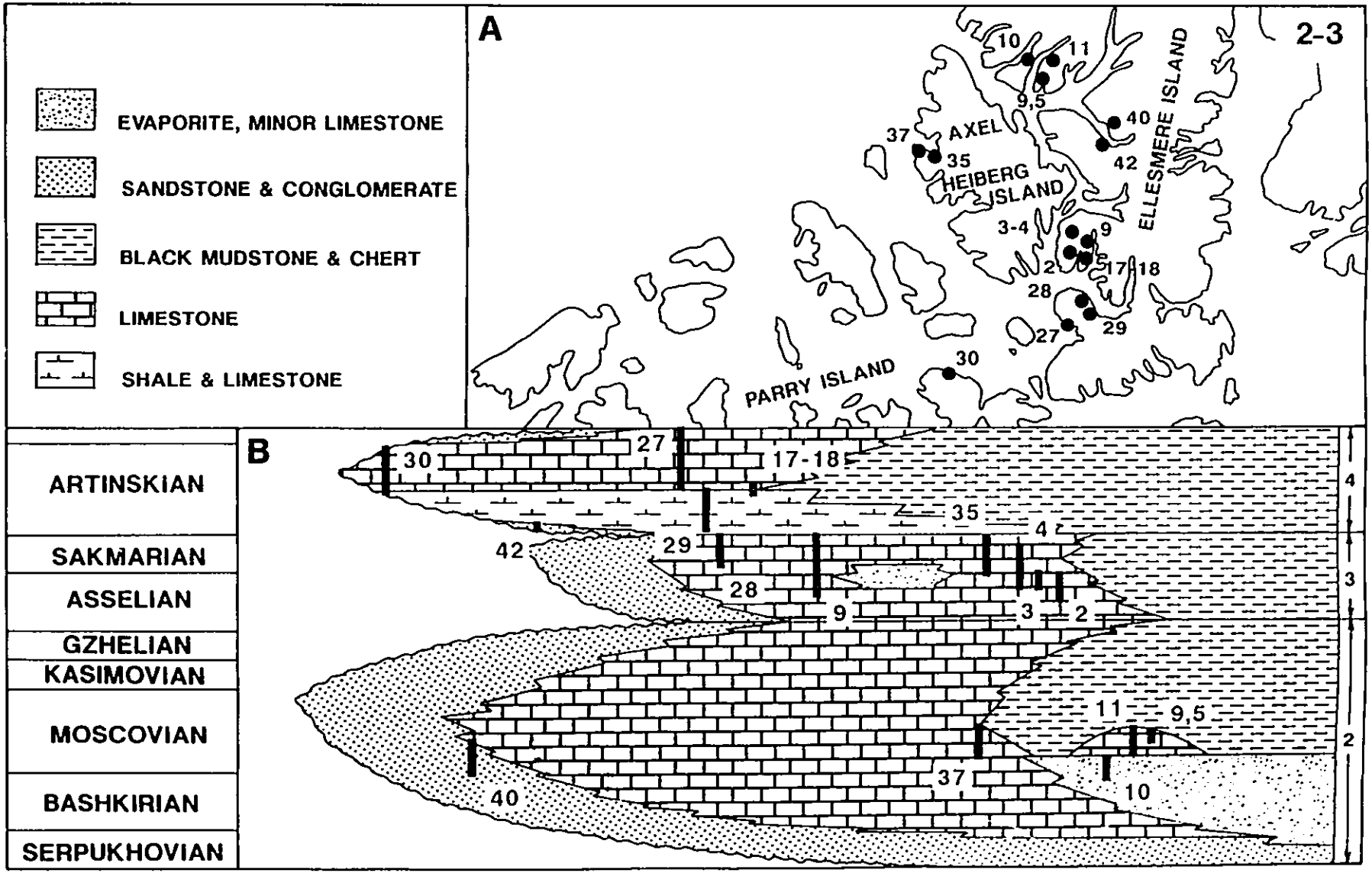
A
2-3
EVAPORITE, MINOR LIMESTONE
SANDSTONE & CONGLOMERATE
BLACK MUDSTONE & CHERT
LIMESTONE
SHALE & LIMESTONE
AXEL
HEIBERG ISLAND
ELLESMERE ISLAND
PARRY ISLAND
10
11
9,5
40
42
37
35
3-4
9
2
17
18
28
29
27
30
B
ARTINSKIAN
SAKMARIAN
ASSELIAN
GZHELIAN
KASIMOVIAN
MOSCOVIAN
BASHKIRIAN
SERPUKHOVIAN
4
3
2

3. PETROGRAPHY OF CEMENTS

Mineralogically, the most common Recent carbonate cements are low-magnesian calcite (LMC), high-magnesian calcite (HMC) and aragonite (A). Modern sea-floor precipitation is dominated by HMC and A (*e.g.* Shinn, 1969; Schroeder, 1972; MacIntyre, 1977; James and Ginsburg, 1979), both metastable phases. In contrast, LMC cements may precipitate in either burial or meteoric environments, although only in minor quantities in the latter.

HMC and A are rarely encountered in ancient carbonate sequences, which usually contain only LMC. This is - at least in part - a result of mineral stabilization that leads to complete disappearance of the metastable mineral phases and their replacement by diagenetic low-magnesian calcite (dLMC). In the case of A, diagenetic processes frequently induce complete dissolution that is eventually followed by calcite precipitation into the molds, and may result in a fabric ranging from coarse calcite crystals in large moldic cavities to fine crystals in minute botryoidal ghosts. The textures that can be generated depend on (1) the relative rates of aragonite dissolution and calcite precipitation, and (2) the scale at which replacement takes place (Sandberg, 1985). In the case of HMC, the stabilization can operate without apparent textural change (Friedman, 1964; Towe and Hemleben, 1976). However, such samples frequently contain microdolomites, observed by SEM, considered to be secondary products of HMC recrystallization (Macqueen and Ghent, 1975; Lohmann and Meyers, 1977). Blotchy (or

composite) CL patterns are also believed to result from stabilization of HMC (e.g. Meyers, 1978).

It has been suggested that marine cements could have been of calcite mineralogy ("Calcite Seas") only with a cyclical reappearance of aragonite ("Aragonite Seas") during the Phanerozoic (Pigott and Mackenzie, 1979; Wilkinson, 1982; Sandberg, 1983). This scenario, even if confirmed by broad petrographic observations, almost certainly represents an oversimplification of the real situation. For instance, Savard *et al.* (1990 b) identified aragonite relics around cold-seep vents in the Cretaceous, a time of the proposed "Calcite Seas". Such findings suggest that the mineralogy of authigenic marine precipitates depends on a complex interplay of multiple factors.

This chapter concentrates on the petrographic description and classification of Late Paleozoic cements of the Sverdrup Basin that are preserved today as calcite. Questions of their origin and of diagenetic pathways will be deferred to after discussion of their geochemical parameters.

3.1 TECHNIQUES AND DESCRIPTIVE PARAMETERS

Light microscopy and cathodoluminoscopy (CL) have been utilized to systematically study 150 large and 150 standard polished thin sections. Sections were

half-stained with conventional mixed solutions of Red Alizarin S and potassium ferricyanide (Dickson, 1965). After staining for four minutes, the samples were dried, and the stained portions varnished. The usual working conditions with the cathodoluminoscope (Technosyn model) were 12-14 Kv and 530-580 μA for an unfocussed electron beam. CL pictures were taken under constant conditions: 13-14 Kv and 580-590 μA.

Samples for studies by Scanning Electron Microscope (SEM) either have been polished, or their broken surfaces have been slightly etched with 50 % acetic acid for two minutes.

The classification of calcite cements is based on their extinction pattern, crystal shape, fabric and luminescence patterns (Table 3-1). Additional criteria include: the abundance of inclusions in crystals; the qualitative iron content as defined by staining tests; the relationship of cement generations to marine sediments and microfractures; and their chronologic rank.

Table 3-2 contains an inventory of all cements and replacive phases examined for the present study. A detailed description of calcite cements will be presented in the next section. Detailed petrography of silica, dolomite and bitumen is not included in this manuscript (for silica see Savard *et al.*, 1990a). The geochemical signatures of these

calcite cements, their regional distribution and their significance will be discussed in chapters 4 and 5.

3.2 EARLY MARINE CEMENTS - NEOMORPHIC CEMENTS

If present, early calcite cements are invariably the first generation. Four types (Table 3-2) have been recognized by optical microscopy:

(a) **Botryoidal Calcite:** inclusion-rich and inclusion-poor anhedral spar with irregular boundaries, present as ghosts of very long needles that form small or giant botryoids;

(b) **Isopachous Calcite:** inclusion-rich needles, fibres and blades, generally with faint boundaries and undulous extinction that form splays or palisades in single, or several superimposed, isopachous layers;

(c) **Rhombohedral Calcite:** inclusion-rich rhombohedral crystals with unit extinction, and postdating cements (a) and (b); and,

(d) **Tangential-Ooidic Calcite:** inclusion-free microspar in concentric cortex layers of ooid ghosts similar to the tangential fabric of Richter (1983).

Except for the cement type (d) that has been sampled in grainstones of a shallow-water inner shelf environment, all other types have been found in cavities of mud mounds within the relatively deep-water outer shelf. The cathodoluminescence patterns of these cements are listed in table 3-3.

The early calcite cements of types (a), (b) and (c) commonly alternate with encrusting marine organisms and/or marine sediments. They play a significant role in mud mound edifices because they solidify the fragile structure of bryozoans and/or algae, thus preventing compaction during later burial. In the "Waulsortian" mud mounds, cements comprise up to 80 % of the volume of the biolithites and fill up to 90 % of the primary pore space (fig. 3-1 a, b). Davies and Nassichuk (1989) used the term "cementstone" to describe such a texture. This term will be adopted in the subsequent text. Pieces of broken cementstone intermixed with marine sediments, fill marine fractures (neptunian dykes). Confirming the early nature of these cements. The walls of marine fractures are, in turn, often covered by similar cements.

3.2.1 Botryoidal calcite - calcitized aragonite (A)

The occurrence of early marine cements in the form of small and large botryoids of calcite is restricted to the Bashkirian and Moscovian mud mound cavities. Such cements have not been observed in the Permian rocks. In the Bashkirian beserellid mounds of the Otto Fiord Formation, they constitute the most abundant abiotic carbonate component, forming giant structures up to 10 cm in radius. These large botryoids (fig. 3-2 a) resemble large mamelons of aragonite that were observed in the Pleistocene reefal terraces of the Red Sea (Aïssaoui, 1985), and Holocene forereef of Belize (James and Ginsburg, 1979).

The botryoidal calcite either predates or postdates other forms of early calcite cements. The small botryoids are texturally comparable to the calcite pseudospar of Mazzulo (1980), a replacive phase after marine acicular aragonite in the Capitan Limestone (Permian Reef Complex) of New Mexico and Texas.

Botryoidal calcite with the best preserved internal texture consists of imbricated anhedral calcite containing needle-like strings of inclusions (fig. 3-2 c). Boundaries of the calcite crystals which are irregular and elongate in the same direction as the acicular ghosts, may be either inclusion-rich or poor (fig. 3-3 a, d). The crystals form mosaics with patchy extinction. In some cases, poor textural preservation spared only the outer boundaries of the botryoids, with the needle-like internal texture having been completely destroyed and replaced by irregular anhedral crystals (figs. 3-2 b, 3-3 f, 3-5 c). These mosaics of irregular imbricated crystals are likely a result of the texturally disruptive transformation of metastable aragonite into the more stable diagenetic calcite (see Sandberg, 1985 for a review).

Previous studies dealing with the petrography of diagenetic calcites that replaced original aragonite cements omitted to document the details of luminescence patterns in the diagenetic anhedral calcites (Davies, 1977; Assereto and Folk, 1980; Mazzulo, 1980; Sandberg, 1983, 1985; Wilkinson *et al.*, 1984; Aissaoui, 1985; Tucker and Hollingworth, 1986). In the present study, the staining tests revealed that the replaced aragonite is

composed of composite iron-free and iron-poor zones. On a finer scale, however, the CL shows a more complex zoning, with nonluminescent, luminescent and dull calcites.

Based on the relationship between replacive calcite crystals, as revealed by cathodoluminescence, and on the state of preservation of the former aragonitic ultrastructure (acicular ghosts), five cathodoluminescence patterns have been recognized. These are:

Irregular pattern (AIR) - Nonluminescent elongate irregular calcite crystals aligned parallel to the axis of former needles, but with crystal boundaries overstepping the original crystal limits (fig. 3-4 a).

Fine needle pattern (AFN) - Luminescent and dull needle-like fine zones (2 to 10 micrometres wide) developed successively after the nonluminescent irregular pattern (fig. 3-4 b). The dull and luminescent calcite seems to have replaced the nonluminescent one. This chronology is supported by the observation that luminescent and dull calcites occiude voids that are lined at the periphery by nonluminescent calcite (see void patterns below).

Mold pattern (AMD) - Nonluminescent and luminescent elongate calcite crystals that are laterally restricted by molds of the former aragonite needles (figs. 3-4 c, d, 3-5 d). The molds are 20 to 50 micrometres wide and 2 to 3 centimetres long.

Microcrystal pattern (AMY) - Composite texture made of dot-like nonluminescent and luminescent microzones (with an average diameter of 0.01 mm) and of films of dull overgrowths (fig. 3-5 b). Some samples show only dull calcite.

Void patterns (AVO) - Regular luminescent and dull calcite overgrowths on nonluminescent calcite. These luminescent and dull portions represent typical layers grown in dissolution voids (figs. 3-3 b, g, h, 3-4 b, e).

The irregular and solution patterns represent the most frequently encountered textural features. They have been observed to coexist in the same samples, some accompanied by fine needle, mold and microcrystal patterns. Admittedly, these patterns reflect conditions that prevailed during calcitization. Their coexistence, therefore, argues for heterogeneity of dissolution pathways for aragonite at the hand specimen scale. The nonluminescent irregular pattern has probably been generated by microscale, partly closed-system recrystallization. At the other extreme, a macroscale open-system dissolution probably accounts for the void pattern. The remaining three textures probably represent intermediate conditions.

3.2.2 Isopachous calcite - recrystallized magnesian calcite (HM)

The most common early marine cements form dark to pale isopachous layers up to 0.5 centimetre thick (fig. 3-1 a, c). They consist of inclusion-rich needles, fibres and blades, generally with faint boundaries and radiaxial, fascicular or undulous extinction

(fig. 3-6 a, b, c, d, e, g, h). Crystals can be perpendicular to the substrate and form palisades (fig. 3-9 d) or they can form small splays in single (figs. 3-1 c; 3-6 b,c,h) or several (fig. 3-1) superimposed isopachous layer(s). Crystals are mostly composed of iron-free low-magnesium calcite, rarely of iron-poor calcite. Neogene bladed and fibrous HMC (7.6 to 13.5 and 14.4 to 16.9 % $MgCO_3$) with similar textures have been described by Aïssaoui (1988).

SEM observations revealed several elongated subcrystals within each needle and fibre as well as anhedral equant subcrystals within fibrous and bladed crystals (fig. 3-7). The typical fascicular optic and radiaxial extinction of these cements could result from the deployment of subcrystals with quasi-parallel c-axes. It may well be a primary feature, as proposed by Coniglio (1985), Kendall (1985), Sandberg, (1985) and Saller (1986). The inclusion-rich texture shows well under SEM. The inclusions consist of perfect empty micro-rhombohedral voids (probably etched dolomite), subordinate silica (see Savard *et al.*, 1990 a), some deformed fluid inclusions, voids between microcrystals, and irregular microvoids (fig. 3-7). The last variety could be microborings: traces of infestation by endolithic organisms soon after crystallization (Videtich, 1985; Saller, 1986). Insignificant proportions of organic matter is still present in a few crystals, an observation based on the white card technique of Folk (1987).

Based on the proportion and distribution of nonluminescent, luminescent and dull zones within the bladed, fibrous and acicular cements, six cathodoluminescence patterns have been recognized. They are described below.

Uniformly nonluminescent (HM1) - Uniformly nonluminescent zones without an identifiable crystal shape and with only traces of luminescent zones (fig. 3-8 a).

Fibrous nonluminescent (HM2a) - Nonluminescent zones with identifiable shape (fibrous or bladed) surrounded by luminescent or dull films (fig. 3-8 b), similar to Frykman's cloudy blades (1986, p.408).

Patchy nonluminescent (HM2b) - Nonluminescent zones with no recognizable shape, with the luminescent and dull zones covering up to 50 % of the surface (fig. 3-8 c, d).

Composite dull (HM3) - Surface dominantly covered by dull zones, generally with no recognizable shape and containing nonluminescent and luminescent microzones (fig. 3-8 e).

Fibrous luminescent (HM4a) - Luminescent zones with fibrous shapes or palisade-like fabrics and containing nonluminescent patches (fig. 3-8 c, d).

Patchy luminescent (HM4b) - Luminescent zones with no recognizable fabric in which the nonluminescent zones can cover up to 50 % of the surface (fig. 3-8 e).

When present in the same isopachous layers, the above patterns have vague lateral contacts indicating that the luminescence patterns are produced by recrystallization (figs. 3-8 d, e; 3-9 a, b). On the other hand, the contacts between stratigraphically successive patterns may also be sharp and clear - like primary layers in succession (fig. 3-9 c, d) - or irregular (fig. 3-9 b, c). Unless precipitated under extraordinary conditions (Adams and Schofield, 1983), Recent marine cements are nonluminescent. The precipitation of luminescent and dull calcite is usually a product of shallow to deep burial diagenesis. This consideration again suggests that the existence of nonluminescent, luminescent and dull zones in the isopachous calcite (often of irregular and composite patterns) is a result of recrystallization. As already stated for the botryoidal calcite, cathodoluminescent patterns in the isopachous calcite may well reflect the dissolution/reprecipitation processes involved in neomorphism.

Even in the best preserved samples (HM1 and HM2a; fig. 3-8 a, b), inclusions of euhedral microdolomite with reddish luminescence are present (see also figs. 3-9 b, c, 3-7). The presence of microdolomite was first interpreted as a result of HMC conversion into LMC (Macqueen and Ghent, 1970; Lohmann and Meyers, 1977) and used as a criterion for recognition of a HMC precursor (Davies, 1977; Kerans *et al.*, 1986; Savard, 1986; and many others). Subsequently, it has been interpreted as a secondary dolomite

in microvoids (Mirsal and Zankl, 1979) or as a microcavity co-precipitate of marine LMC (Saller, 1986). In the present study, the isolated small dolomite inclusions have a perfect rhombohedral shape that could not possibly have resulted from microvoid filling. This assertion is supported also by the observation that many ossicles of echinoderms contain abundant microdolomite crystals that have the same size and luminescence as those present in the isopachous cements (fig. 3-8 f). Ancient echinoderms are believed to have had a HMC composition (Macqueen and Ghent, 1970).

In summary, the radiaxial extinction of the cements could be a primary feature, but the cathodoluminescent patterns and the microdolomite distribution are consistent with the hypothesis of the recrystallization of magnesian calcite.

3.2.3 Rhombohedral cements - recrystallized magnesian calcite (HMRH)

In light microscopy, large calcite crystals have inclusion-rich and inclusion-free sub-zones (fig. 3-10 a, b). The inclusion-rich portions mimic rhombic crystals (fig. 3-10 a, b) and are superimposed either over earlier marine isopachous calcite cements or on cavity walls. They are iron-free, generally covered by iron-rich, inclusion-free sub-zones.

Even where the rhombohedral ghosts are poorly defined under light microscope, the rhombohedral sub-crystals are perfectly discernible by CL (compare figs. 3-10 b, 3-13 b with 3-11 a, b). The inclusion-rich portions correspond to precisely defined sub-crystals that are comparable to the elongate rhombs of Folk (1974) or to the

scalenohedral or "dogtooth" crystals of Pierson and Shinn (1985), Machel (1986) and Kerans *et al.* (1986). The overall crystal shape is rhombic, and cross-sections of the crystals are perfect triangles (fig. 3-11 c). In the subsequent text, the adjective rhombohedral will be utilized to describe this type of cement.

The inclusion-free overgrowths on the rhombohedral ghosts are devoid of microdolomite, and they are regularly zoned. In contrast, the inclusion-rich rhombohedral portions can have both regular and blotchy CL patterns (fig. 3-11 a, b and c) and they contain abundant microdolomite inclusions. This implies the existence of two mineralogically differing, precursors, with recrystallization affecting only the rhombohedral portions and not the inclusion-free overgrowths. The former thus acquired microdolomites as well as disturbed CL patterns. On balance, all these observations suggest that the inclusion-rich crystals had HMC-precursors, a conclusion advocated previously by Machel (1986) and previously proposed by Folk (1974). The inclusion-free portions correspond to syntaxial overgrowths which precipitated under somewhat different, non marine, conditions (see the later-discussed primary calcite cements).

3.2.4 Tangential-ooidic calcite - calcitized aragonitic ooids (AOO)

Some oosparite samples from the inner-shelf cycles contain neomorphosed ooids that have an average diameter of 200 micrometres. Neomorphism strongly affected these rocks, in some instances preserving only the ghosts of concentric banded cortices

(fig. 3-10 c, d). These ghosts structurally resemble the *in situ* calcitized aragonitic ooids of Richter (1983). Cortical calcite is composed of iron-free calcite and varies in thickness from 10 to 35 micrometres. In contrast, calcite filling moldic cores is iron-rich.

Under CL, the cortices are invariably composed of nonluminescent microspar designated as AOO. It contrasts with the fill of the oomoldic cavities that are occluded exclusively by dull xenomorphic spar (fig. 3-11 d, e). The interparticle pores contain equant nonluminescent crystals with meniscus fabric (and subordinate luminescent overgrowths) as the first generation of cements. The sequence of diagenetic processes may therefore be as follows: (1) microscale recrystallization of aragonitic cortex, with more or less contemporaneous partial cementation of oosparite by nonluminescent equant calcite, (2) dissolution of cores, and (3) precipitation of luminescent and dull sparite.

3.3 PRIMARY CALCITE CEMENTS

3.3.1 NL and zoned cements - meteoric cements

Light microscopy shows that these cements are inclusion-free, iron-free equant calcites with clear crystal boundaries. Because of these textural features, they are believed to have precipitated directly as calcites from waters of meteoric derivation. Cathodoluminoscopy allows their subdivision into two categories.

Equant NL Calcite (MT1) - Equant, anhedral, nonluminescent crystals (10 to 100 micrometres) occur within mosaic fabric in fenestral cavities of calcrete or within meniscus fabric in calcitized, texturally disrupted and originally aragonitic ooidic grainstones (figs. 3-11 d, 3-12 a, b). In some places, these cements bear diagnostic features of meteoric diagenesis such as fine equant size and meniscus (?) fabric. They appear in sedimentary environments susceptible to meteoric influence, specifically in shallow-shelf environment and in calcrete horizons.

Equant Zoned Calcite (MT2) - Equant, anhedral crystals (up to 0.6 mm) with multiple nonluminescent/luminescent couplets, having up to 40 zones (fig. 3-12 c, e). *A priori*, the probability for these cements to have formed from meteoric water appear to be low, because some are present in the relatively deep water outer shelf patch reef mounds (sections 2, 3 and 4). Others, such as the MT2 cements from section 35, occur in patch reefs of the inner shelf that were probably affected by the Early Artinskian regression.

CL zonation, a typical feature of the MT2 cements, are usually believed to signify differences in composition that, in one explanation, can be generated by variations in parent water chemistry. In this interpretation, the fine nonluminescent/luminescent zonations are related to rapid fluctuations in pore water chemistry (redox), and attributed to the influx of ground water into an aquifer (Meyers, 1974, 1978; Frank *et al.*, 1982; Grover and Read, 1983; Niemann and Read, 1988; Horbury and Adams, 1989; Emery and Dickson, 1889; Lee and Harwood, 1989; McLimans and Videtich, 1989). This

concept, based solely on CL petrography, is highly controversial. Bulk solution disequilibrium precipitation, nonlinear dynamic behaviour of solutes and to a minor extent, sector zoning, could also explain CL couplets (Have and Heijen, 1985; Machel, 1989, 1990; Reeder and Paquette, 1989; Middleton, 1990; Fowler, 1990; Paquette and Reeder, 1990). Furthermore, CL zoning has also been reported from an early *burial* equant spar within deep water carbonates that were never subjected to meteoric diagenesis (Coniglio, 1989). Nonetheless, in a purely statistical sense, case studies of multiple nonluminescent/luminescent zones in cements seem to favour the meteoric interpretation. The CL equant zoned cements are therefore tentatively included in the "meteoric cement" category. Further clarification, based on geochemical data, is essential for more definite assertions (see chapter 4).

Fibrous Isopachous Calcite (MT3) - Fibres arranged in isopachous layers form a typical calcrete crust. Although petrography suggests recrystallization, the diagenetic history of this crust could not be established, because only one sample from an Artinskian calcrete horizon was studied.

3.3.2 Late cements - burial (?) cements (L)

If present in the same cavities, clear calcite cements are always superimposed on the above described early marine and meteoric cements. Such clear calcite cements consist of low-magnesium calcite (LMC) with 0.6 mole % $MgCO_3$. They appear in all kinds of cavities, including tectonic fractures. In hand specimens, late calcite crystals are

translucent, white or yellow. On a microscopic scale, they invariably have unit extinction, are inclusion-free, and either iron-rich or iron-poor. Their grain boundaries, as for MT1 and MT2 cements, are clearly defined, no secondary minerals have been found by SEM, and only regular and pristine patterns were observed with CL. Since they do not show textural signs of alteration, their geochemical attributes should be primary.

The terms "poikilotopic" or "poikilitic" have been popularly adopted to describe the arrangement of these coarse burial cements (Moore and Druckman, 1981; Scholle and Halley, 1985; Koch and Schorr, 1986; Emery *et al.*, 1988; Hurley and Lohmann, 1989; Moore, 1989 Choquette and James, 1990). However, these textural terms apply only to coarse crystals that enclose several depositional grains, a texture encountered only a few times in this study. The term "coarse mosaic calcspar" utilized by Choquette and James (1990) for description of large burial cements constitutes an alternative. However, "xenomorphic" is herein suggested as a better textural term for anhedral coarse crystals with high frequency of enfacial junctions.

A combination of crystal shapes and cathodoluminescent patterns yields five categories of late calcite cements (table 3-4). They are described below.

Stubby NL Calcite (L1a) - Fine stubby to bladed nonluminescent crystals (10 to 50 micrometres), generally overgrown by a film of brightly luminescent calcite. They can

appear directly on cavity walls, or as overgrowths on earlier generations of cements (figs. 3-6 e, f, i; 3-14 b). In terms of abundance, this category is of minor importance.

Stubby Zoned Calcite (L1b) - Fine stubby or bladed crystals (30 to 300 micrometres) showing only one or two alternations of nonluminescent, luminescent and dull calcite layers, and appearing directly on walls of corals (fig. 3-14 a). In terms of abundance, this category is of minor importance.

Xenomorphic Dull Calcite (L2a) - Uniformly dull, coarse calcite crystals that show high frequency of enfacial junctions in a mosaic arrangement. Development of characteristic habits of the rhombohedral system has been prevented by competitive growth and by the lack of space, resulting in poikilotopic (fig. 3-13 a) and xenomorphic (xenotopic; figs. 3-13 c, d; 3-14 a) textures. This is the most abundant category of late cements. In some cases, it is present within microfractures that postdate stylolites, is invariably iron-rich and sometimes contains inclusions of bitumen (3-13 d).

Xenomorphic Zoned Calcite (L2b) - Coarse luminescent/dull calcite crystals appearing as a mosaic in the center of cavities (fig. 3-14 b). In microfractures they occasionally postdate stylolitization. In terms of abundance, this category is of minor importance.

Xenomorphic Luminescent Calcite (L2c) - Coarse (up to 0.5 mm) luminescent calcite crystals that appear as a mosaic in the centre of cavities or fill microfractures. In

microfractures they occasionally postdate stylolitization. In terms of abundance, this category is of minor importance.

Cements of the L1 type do not bear any petrographic attributes typical of early marine cements, and in their shapes, they differ only slightly from the meteoric cements of the MT1 type, yet, no sedimentological criterion supports their formation in a surficial meteoric diagenetic environment. Chronologically, they postdate marine cements and appear to precede compactional breakage and thus might be of shallow burial origin. This proposition is consistent with their stable isotope composition (Savard and Bourque, 1989; Hurley and Lohmann, 1989), but geochemical criteria may not always be unequivocal (Choquette and James, 1990). Tentatively, the L1 type of cements are interpreted as shallow burial products.

The inclusion-free coarse crystals of the L2 type are typical of slow growth at low supersaturation level (Scholle and Halley, 1985). Because they commonly post-date fracturing and stylolitization, they are labelled here as burial cements *stricto sensu*. In some instances, they postdate pyrobitumen, and this also suggests a deeper burial origin.

3.4 SUMMARY

Inclusion-rich isopachous and botryoidal calcites are inferred to be neomorphic LMC after marine HMC and A, respectively. If the primary mineralogy was as suggested, it should be reflected in the geochemistry of the successor dLMC. In the latter, many CL patterns have been recognized and their intersecting and entangling relationships suggest that stabilization has been accomplished in more than one dissolution/reprecipitation step. These CL patterns can be regarded as distinct degrees of textural preservation. The disruption increases from the AIR to the AMY patterns for calcitized aragonite, and from the HM1 and HM2a to the HM3 and HM4 patterns for recrystallized HMC. In theory, the texturally "best" preserved samples should have the "best" marine isotopic signal, and this assertion will be verified in the next chapter.

The "primary" cement category comprises all LMC cements devoid of recrystallization features and includes meteoric and late cements. The calcitic meteoric cements constitute the best material for extraction of the isotopic meteoric signals. However, some of these cements (*e.g.* MT2) have been only tentatively included in the meteoric category, and geochemical investigations are required to confirm their origin.

The "xenomorphic" late cements include calcite with numerous CL patterns, the most abundant one being "uniform dull" (L2a). In some cases, these dull cements are associated with textural features of undeniably "deep burial" origin, whereas in others

there are no petrographic clues as to the depth or environment of their origin. Again, geochemical criteria may help to decide whether these cements are of phreatic (marine or meteoric), or of burial origin.

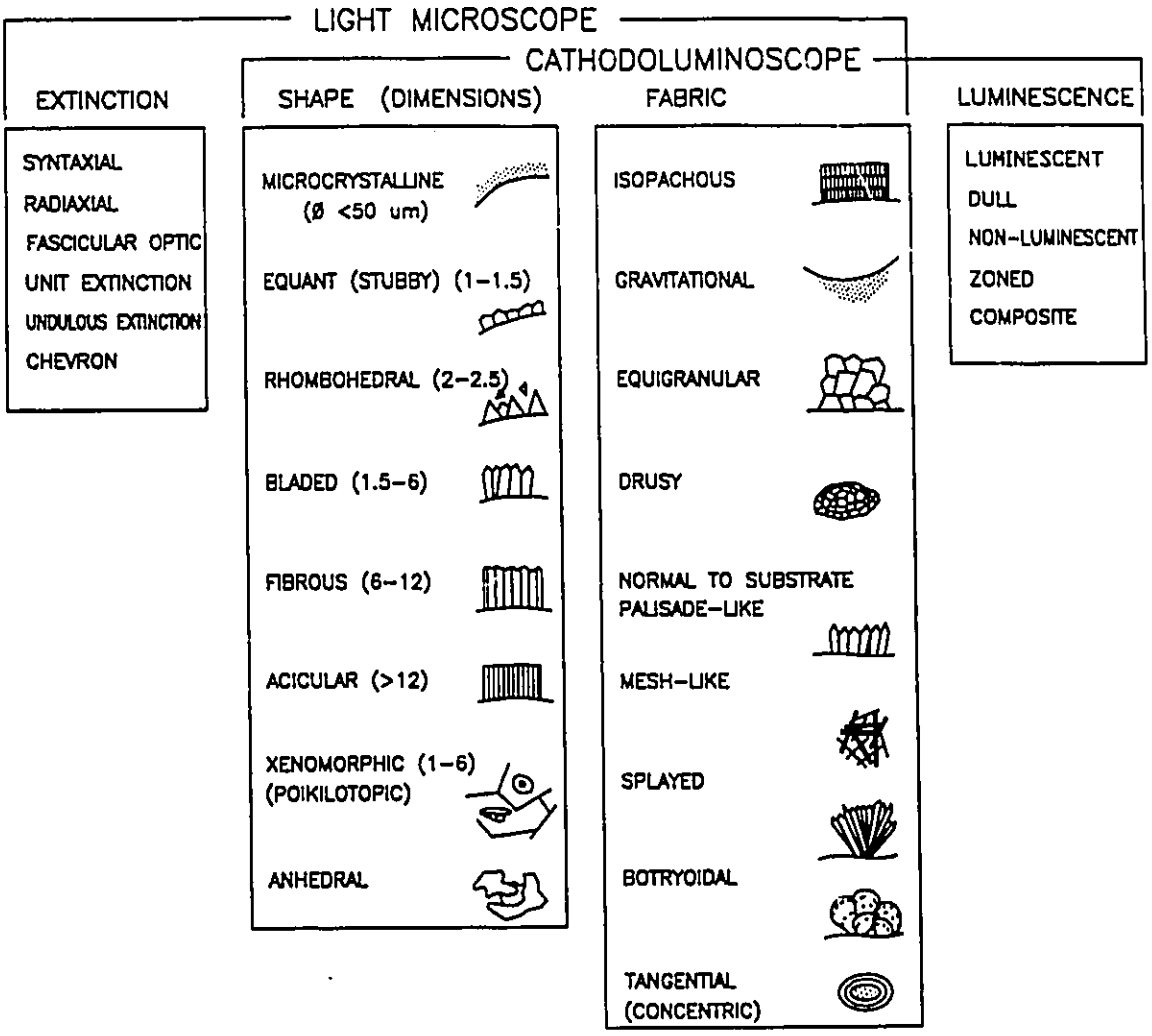

TABLE 3-1. PETROGRAPHIC PARAMETERS. LIGHT MICROSCOPY: SHAPE, DIMENSIONS (LENGTH TO WIDTH RATIOS), FABRIC AND EXTINCTION. CATHODOLUMINESCOPY: SHAPE, DIMENSIONS, FABRIC AND LUMINESCENCE.

CEMENT	SHAPE	FABRIC	CL
NEOMORPHIC CALCITE	ACICULAR GHOSTS FIBROUS, BLADED RHOMBOHEDRAL GHOSTS MICROSPAR	BOTRYOIDAL ISOPACHOUS TANGENTIAL OOLITIC	COMPOSITE COMPOSITE COMPOSITE NL
PRIMARY CALCITE	EQUANT POIKILOTOPIC	----------	NL, LUM, ZONED LUM, DULL
SILICA	FIBRES – QUARTZINE – LUTECITE CHALCEDONY SUBAUTOMORPHIC AUTOMORPHIC – MEGAQUARTZ XENOMORPHIC – MICROQUARTZ – MEGAQUARTZ	 SPHERULITIC SPLAYED SPHERULITIC CHAIN–LIKE ISOLATED MESH–LIKE MOSAIC–LIKE	 NL NL NL NL NL NL NL
DOLOMITE	MICRORHOMBOHEDRAL RHOMBOHEDRAL "BAROQUE" ANHEDRAL	----------	ZONED, NL ZONED, NL NL, LUM NL, LUM
BITUMEN	DROPLET	----------	----------

TABLE 3–2.
COMPILATION OF CEMENTS OBSERVED IN THE STUDIED CARBONATE SEQUENCES OF THE SVERDRUP BASIN.

SHAPE	FABRIC	EXTINCTION	CL PATTERNS
EQUANT IRREGULAR	BOTRYOIDAL	UNIT	IRREGULAR ELONGATIONS FINE NEEDLES ACICULAR MOLDS MICROCRYSTALS SOLUTION VOIDS
FIBROUS AND BLADED	ISOPACHOUS	RADIAXIAL, FASCICULAR, UNDULOUS	NL NL FIBRES NL PATCHY (BLOTCHY ?) DULL COMPOSITE LUM PALISADE-LIKE LUM PATCHY
RHOMBOHEDRAL	--------	UNIT TO UNDULOUS	NL PLAIN TEXTURE NL PATCHY TEXTURE
EQUANT IRREGULAR	TANGENTIAL	UNIT	NL

TABLE 3-3. PETROGRAPHY OF NEOMORPHIC CALCITE CEMENTS INTERPRETED AS MARINE.

SHAPES	LUMINESCENCE
STUBBY	NL and NL/LUM ZONED (EQUANT)
STUBBY to BLADED	NL LUM and DULL/LUM ZONE (OVERGROWTHS)
POIKILOTOPIC, XENOMORPHIC	DULL

TABLE 3-4. SHAPE AND LUMINESCENCE OF PRIMARY CALCITE CEMENTS.

MEGASCOPIC OBSERVATIONS - EARLY CEMENTS

Figure 3-1

a) Phylloid algal *cementstone* from Moscovian *Waulsortian* mud mounds, Hare Fiord Formation. Isopachous layers of early, inclusion-rich fibrous calcite fill up to 85 % of the pore volume. Polished hand specimen. Length of the picture (long axis) is 13 centimetres. Sample number (S N): 32173.

b) Phylloid algal *cementstone* from Moscovian *Waulsortian* mud mounds, Hare Fiord Formation. Neomorphic low-magnesium calcite after aragonite (A) and high-magnesium calcite (H), and late inclusion-free calcite (L) fill up to 55, 35 and 10 % of the primary pore volume, respectively. Polished hand specimen. Length of the picture is 7 centimetres. S N: 31179

c) *Paleoaplysina* (P) boundstone. Shelter (growth) cavity filled by multilayered, inclusion-rich, isopachous fibrous calcite (H). Polished hand specimen. Length of the picture is 6 centimetres. S N: 31733.

A

B

C

BOTRYOIDAL FABRIC

Figure 3-2

a) Giant botryoidal neomorphic calcite on the wall of a marine fracture. The well preserved strings of inclusions show primary growth steps of the former aragonitic botryoids. Hand specimen. Length of the picture is 10 centimetres. S N: 31183.

b) Poorly preserved small botryoids of calcitized aragonite for which only ghosts of the outer boundaries are recognizable. Plane-polarized light. Length of the picture is 14 millimetres. S N: 171267.

c) Well preserved acicular ghosts of aragonite within elongate anhedral neomorphic calcite. Cross-polarized light. Length of the picture is 1.75 millimetres. S N: 171267.

d) Same as c. Cathodoluminescence patterns showing calcitization steps.


A


B


C


D
3-2

TEXTURES IN CALCITIZED ARAGONITE

Figure 3-3

a) Calcitized aragonite with discontinuous ghosts of needles and inclusion-free and -rich portions of replacive crystals. Plane-polarized light. Length of the picture is 1.4 millimetres. S N: 171262.

b) Same as a. Cathodoluminescence view showing that the inclusion-free portion underwent total dissolution. The void was later filled by luminescent calcite. The inclusion-rich portion has nonluminescent and dull CL, the latter associated with microfractures.

c) Microfracture separating the dull and nonluminescent zones in elongated LMC crystals after aragonite. Portions of nonluminescent calcite isolated in the dull zone indicate that recrystallization of the former produced the dull pattern. Cathodoluminescence. Length of the picture is 3 millimetres. S N: 171262.

d) Irregular boundaries of elongated LMC crystals after aragonite, crossed by twin lamellae. Plane-polarized light. Length of the picture is 1.4 millimetres. S N: 171267.

e) Same as d. Cathodoluminescence view. Coexisting CL patterns: nonluminescent irregular (I), fine needle (F) and solution (V).

f) LMC showing poorly preserved texture of former botryoidal aragonite. Relics of needles can only be seen in the outer part (arrows). The centre is made of imbricated anhedral crystals. Plane-polarized light. Length of the picture is 2.8 millimetres. S N:171287.

g) Same as f, under cathodoluminescence. CL patterns are AVO and AFN. They indicate that calcitization proceeded partly by wholesale solution and subsequent void-filling and partly by in situ replacement.

h) Same as g, closer view under cathodoluminescence. Length of the picture is 1.4 millimetres.

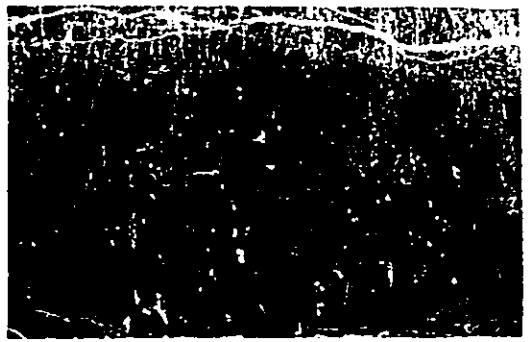

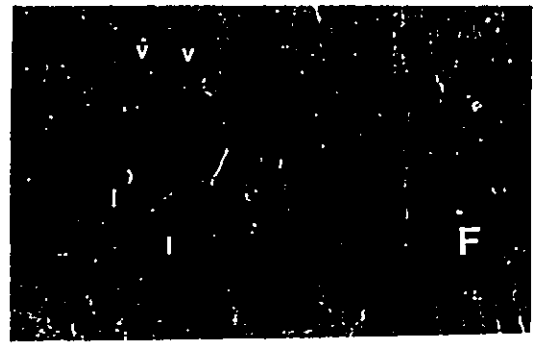

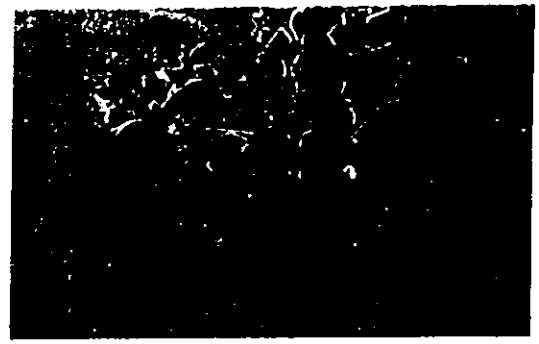

3-3

CATHODOLUMINESCENCE PATTERNS IN CALCITIZED ARAGONITE

Figure 3-4

a) Irregular. Nonluminescent elongated irregular calcite crystals. Luminescent films mark the intercrystalline boundaries. Length of the picture is 2 millimetres. S N: 171262.

b) Fine needle. Luminescent (L) and dull (D) needle-like fine zones (2 to 10 micrometres wide) developed by replacement of the nonluminescent irregular pattern. The centre shows a solution void (V) later filled by luminescent calcite. Length of the picture is 3 millimetres. S N: 171262.

c) Mold. Luminescent and dull elongated calcite crystals that are laterally restricted by molds of former aragonite needles. Length of the picture is 0.6 millimetre. S N: 171288.

d) Mold. Nonluminescent elongated calcite crystals that are laterally restricted by molds of former aragonite needles. Length of the picture is 0.7 millimetre. S N: 171262.

e) Solution. Regular luminescent and dull calcite overgrowths on nonluminescent calcite. The regular crystals grew in free space (dissolution voids). Length of the picture is 1.1 millimetres. S N: 171262.


A

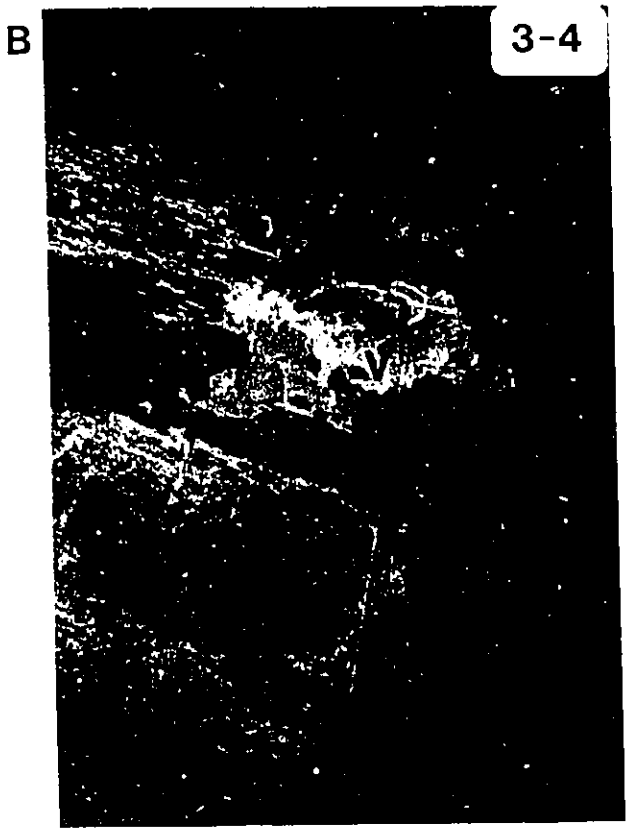
B
3-4


C


D

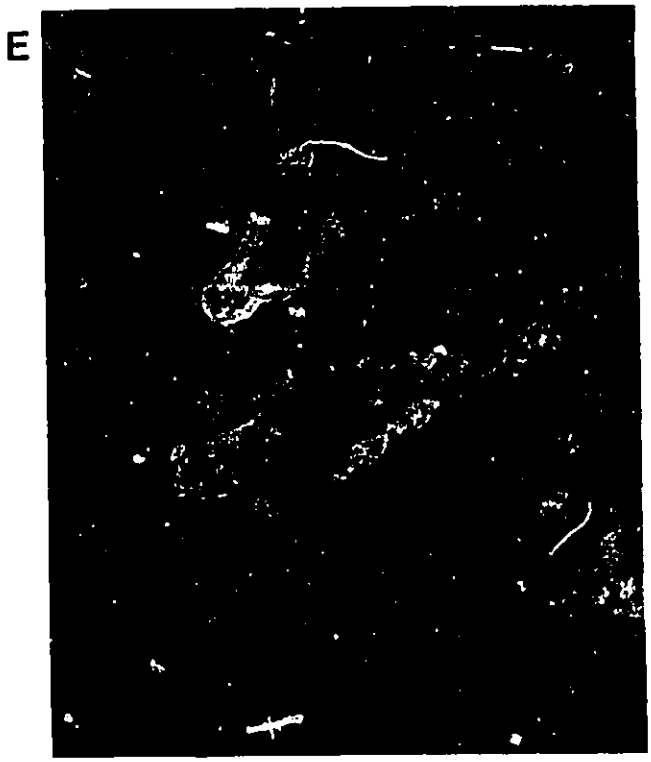
E

TEXTURES IN CALCITIZED ARAGONITE

Figure 3-5

a) Mosaic of irregular calcite crystals. Plane polarized-light. Length of the picture is 1.4 millimetres. S N: 171287.

b) Same as a, under cathodoluminescence. **Microcrystal pattern.** Composite texture made of dot-like nonluminescent and luminescent microzones and of films of dull overgrowths.

c) Mosaic of irregular calcite crystals within a faint oval mold (arrows). Plane polarized-light. Length of the picture is 4 millimetres. S N: 171287.

d) Same as c, under cathodoluminescence. **Mold pattern.** Zoned luminescent and nonluminescent calcite within dissolved needles. Late micro-fractures are filled by luminescent (L) and dull (D) calcite.

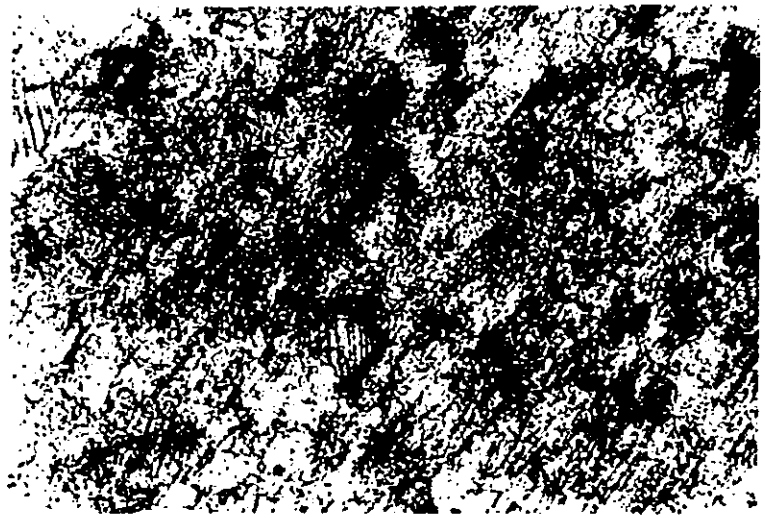

A

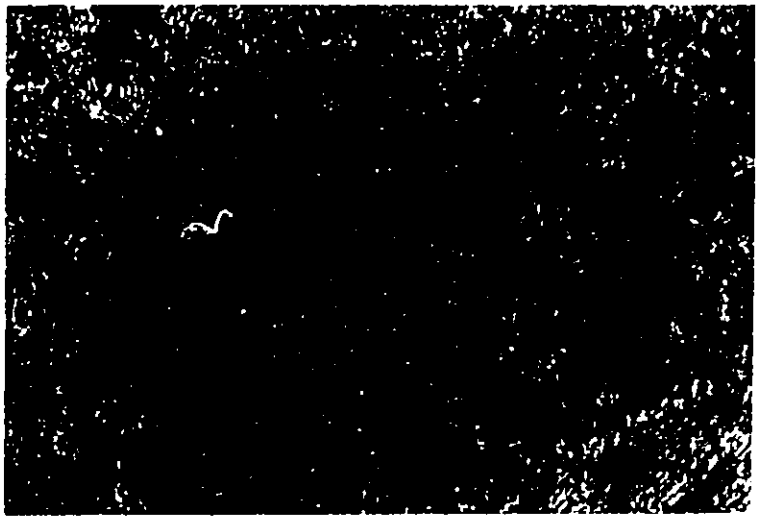

B

C

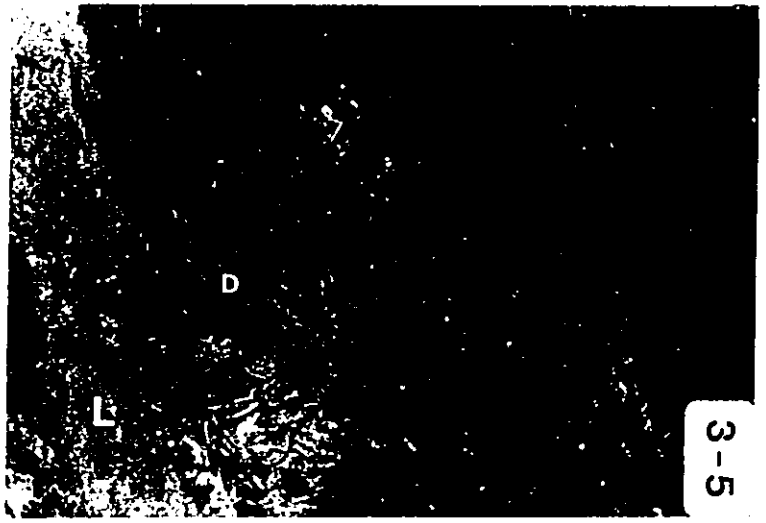

D

TEXTURES IN RECRYSTALLIZED HMC

Figure 3-6

a) Inclusion-rich, splayed faint sub-crystals. C-axis is shown by the extinct portion of the crystal at the centre of the picture. Cross-polarized light. Length of the picture is 0.7 millimetre. S N: 123236.

b) Larger view of the same cavity filling. Extinction of all crystals is sweeping. Cross-polarized light. Length of the picture is 4 millimetres.

c) Inclusion-rich and -poor portions within calcite crystals devoid of clear boundaries. Plane polarized light. Length of the picture 3 millimetres. S N:123236.

d) Same as c. Inclusion-rich and -poor portions in fibrous crystals with clear irregular boundaries. Cross-polarized light.

e) Inclusion-rich early marine cement followed by inclusion-free xenomorphic calcite in pore centre. The boundary of early and late calcite is not clear. Plane-polarized light. Length of the picture is 1.5 millimetres. S N: 171256.

f) Same as e, under cathodoluminescence. The early cement shows composite luminescence whereas the late one has a uniform dull luminescence. Nonluminescent bladed to stubby crystals occur between the early and late cements.

g) Early irregular fibrous cement covered by xenomorphic cement. Cross-polarized light. Length of the picture is 1.5 millimetres. S N: 123191.

h) Same as g. The early cement is inclusion-rich and the late one is inclusion-free. Plane-polarized light.

i) Same as g, under cathodoluminescence. Nonluminescent blotchy early cements are followed by bladed nonluminescent crystals, luminescent overgrowths and xenomorphic luminescent and dull calcite.

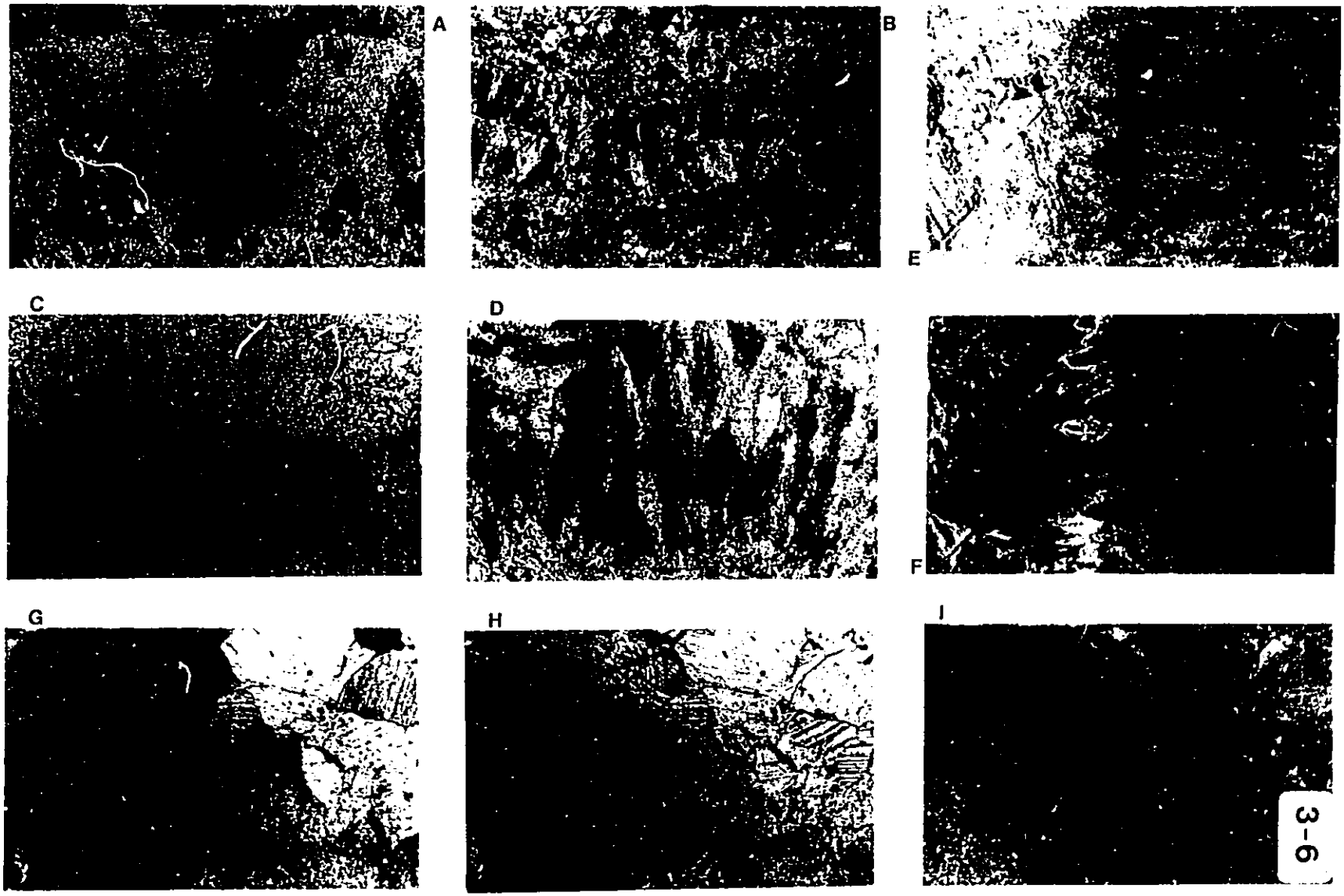
A
B
E
C
D
F
G
H
I

MICRO-SCALE TEXTURES OF EARLY CEMENTS

Figure 3-7

a) Anhedral equant microcrystals (calcitized aragonite) covered by elongated fibrous crystals containing a plethora of rhombohedral micro-voids. SEM. The scale is on the picture. Polished and etched surface. S N: 131740.

b) Irregular fibrous crystals containing a plethora of rhombohedral micro-inclusions. SEM. Broken and etched surface. Scale is on the picture. S N: 171284.

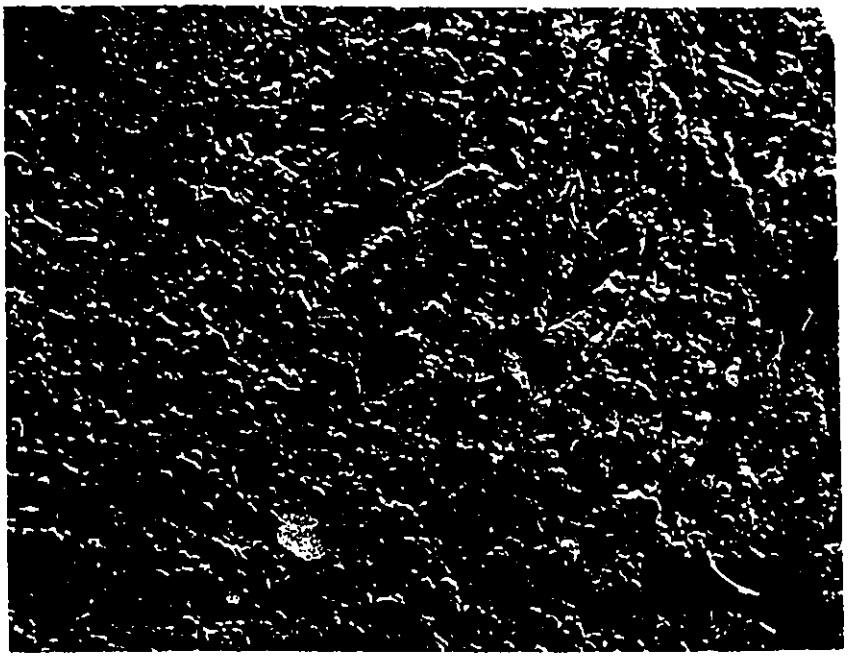

A

B

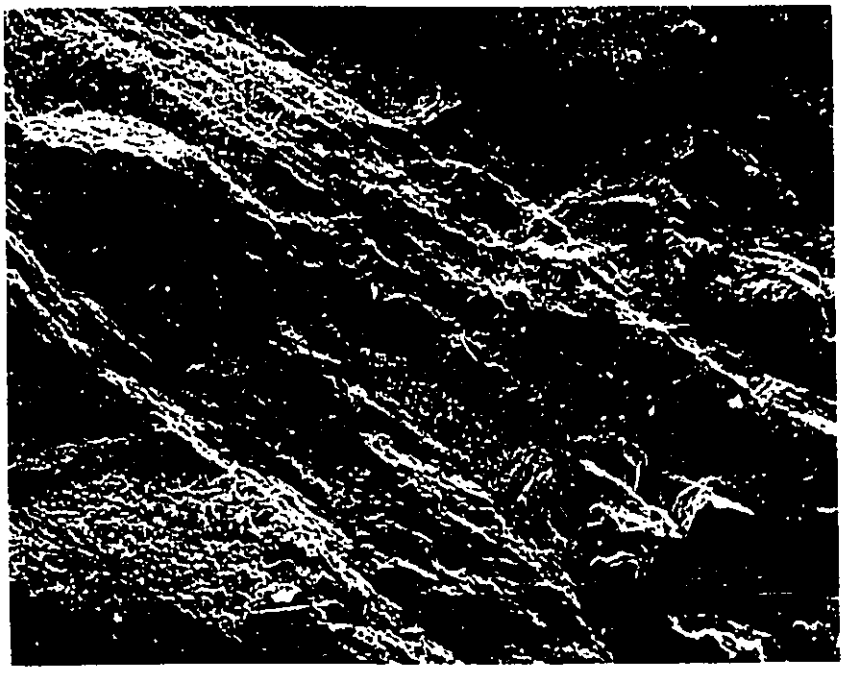

CATHODOLUMINESCENCE PATTERNS IN RECRYSTALLIZED HMC

Figure 3-8

a) Uniformly nonluminescent. Nonluminescent calcite (U) without identifiable crystal shape, covered by blotchy rhombohedral cement (R), itself followed by uniformly dull centre pore calcite (D). Length of the picture is 2.6 millimetres. S N: 123236.

b) Fibrous nonluminescent. Nonluminescent fibrous crystals. Boundaries between crystals are underlined by intercrystals of dull calcite. Length of the picture is 0.7 millimetre. S N: 171289.

c) Patchy nonluminescent. Layer of patchy nonluminescent (P) calcite covered by fibrous luminescent (F), in turn covered by luminescent to dull xenomorphic calcite. Length of the picture is 2 millimetres. S N: 123191.

d) Fibrous luminescent. Fibrous luminescent (F) passing laterally, within one layer of early cement, to patchy nonluminescent (P) calcite. Length of the picture is 1.2 millimetres. S N: 171320.

e) Patchy luminescent. Luminescent zones (L) covering 50 % and more of the surface, with no recognizable shape. The centre of the area is *composite dull* (C). Length of the picture is 0.7 millimetre. S N: 171256.

f) Nonluminescent crinoid ossicle containing abundant *reddish* micro-dolomite crystals (example in the circle). The ossicle is surrounded by luminescent to dull calcitic mud. Length of the picture is 0.6 millimetre. S N: 171270.

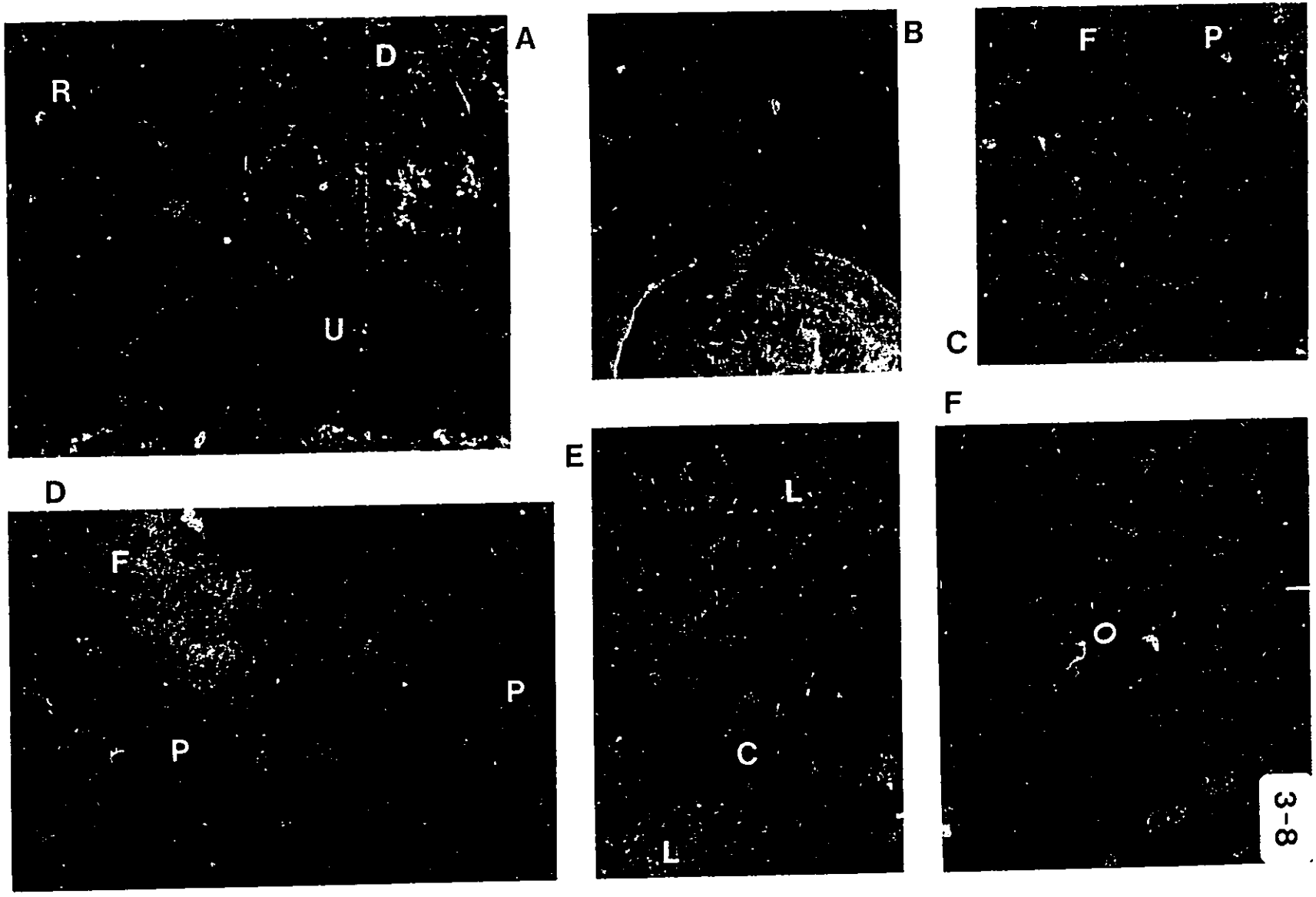
A
D
R
U
B
C
F
P
D
F
P
P
E
L
C
L
F
O

CATHODOLUMINESCENCE PATTERNS IN RECRYSTALLIZED HMC

Figure 3-9

a) **Nonluminescent fibrous** (N) and **luminescent fibrous** (L) patterns coexisting within the same layer of calcite. Lateral passage is irregular whereas vertical passage, between two layers, is abrupt (arrows). Length of the picture is 1.1 millimetres. S N: 171279.

b) **Nonluminescent fibrous** (N) and **luminescent fibrous** (L) patterns with either sharp (S) or irregular vertical contacts (arrows). Length of the picture is 1.4 millimetres. S N: 171279.

c) **Palisade-like luminescent** and **composite dull** patterns. Palisade-like luminescent (L) calcite passing abruptly to composite dull pattern (C). The latter is dominantly made of dull calcite with no recognizable shape and containing nonluminescent and luminescent microzones. Patchy nonluminescent (P) calcite is interlayered with the two other patterns. Length of the picture is 1.3 millimetres. S N: 171320.

d) **Palisade-like luminescent** calcite (L) with sharp vertical contacts with interlayers of **composite dull** calcite (C). Length of the picture is 1.0 millimetre. S N: 171320.

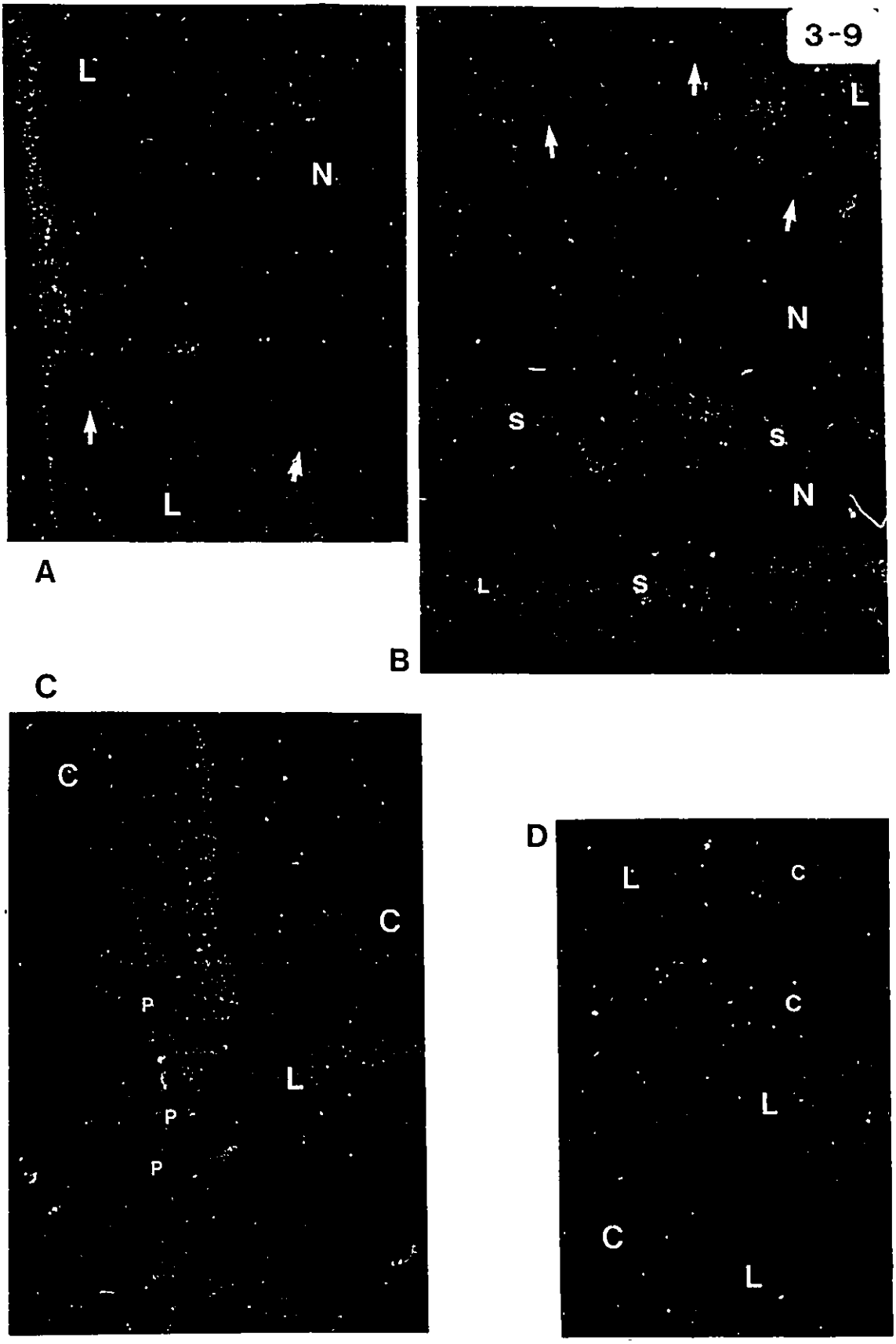
3-9
L
N
L
A
L
N
S
S
N
L
S
B
C
C
C
P
L
P
P
D
L
C
C
L
C
L

RHOMBOHEDRAL CEMENTS and PRIMARY CEMENTS

Figure 3-10

a and b) Low-magnesium calcite with inclusion-rich (R) and -free (P) sub-zones. In (b), polysynthetic twin lamellae are visible throughout the entire crystals. See figure 3-11 (a) for corresponding CL view. Plane-polarized light. Length of the picture is 0.7 and 1.5 millimetres on a and b, respectively. S N: 171287.

c) Well preserved cortex texture of a recrystallized oolite. See (d) for details. Oolite core has been replaced by anhedral inclusion-free calcite. See 3-11 (e) for corresponding CL view. Plane-polarized light. Length of the picture is 0.4 millimetre. S N: 119424.

d) Anhedral equant dLMC crystals forming oolite cortex after tangential aragonite. Interlayer voids mark the limit between former aragonite generations. Core is formed of recrystallized intraclastic carbonate micrite. Polished and etched surface. SEM. The scale is on the picture. S N: 119424.

e) Poorly preserved oolitic texture. Only mold of former oolite is preserved (arrows). In this example, the entire oolite is now replaced by a single late spar crystal. Plane-polarized light. Length of the picture is 1 millimetre. S N: 119424.

f) Grainstone with interparticle xenomorphic calcite and geopetal texture. Former aragonite mold has been dissolved away and later filled-up by inclusion-free anhedral calcite. Plane-polarized light. Length of the picture is 1.5 millimetres. S N: 171306.

g) Same as f, under cathodoluminescence. **Equant nonluminescent.** Anhedral and equant calcite precipitated between particles and inside the geopetal texture predating the solution of the aragonitic component. The mold has been later filled by stubby nonluminescent crystals and luminescent and dull overgrowths.

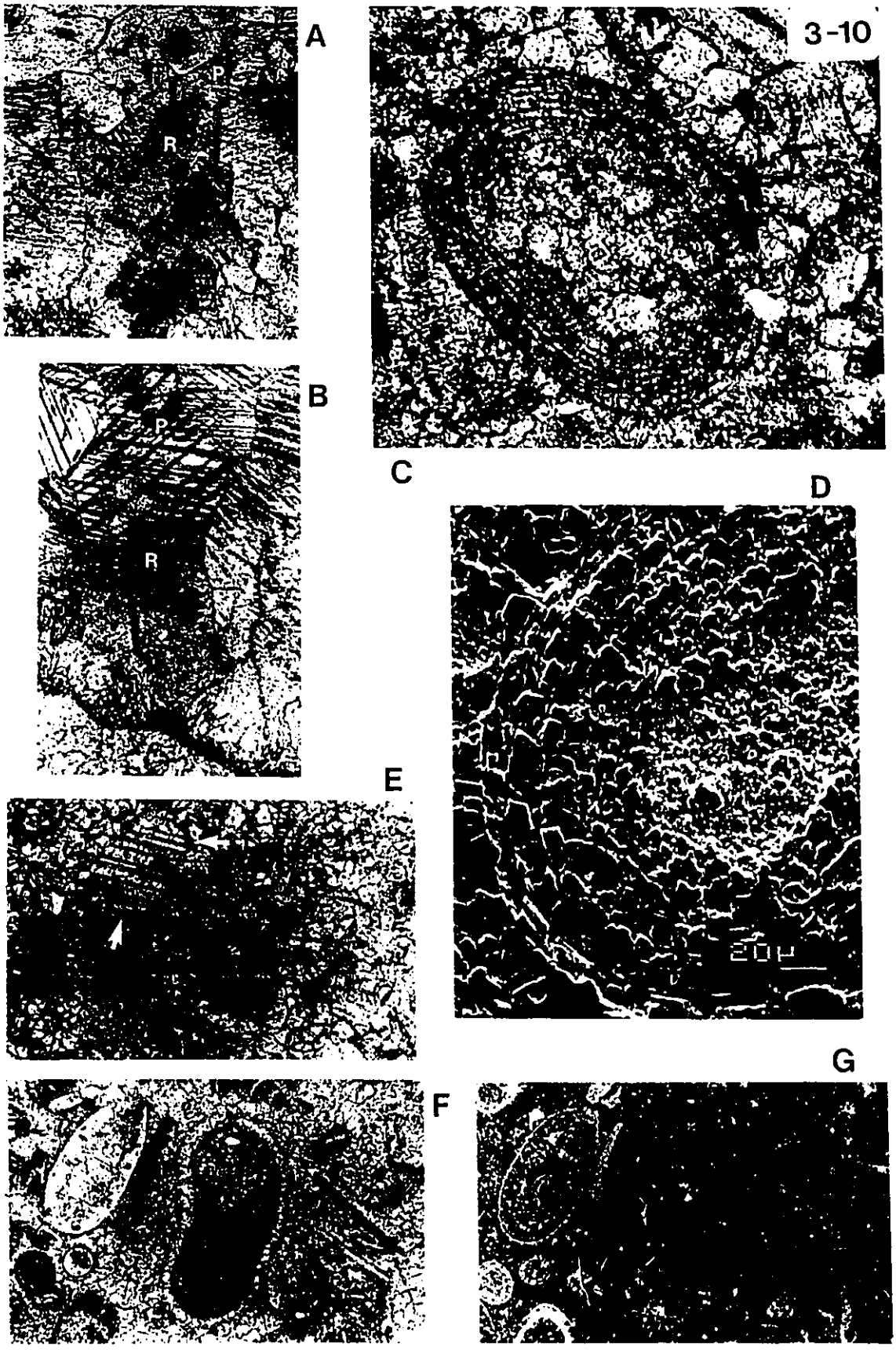
A
P
R
B
P
R
3-10
C
D
20μ
E
F
G

RHOMBOHEDRAL HMC and EQUANT REPLACIVE CALCITE

Figure 3-11

a) Closer view of 3-10 (b), under cathodoluminescence. Nonluminescent bladed crystals (arrows) with two interlayered luminescent zones contain abundant *reddish* microdolomitic rhombohedrons (examples in circles). The late luminescent and dull overgrowths are devoid of microdolomites. Polysynthetic twin lamellae traverse the entire crystals. Length of the picture is 1.5 millimetres.

b) **Rhombohedral** nonluminescent blotchy calcite overgrown by uniformly dull (to luminescent) late calcite. See 3-13 (b) for corresponding plane-polarized light. Length of the picture is 0.6 millimetre. S N: 123236.

c) **Rhombohedral** nonluminescent crystals with triangular cross-sections. Crystals contain numerous microdolomite inclusions. Length of the picture is 0.5 millimetre. S N: 171287.

d) Oosparite with grainstone texture including anhedral crystals in meniscus fabric (M). Cortex layers are now composed of nonluminescent anhedral calcite. Cores of oolites have been dissolved and later filled by uniformly dull xenomorphic calcite. Length of the picture is 1.0 millimetre. S N: 119424.

e) Smaller magnification of 3-10 (c), under cathodoluminescence. The replacive anhedral crystals are nonluminescent. Inter-oolite pore space has been filled by larger equant nonluminescent crystals. The dissolved cores of oolites have been replaced by uniformly dull xenomorphic late calcite. Length of the picture is 0.8 millimetre.

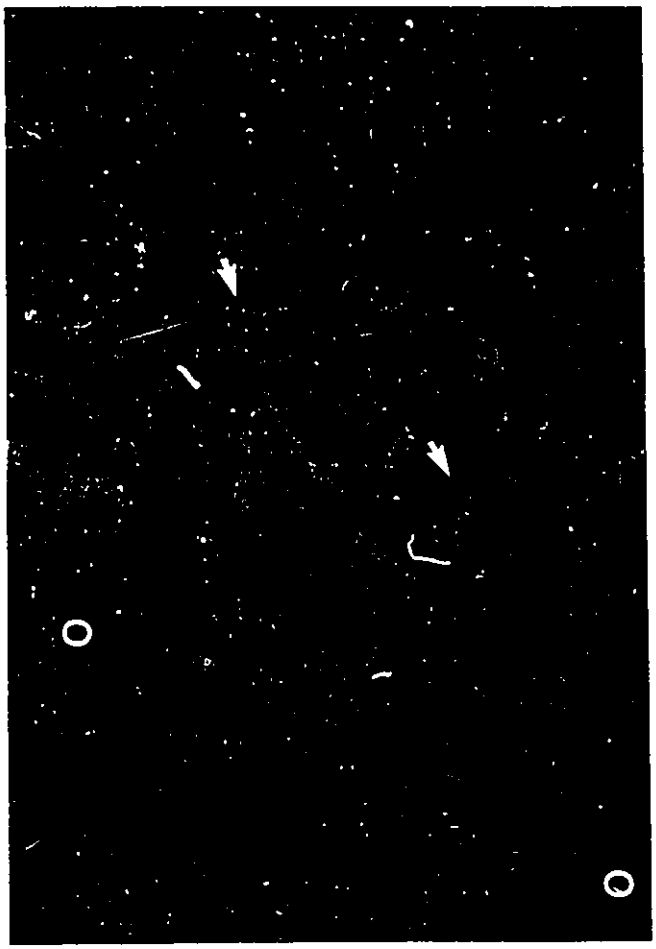

A

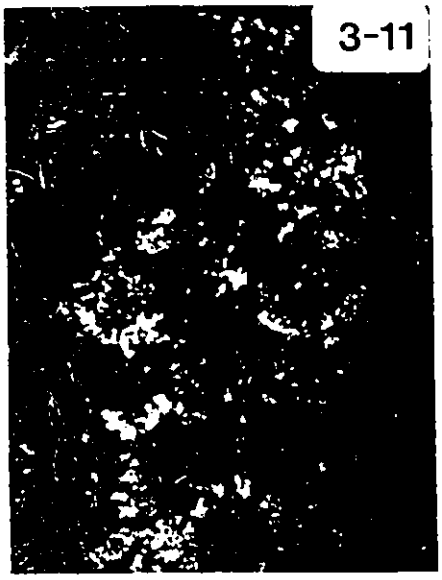

B

C

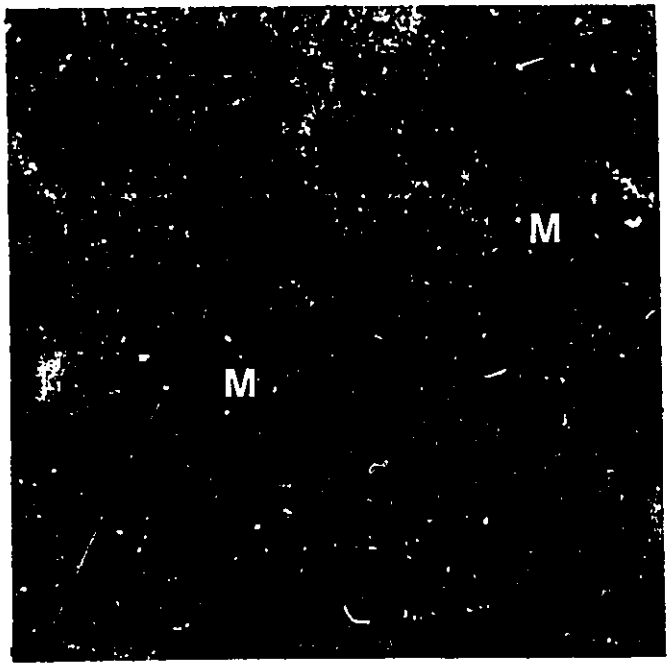

D

E

METEORIC CEMENTS

Figure 3-12

a and b) Subhedral nonluminescent crystals within a fenestral cavity of a calcrete. Centre pore is filled-up by younger luminescent and dull overgrowth. Lengths of the pictures are 0.25 and 0.50 millimetre, respectively. S N: 170121, 170127.

c) Zoned equant cement in a grainstone. Sector zoning is common in the crystals (sets of arrows). Length of the picture is 0.6 millimetre. S N: 115251.

d) Equant calcite crystals infilling a mold after a sulfate mineral (?). The mold cuts through fibres of former HMC from section 37. Plane-polarized light. Length of the picture is 0.5 millimetre. S N: 115613.

e) Same as (d), under cathodoluminescence. Late calcite is zoned equant.

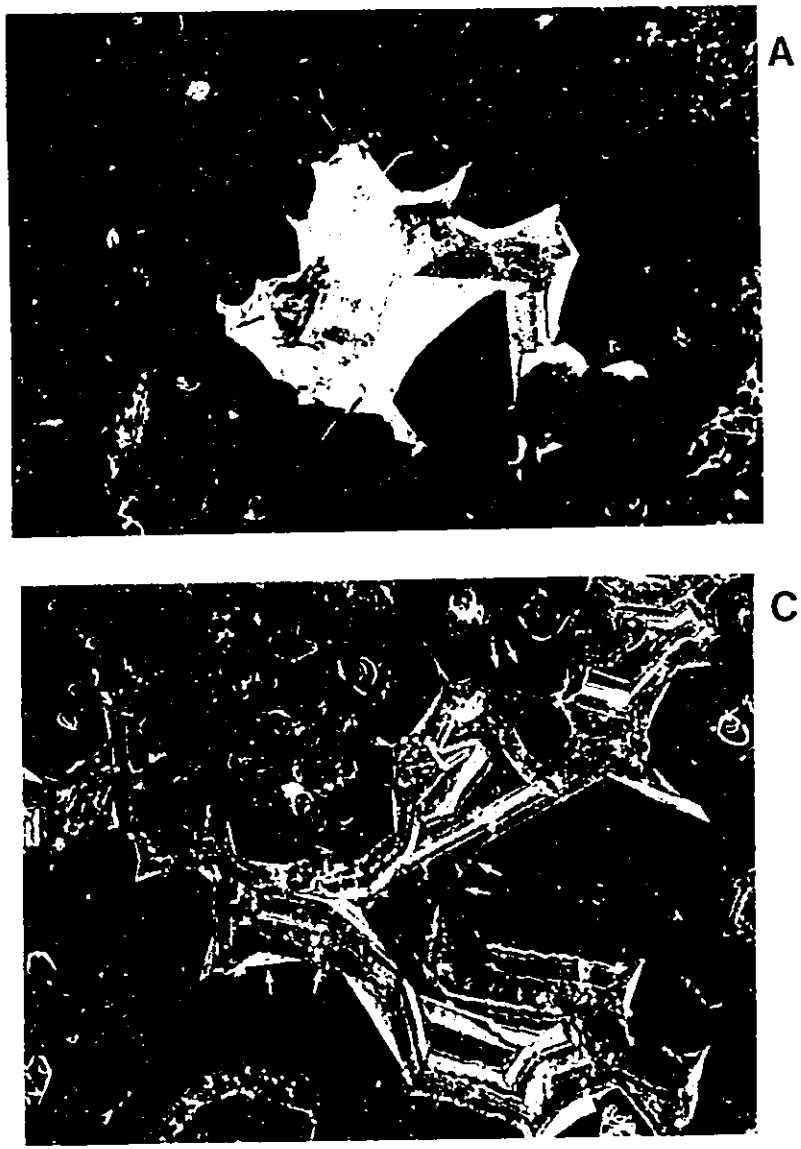
A
B
C
D
E
3-12

LATE CEMENT

Figure 3-13

a) Poikilotopic coarse late calcite engulfing fine particles. Plane polarized light. Length of the picture is 1.0 millimetre. S N: 123115.

b) Same as 3-11 (b), in plane polarized light. Inclusion-rich sub-zones are followed by inclusion-free late cements present within each crystal. Length of the picture is 0.6 millimetre.

c) Intracoral pores infilled by inclusion-free "drusy" calcite. Plane polarized light. Length of the picture is 3 millimetres. S N: 119409.

d) Corroded (arrows) early fibrous calcite superseded by late calcite that has trapped bitumen (opaque black, B). Plane polarized light. Length of the picture is 1.5 millimetres. S N: 171307.

e) Late inclusion-free calcite in intra-organism cavity. Cement post-dates microfracturing (fills a micro-fracture; F) but is in turn postdated by stylolites (arrows). Polished hand specimen. Length of the picture is 3.8 centimetres. S N: 171287.

A

3-13

B

C

D

E

CATHODOLUMINESCENCE TEXTURES OF LATE CEMENTS

Figure 3-14

a) Same as 3-13 c. Late cements within corallites. L1b: 1. L2a: 2. Length of the picture is 3 millimetres.

b) Microfractures (F) cutting through uniformly dull to nonluminescent early cement and stubby to bladed non luminescent crystals (L1a: 1). Zoned overgrowths (L2b: 2) fill the microfractures. The microfractures probably fed the pore centre cementation. Note that the dull late calcite is zoned. Length of the picture is 1.2 millimetres. S N: 171320.

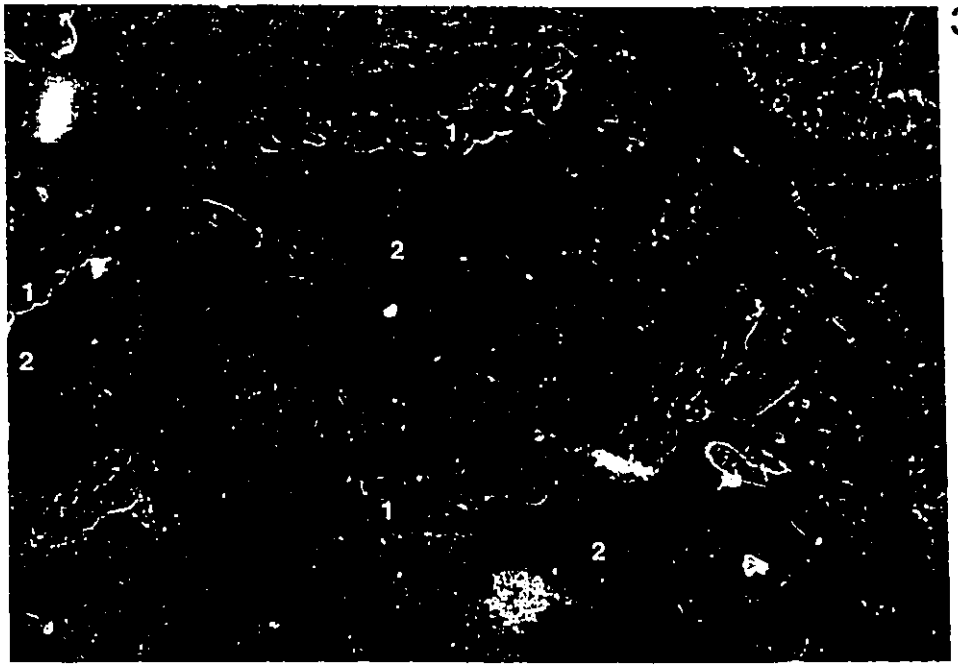

A

B

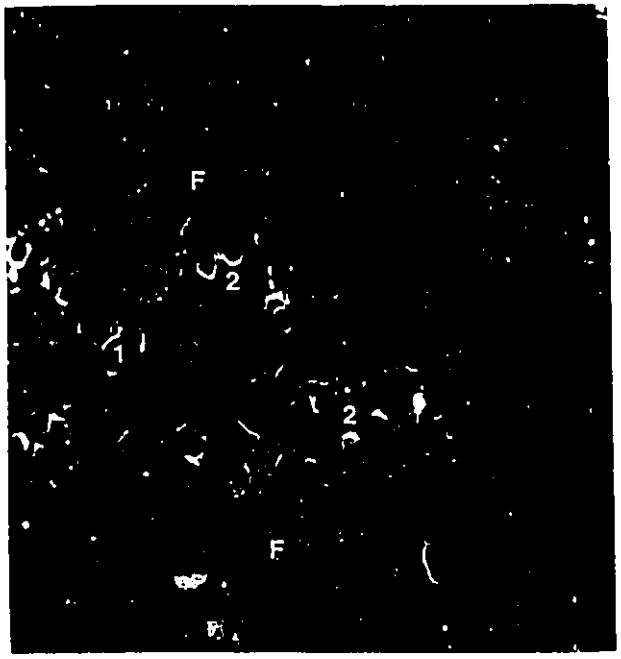

4. GEOCHEMISTRY OF CEMENTS

Chemical species incorporated into the $CaCO_3$ lattices of cement crystals reflect, to a lesser or greater degree, the nature of pre-existing ambient pore fluids. Detailed geochemical studies can therefore provide information related to composition, temperature and the flow of parent waters. The tracers usually utilized for such purposes are Mg, Sr, Fe, Mn, and the isotope ratios of Sr, C and O. For decades, electron microprobes and atomic absorption spectrophotometers (AAS) were the preferred tools for minor element chemical studies. Whereas the former usually offer detection limits that are too high for Sr, Fe and Mn in carbonates, the latter not only demand laborious mechanical separation of cement phases but may also require large quantities of powde.. None of these techniques is suitable for studies of microscale luminescent cement layers. Recently, secondary ion mass spectrometers (SIMS) have been calibrated for detection of trace elements in carbonates (Veizer *et al.*, 1987; Mason, 1987; Swart, 1990). Such instruments have not been previously utilized for systematic investigation of cements, and this work represents the first study where the spatial resolution of tens of micrometres is attained at trace element detection limits in low ppm range.

Geochemical work on cements was planned to assist interpretation of microscale textural phenomena as well as diagenetic evolution on a basin scale. Taking petrographic and stratigraphic criteria as the basis of sample selection, 280 microsamples were separated for C and O isotopes, 59 for $^{87}Sr/^{86}Sr$, and 229 for trace elements by ion

microprobe. Samples for isotopic analysis were drilled at the University of Ottawa, utilizing a Jensen microsampler with small bits of 0.3, 0.4, 0.79 and 1.59 millimetre in diameter.

4.1 ANALYTICAL TECHNIQUES

Stable Isotopes

CO_2 gas was extracted by reacting 8 mg of carbonate powders for twelve hours with phosphoric acid at 25°C. The liberated gas was analyzed on the VG-SIRA 12 mass spectrometer at the Derry Rust Laboratory, University of Ottawa. The results are expressed in the usual delta notation and given in per mil relative (‰) to the Peedee Belemnite standard (PDB). All values are corrected for the presence of ^{17}O, for the geometry of the mass spectrometer and for linear deviation from standard values (Gilles St-Jean, 1990, pers. comm.). Precision of the data is ± 0.1 ‰.

Strontium Isotopes

Samples for Sr isotopic analysis were analyzed at the Geological Institute of the Ruhr University-Bochum, Germany (Buhl *et al.*, 1991). Powdered samples, weighing from 2.0 to 4.4 mg, were dissolved in 2.5 N supra pure HCl in 5 ml SAVILEX PFA beakers, Sr separated by standard ion exchange technique and loaded on a single Ta filament. Mass spectrometry was performed on a 5 collector FINNIGAN MAT 262 mass spectrometer

and the data normalized to $^{88}Sr/^{86}Sr$ of 8.375209. The standard NBS 987, run between May 1989 and June 1990, gave an average value of 0.710238 ± 8 ($\pm\sigma$). The EN-1 $CaCO_3$ (USGS) standard gave a mean value of 0.709134 ± 17 ($\pm\sigma$). The $\pm\sigma$ for single specimen measurements was usually better than ± 20 x 10^{-6}

Trace Elements

Forty two samples that were selected for chemical investigations were polished, cleaned twice with acetone and coated with gold. Based on optical microscope and CL observations, only the areas that did not have any detectable inclusions were selected for analysis. Over a period of 20 days, 229 spot determinations were performed by Secondary Ion Mass Spectrometry with a Cameca IMS 4f at the Grant Institute, University of Edinburgh, Scotland. All spots were analyzed by the author. The trajectory of the primary beam through the primary column (deflectors, lenses, apertures, stigmators...) and of the secondary beam through the mass spectrometer were aligned every morning by John Craven of the University of Edinburgh. The primary $^{16}O^-$ beam had an accelerating voltage of 10.63 Kv, an intensity of 5 nA and a diameter of 25 micrometres. Three minutes were allowed for the beam to pierce the gold coating. The secondary ion intensities were recorded at low mass resolution of 300. Energy filtering (see also Swart, 1990) was applied for the secondary beam, with the discrimination threshold set at 10 % of the maximal energy peak. The usual voltage offset was 75 volts. The total counting time was 925 seconds, with five cycles of 20 seconds for each element, except for Ca with 5 seconds. Na, Mg, Al, Si, Ca, Fe, Mn, Sr, Ba and Ce were measured

on masses 23, 26, 27, 28, 44, 54, 55, 88, 138 and 140, respectively. These peaks were selected either because they represent an abundant isotope of the element in question, or because interferences by molecular complexes were minimal. The standard, a Derbyshire Iceland Spar (DIS), was analyzed every morning in order to establish the ion yield for every element. Over 20 days of investigation, the obtained ion yields remained consistently around 0.35, 0.17, 0.29 and 0.68 for Mg, Fe, Mn, and Sr, respectively. In the same order, 12, 6, 6 and 6 % were the precisions obtained for 17 analyses of DIS. They were calculated as standard deviation (sigma) multiplied by the student factor "t", 1.75, for 15 degrees of freedom at the 95 % confidence level, and expressed in relative percent. The signal to background ratios were always very high (generally thousands of counts compared to a maximum of 0.03 of count per second). The detection limits ((6÷counts in the sample/ppm) x (background counts/second)$^{1/2}$) of the ion probe was generally less than 5 ppm, specifically 4.3, 0.5, 0.2, 0.1, 10 and 10 ppm for Fe, Mg, Mn, Sr, Ba and Ce, respectively.

Because their concentrations in the standard were not known, the estimation of the ion yields for Na, Al, Si, Ba and Ce has been based on the periodic nature of the yield, relative to the calcium ion yield (Iy_{Ca}). The Na, Al and Si concentrations are therefore only approximate order-of-magnitude estimates. They were here utilized solely for comparative purposes, such as screening of samples with higher proportions of clay, chert or other non-carbonate inclusions. The utility of Na as a tracer is further complicated by the fact that sodium may be present not only in the carbonate but also

in the non-carbonate impurities (Veizer, 1983a), in interstitial positions, in crystal defects (making Na incorporation highly dependent on the rate of crystal growth; Mucci and Morse, 1990), and as a surface contaminant (this study). Ba and Ce concentrations hover around their detection limits (about 10 ppm), and the present results for these two elements are therefore meaningless. The calculated ion yields for the replicates of Na, Al, Si, Ba and Ce were not constant and the standard deviations for DIS were poor.

The Secondary Ion Mass Spectrometry technique employs a primary ion beam for bombardment of selected points. Ions liberated from this surface form the secondary ion beam that is accelerated in a mass spectrometer. The signal/background ratio of the spectrometer is very high, thus enabling exceptionally high sensitivity. The technique produces an open microcrater that allows verification of spot location in bands of diverse luminescence or in any other target. The spot diameter in a polished thin section is about 20 to 25 micrometres. This opens the microscale world to direct study without the laborious mechanical separation that is necessary for standard techniques such as the Atomic Absorption Spectrophotometry or Induced Coupled Plasma Mass Spectrometry. Furthermore, in contrast to electron microprobe, SIMS has considerably lower detection limits. The application of SIMS to diagenetic studies of carbonates is still in its infancy. As of this date, only three studies have been published (Veizer *et al.*, 1987; Mason, 1987; Swart, 1990). A wider application of the technique is hampered by the scarcity of available instruments and the high commercial costs, with a minimal charge of $300 per hour.

The main technical problem encountered in the ion microprobe studies is the mass interference. For example, for carbonates, $^{12}C^{16}O$, $^{40}Ca^{16}O$, $^{40}Ca^{14}N$, $^{28}Si^{16}O$, $^{28}Mg^{16}O$, $^{44}Ca_2$ and many other ionic complexes can interfere at mass peaks ^{28}Si, ^{56}Fe, ^{54}Fe, ^{44}Ca, ^{42}Ca and ^{88}Sr. Spectral stripping, high mass resolution and energy filtering are the three techniques that can potentially overcome the mass interference problem. The first technique corrects for contribution from the interfering molecular species. In this case, neighbouring peaks of the supposed interfering species are measured for different molecular complexes (Reed, 1989). This approach is time consuming and the identification of interfering species is not always definitive. The high mass resolution technique exploits small mass differences between a given isotope and the interfering molecular complex. Mass resolution is defined as the mass divided by peak width. The high mass resolution usually ranges between 2000 and 7000. This demands a narrowing of the spectrometer slits, which inevitably reduces the intensity of the signal, and thus diminishes the sensitivity of the technique (Reed, 1989). In addition, it is not always possible to attain the resolution that is necessary for separation of some ions, such as, for example, $^{16}O^{28}Mg$ and ^{44}Ca, or $^{44}Ca_2$ and ^{88}Sr. The third technique, energy filtering, is only attainable with instruments having an adequate design (eg. Nier design). Molecular complexes tend to dissociate at high energies whereas the atomic ions cover a much greater range of kinetic energy (Schimizu *et al.*, 1978). Collection of high energy ions therefore avoids interference of molecular complexes. Energy filtering is achieved either by moving the energy slit or by reducing the accelerating voltage of the secondary beam (voltage offset). Apparently, the only disadvantage of this technique is that it lowers the

intensity of the measured atomic beam. Preliminary experiments at the Grant Institute indicate the applicability of this technique for studies of trace elements in carbonates (Research Group, IMS, Grant Institute, 1989).

The ion yield relative to Ca (RIy) for a given element (Me) is calculated for the standard (st) according to the formula:

$$\frac{\left(\frac{Me\ counts/cycle/second}{Me\ (ppm)/atomic\ weight_{Me}}\right)}{\left(\frac{Ca\ counts/cycle/second}{Ca\ (ppm)/40.08}\right)} = \frac{Iy_{Me}}{Iy_{Ca}} = RIy_{Me\ st}$$

where the counts of the cations, Me and Ca, are normalized from isotopic to elemental abundances and where Iy represents the measured elemental yield.

Taking into account the isotope to element normalization and assuming that

$$RIy_{Me\ un} = RIy_{Me\ st}$$

the concentration in ppm of the element (Me) in the unknown (un) can be calculated as follows:

$$[Me_{(ppm)}] = \frac{Counts\ corrected_{Me\ un} \times Atomic\ Weight_{Me}}{Counts\ corrected_{Ca\ un} \times RIy_{Me\ st}}$$

Precision and Accuracy

The main constraint on the precision of the technique is the inhomogeneity of the standards which induces an error in the calculated ion yields. The elemental contents of Mg, Fe, Mn, and Sr, previously evaluated by AAS and ICP for the standard (DIS) were 723, 1033, 760 and 111 ppm, respectively. For comparison, the average values ($\pm$ 1 σ) for 17 SIMS analyses of the same standard were 780 $\pm$ 90, 960 $\pm$ 60, 780 $\pm$ 50 and 90 $\pm$ 5 ppm. ^{54}Fe in sample 115251-2 gave 460 counts for 100 seconds, wich constitutes the lowest count rate for all samples and elements. Even this number of counts yields an excellent counting error of 5% (100 x number of counts$^{-1/2}$).

4.2 STABILIZATION OF SHELF CARBONATES: GENERAL CONSIDERATIONS

Brand and Veizer (1980) proposed the now well-accepted model for trace element repartitioning in the process of diagenetic stabilization of carbonate components (fig. 4-1 a). Lohmann (1988) modelled the covariation patterns for oxygen and carbon isotopes during meteoric stabilization of marine carbonates under conditions of varying rock-water ratios (fig. 4-1 b). These models suggest that the $\delta^{18}O$, $\delta^{13}C$ and trace

elements compositions of recrystallized carbonates reflect diagenetic systems that tend to have low water-rock ratios; the systems are buffered by the marine precursors. The recrystallized marine phases and LMC cements produced in a meteoric environment have geochemical attributes that vary according to the site and time of (re)precipitation. Rock imprint on the geochemical attributes increases with distance from the recharge area, whereas, at a given site, it diminishes with time (fig. 4-1).

Meteoric stabilization is a relatively well documented diagenetic pathway for marine carbonates from the petrographic (James and Choquette, 1990; Sandberg, 1985) and geochemical points of view (e.g. Brand and Veizer, 1980, 1981; Veizer, 1983 a, b; Lohmann, 1988; Al-Aasm and Veizer, 1986 a, b). Meteoric dissolution-reprecipitation of carbonates is driven by the kinetics of the $CaCO_3$-CO_2-H_2O system, and is controlled mainly by the flux of meteoric waters and their level of undersaturation with respect to carbonate minerals. Carbonates can thus undergo micro- or macroscale dissolution that may result in anything from partial to total disruption of the primary features.

Under modern shelves, freshwater lenses can spread out as far as 100 kilometres away from the shore (e.g. Florida shelf: Manheim and Sayles, 1974). However, meteoric stabilization may not be the dominant or sole diagenetic pathway for marine cements throughout the entire Phanerozoic (Bathurst, 1975). Marine and shallow burial pathways are feasible alternatives and they have been addressed, for example, in Neugebauer (1974), Baker *et al.* (1982), Elderfield *et al.* (1982), Veizer (1983 a), Tucker (1985) and

Saller (1986). These studies point out that marine, burial and meteoric stabilizations can all result in comparable geochemical trends, although not necessarily of the same magnitudes. This has been well illustrated by Banner and Hanson (1990) in their mass balance modelling of simultaneous isotopic (C, O and Sr) and trace element (Nd, Sr and Mn) variations in recrystallized carbonates (fig. 4-2). Thus stabilization of shelf carbonates should not be regarded as an exclusive product of meteoric diagenesis.

The geochemical interpretation of diverse cement types relies heavily on the identification of signals from two end-members in the broad spectrum of depositional and diagenetic fluids, marine and meteoric waters. Evaluation of the approaches that enable estimates of these end-members will therefore be the first step in discussion of the geochemistry of the Sverdrup Basin cements.

4.2.1 Isotopic composition of past seawater or "waltzing with a ghost"

As a standard practice, marine signals for Paleozoic carbonates are derived from measurements on brachiopods or early marine cements. Brachiopods grew in marine waters, and their relatively stable LMC shells are believed to be a particularly suitable material for such purposes. However, the retained isotopic signals may vary considerably, depending on the degree of diagenetic alteration as well as on the depositional environment (basinal vs shelf; Brand, 1989 b). For paleoceanic studies, the best "preserved" portions of unaltered brachiopods are currently selected on the basis of petrography - particularly cathodoluminescent properties - and trace element chemistry

(Veizer *et al.*, 1986; Popp *et al.*, 1986; Brand, 1989 b). Brachiopods incorporate Sr without any isotopic fractionation, but some Paleozoic brachiopods may have incorporated fractionated carbon isotopes at the generic level (Veizer *et al.*, 1986). Similarly, some modern species secrete shells with $\delta^{13}C$ and $\delta^{18}O$ variations of ± 1 ‰ within and between specimens (Hiebert *et al.*, 1988).

A recent case study of Jurassic brachiopods from a section topped by a discordance, suggests that they may have had their chemical attributes reset by post-depositional exchange with meteoric waters, even though the brachiopods possess a uniform nonluminescent cathodoluminescence pattern (Rush and Chafetz, 1990). Similarly, Wadleigh and Veizer (1991) found that nonluminescent portions and whole shells of brachiopods gave more or less identical oxygen and carbon isotope values. Both studies therefore indicate that cathodoluminescence alone is not the definitive discriminant for selection of unaltered samples. This assertion, at least for biogenic carbonates, is confirmed by the study of Recent skeletal material by Barbin *et al.* (1991) that documents unequivocal luminescence in clearly unaltered modern shells (foraminifera, molluscs, coralline algae).

Utilization of marine cements as recorders of the isotopic composition of past sea water may help to overcome the biogenic fractionation problems. In general, marine cements grow on moderately deep shelves, and thus in relatively uniform marine environments. A problem, however, arises from the fact that these cements are

composed either of HMC or A, both metastable minerals that are highly susceptible to diagenetic alteration, and thus are almost invariably neomorphosed to dLMC. After neomorphism, the different isotope systematics will be variously affected, depending on the composition of diagenetic water, the water-rock ratio, the openness of the system and the extent to which equilibrium is attained during the transformation (Banner and Hanson, 1990). Rock buffering of their chemical budgets in diagenetic environments of early recrystallization enables sequestering of the original $^{13}C/^{12}C$ and $^{87}Sr/^{86}Sr$ into the successor phase. In contrast, unless cement recrystallization takes place very early and very rapidly, and/or in isotopically marine-like waters, the $\delta^{18}O$ can hardly be preserved. In order to do so, the solution-reprecipitation must be accomplished in a relatively closed-system and within a time interval of one to two hours (Veizer, 1983a; Land, 1989). In any case, ancient marine signals for oxygen and carbon isotopes are generally derived from cements displaying the highest delta-values. Given and Lohmann (1985) were able to obtain Permian (Guadalupian) seawater isotopic composition from isotopic covariation in former A and HMC marine cements. They found that the nonluminescent portions of recrystallized cements kept their original marine isotopic signal, whereas an increase in the proportion of luminescent calcite usually signified an increase in the degree of alteration as well.

In summary, both ancient brachiopods and early marine cements can only give what can be termed the "best estimates" for isotopic composition of ancient marine calcites. In theory, brachiopods appear to better retain the oxygen, and cements, the

carbon isotopic ratios. In the subsequent discussion, published data for coeval brachiopods will be utilized as an initial estimate for a $CaCO_3$ phase that would be precipitated in approximate equilibrium with the coeval seawater. The diagenetic signal of cements will then be considered relative to this reference composition. Finally, after discussion of the trends for cements, the topic of the isotopic composition of the coeval seawater will be reviewed from the point of view of both cements and brachiopod shells, and from the perspective of the present as well as published data.

4.2.2 Isotopic composition of past meteoric water

Isotopic differences between modern marine and meteoric tropical waters are estimated to be less than about 4 ‰ for oxygen, but due to the Rayleigh distillation process, the difference increases with latitude and altitude. In the case of carbon isotopes, the difference is highly variable due to the incorporation of soil-derived CO_2 into surface waters. This ^{12}C depleted signal is, however, quickly obliterated as meteoric waters interact with marine carbonates. Frequently, marine and meteoric precipitates may have comparable $\delta^{13}C$ signals (see "J" and "L" curve of Lohmann, 1988 and Al-Aasm and Veizer, 1986 b). A direct estimate of the attributes of meteoric water can perhaps be provided by coeval calcrete. This approach will be utilized in the present study. Waters that precipitate calcrete can, however, be up to 3 ‰ enriched in ^{18}O, due to surface evaporation. This enrichment is unlikely for carbonates precipitated from phreatic meteoric waters.

4.3 GEOCHEMICAL ATTRIBUTES OF CEMENT CATEGORIES

This section discusses the general geochemical characteristics for cement types that have been established by petrography. It deals with geochemical trends that relate directly to the nature of the cements. Attributes inherited from secular variations in seawater composition, from local hydrologic systems, and from other related phenomena will be discussed in the subsequent Chapter 5.

Despite considerable overlap, the comparative plots of tracers indicate that the main petrographic categories of cements have distinctive geochemical attributes (fig 4-3 and 4-4). These plots include all results, regardless of their CL patterns (for neomorphic cements), age, or position within the basin.

For trace elements, the notable feature is the Sr content in excess of 1000 ppm for botryoidal calcite (fig. 4-3 b) of presumed original aragonitic mineralogy. The remaining cements have mean Sr contents of about 250 ppm. The Mg contents of the recrystallized marine cements are slightly higher than those of the burial (L2) and meteoric ones (fig. 4-3 a). In contrast, except for the botryoidal calcite, the Mn and Fe concentrations seem to increase slightly with the level of burial.

However, the most notable overall feature is the depletion in ^{18}O and ^{13}C, and enrichment in ^{87}Sr, from early marine to late (L1), to burial cements *stricto sensu* (L2),

and finally to meteoric cements. Most, if not all, of these geochemical trends are compatible with the theoretical considerations of the behaviour of trace elements and isotopes during diagenesis (e.g. Veizer, 1983 a, b). Their details will be explored in the subsequent text.

4.4 EARLY MARINE CEMENTS - NEOMORPHIC CEMENTS

4.4.1 Botryoidal Calcite - Calcitized Aragonite

Factor analysis (table 4-1 a) for botryoidal calcite, although based on only ten samples, suggests that a single factor controls the entire trace element distribution pattern. This factor, with negative loading for Sr and positive for Fe, Mn and Mg, can be interpreted as diagenetic stabilization of the original aragonitic cements. The higher the water/rock ratio, the more pronounced are the gains in Fe, Mn and Mg, and the depletion in Sr. The trend (fig. 4-5 a) mimics entirely the theoretical pattern given in figure 4-1 a.

Neomorphic cements texturally recognized as calcitized aragonite have the highest observed Sr concentrations, although the overall spread is considerable (400 to 3300 ppm; fig 4-3 b). Davies (1977) reported spot values as high as 10000 ppm in botryoids of the same age and location (Moscovian, Sverdrup Basin). These high Sr

values are in accordance with petrographic evidence that the cement represents neomorphic calcitization of a Sr-rich precursor, such as botryoidal aragonite.

The above diagenetic trend can be documented not only statistically, but also directly on traverses in thin sections. For example, the nonluminescent irregular calcitized aragonite (AIR pattern; points 8 and 9) in figure 4-6 contains the highest Sr and low Mg contents as well as the least radiogenic Sr isotopic signal (see Appendix). The adjacent isopachous calcite (HM3 pattern; points 5 and 6), a former HMC, has the opposite attributes with high Mg and low Sr contents. This partitioning is in accord with the trends expected from stabilization of A and HMC in partially closed systems. In contrast to calcitized aragonite in figure 4-6, the example in figure 4-7 shows much more pronounced textural disruption. The microcrystals (points 1 and 2) are juxtaposed with a void pattern (points 4, 5, 6, and 7). These patterns are likely a result of diagenetic stabilization in a system with a higher W/R than the one in figure 4-6. As a result, the phantom needles (points 1 and 2) have higher Mg and lower Sr contents than aragonites in figure 4-6. The Mg and Sr concentrations are comparable to the free-grown calcite of the voids (points 4, 5, 6 and 7). The *in situ* replaced aragonite differs from the void calcite only in its higher Fe content.

In terms of stable isotopes, most botryoidal calcites follow a trend of invariant $\delta^{13}C$ accompanied by ^{18}O depletion (figure 4-5 b). The $\delta^{18}O$ varies from about -1 ‰, typical of the Moscovian marine carbonates, to about -8 ‰. Such a trend is characteristic of

stabilization in the presence of (1) progressively warmer saline (marine or brine) waters and/or (2) meteoric waters within carbonate buffered aquifers. These two possibilities for calcitization of the original A will be discussed, together with the recrystallized HMC, in the next section.

4.4.2 Isopachous Calcite - Recrystallized High Magnesium Calcite

Spot analyses of marine isopachous calcite range from 1000 to 7300 ppm, and 100 to 680 ppm, for Mg and Sr, respectively. These calcites are therefore enriched in Mg and impoverished in Sr, if compared to calcitized aragonite (fig. 4-3 b); in accord with the proposed HMC nature of their precursors (see section 3.2.2).

Factor analysis of all isopachous cements reveals that two factors control their chemical and isotopic composition (table 4-1 b). Factor 1, that explains 57 % of the total variation, may represent diagenetic loss of Mg and Sr, because their partition coefficients are less than one (fig. 4-8 a, b). The most impoverished samples have also the most radiogenic $^{87}Sr/^{86}Sr$ (see Appendix). However, the positive loading of Fe on this factor is surprising and at odds with the post-depositional repartitioning theory. It appears that this factor reflects, at least in part, regional overprint. The samples high Fe and Mg, samples are all confined to the Moscovian section 11 in the northeastern part of the basin (sequence 2 - east; see chapter 5). With these samples separated into a distinct population, the Fe and Mg distribution pattern would follow the predicted theoretical repartioning (fig. 4-8 a).

Factor 2, accounting for 29 % of the total variation, has positive loadings of $\delta^{18}O$, $\delta^{13}C$ and Mn and is clearly controlled by a population of the later-discussed carbonates of hydrothermal origin that are depleted in ^{18}O, ^{13}C and Mn (chapter 5). This factor is thus a reflection of the mixing of two populations of HMC cements.

On a scatterplot of Sr and Mn data, the isopachous early marine cements are depleted in Sr and somewhat enriched in Mn if compared to their theoretical marine precursors (fig. 4-8 b). Despite the fact that the overall diagenetic trends are overprinted by regional phenomena, the predicted pattern for stabilized HMC is still discernible.

During recrystallization of partly lithified, mixed aragonitic-calcitic marine sediments, theory and observation indicate that trace element repartitioning in the presence of marine waters can result in comparable trends to those imposed by meteoric diagenesis (Baker *et al.*, 1982; Veizer, 1983 a; Brand and Veizer, 1980; Lohmann, 1988; Banner and Hanson, 1990; Morse and Mackenzie, 1990; Hesse, 1990). In a meteoric system, near recharge areas, the produced dLMC (primary LMC as well) will have, for instance, a Sr/Ca ratio much lower than the original phase; the departure from the original ratio depends on W/R, the composition of the water, and the distribution coefficient (D). The latter being lower than unity, the system will build up the Sr/Ca ratio towards the discharge area (fig. 4-1 a). According to D, W/R, $Sr/Ca_{calcite}$ and Sr/Ca_{water} estimated by Veizer (1983 a), theoretical Sr-contents would be around 150 ppm upflow, and up to many hundreds of ppm down flow. The importance of the up to down

flow gradient depends strongly on the rate of flow relative to reaction rate. Similarly, within the present-day deep-sea sediment column, carbonates stabilized by marine water have strontium concentrations ranging from 200 to 800 ppm (Baker *et al.*, 1982; Hesse, 1990). A precondition for generation of such a trend is that the system must be rock-dominated (have low W/R). In deep-sea sediments, this condition is maintained by the fact that compaction-induced flow is sluggish relative to aqueous diffusion of trace elements towards the surface; partition coefficients therefore dominate the system. In theory, this could lead to buildup/depletion of a trace-element concentration down-flow and, ultimately, to a successor phase that is identical chemically with the precursor (cf. Veizer 1983 a). Yet, in systems where the rate of recrystallization approaches the rate of diffusion, and where the rate of flow is somewhat faster (but not as fast as to dissipate the generated localized gradients), neomorphism may lead to repartitioning of trace elements without their appreciable buildup/depletion in pore waters. At the top of the sediment column, the diffusion may even totally counteract the D-induced gradient and the produced calcites will show very low Sr-contents. In modern deep-sea deposits, this is the case for the uppermost 150 metres of sediments that are in direct communication with the overlying seawater (cf Baker *et al.*, 1982). Overall, both systems, meteoric and marine phreatic (shallow burial), can theoretically produce the elemental trends shown in figure 4-8.

The bulk of original HMC cements have oxygen and carbon isotopic signatures similar to their theoretical marine precursors (fig. 4-9 a). The samples that plot outside

the "marine" box are almost all from section 37 (sequence 2 - west). These samples are slightly depleted in ^{13}C, heavily depleted in ^{18}O ($\delta^{18}O$ relative to PDB mostly lighter than -7 ‰), have moderately radiogenic $^{87}Sr/^{86}Sr$ (fig. 4-9) and, in terms of their trace elements, they plot in the low Mn, Fe and Mg range of the spectrum (fig. 4-8). As discussed later (chapter 5), these properties can be attributed to stabilization of HMC in warm waters, probably of hydrothermal origin.

Leaving aside the ^{18}O-depleted population, the remainder of originally HMC cements shows gains in Mn and Fe, ^{18}O-depletion of up to -8 ‰ that is accompanied by only slight ^{13}C-depletion, and by a marked ^{87}Sr gain (4-9 a and trend 1 on 4-9 b). At first glance, the combination of these attributes with the trace-element results (an order of magnitude loss of Sr and Mg) argues for a diagenetic system influenced by meteoric waters. Qualitatively, this model could explain the signs of geochemical signals as well as the signatures in the most ^{18}O-depleted part of that population. Yet, such heavily "shifted" samples are not typical of the bulk of the cements. Quantitatively, a paradox arises from the requirement that the order of magnitude losses/gains of trace elements and the incorporation of ^{87}Sr can be accomplished only in a partially open system that enables their transport from/to recrystallization sites. In contrast, the preservation of near-original carbon, and particularly oxygen, isotope ratios requires a relatively closed recrystallization system. This paradox could be reconciled if the recrystallization of most original early marine cements was accomplished in a phreatic zone with essentially marine-derived pore waters. Moreover, the covariation of $\delta^{18}O$ and $^{87}Sr/^{86}Sr$ for trend "1"

is characterized by large gains in ^{87}Sr without significant ^{18}O depletion (fig. 4-9 b). In recrystallizing carbonates, oxygen isotopes attain equilibrium with diagenetic waters at W/R three orders of magnitude lower than strontium isotopes. This argues against recrystallization in a meteoric system, because at W/R necessary to reset Sr isotopes, oxygen isotopes would have to be reset as well. Unless the diagenetic waters were saline - had high concentrations of Sr - the strontium isotopic ratios in the water would have been buffered by the reacting carbonates. At intermediate W/R (fig. 4-2 b), shallow burial waters with radiogenic $^{87}Sr/^{86}Sr$ and low Sr/Ca could have greatly lowered the actual Sr-concentrations of the dLMC without affecting the $\delta^{13}C$-$\delta^{18}O$ marine signal. Thus, the nature of the system responsible for recrystallization of most of the early cements can tentatively be interpreted as water-rock interaction in marine-derived (shallow burial) waters enriched in radiogenic Sr. Such an interpretation is also supported by the fact that most early marine cements originate from mud mounds which, in many cases, have been buried rather than subaerially exposed.

4.4.3 Modes of recrystallization: perspective from chemical data

A typical feature that emerges from the microanalytical approach is the pronounced microscale heterogeneity of Mg in recrystallized HMC and of Mg, Sr and Fe in calcitized aragonite, even for samples showing identical CL patterns (see Appendix). Such heterogeneous distribution could only result from microscale recrystallization that has been controlled by local equilibria (bulk solution disequilibrium system of Veizer, 1978). The complex succession of CL patterns in neomorphic cements

could possibly be a result of progressive or multiple recrystallizations of the metastable phases (see the progression from AIR to AMY to AVO, and from HM1 and HM2 to HM4; figs. 2-3 a, b, c, 2-4 b, e and figs. 2-8 d, 2-9 a, respectively).

In this study, no clear cut relationship has been observed between CL patterns (degree of textural disruption) and C and O isotope systematics. Contrary to expectations, many nonluminescent, well preserved isopachous calcites possess ^{18}O and ^{13}C depleted isotopic signatures, whereas some poorly preserved calcites that have dull or "composite" luminescence are not isotopically depleted (table 4-2). For calcitized aragonite (the statistical coverage is not as good as for HMC calcites) , the best preserved patterns (AIR) gave -7.2 to -0.4 and 6.7 to 7.9 ‰ for $\delta^{18}O$ (PDB) and $\delta^{13}C$, respectively. The poorly preserved ones gave similar ranges of -7.8 to -3.0 and 5.7 to 7.0 ‰. The observed lack of correlation between CL and isotopic signatures is in agreement with conclusions reached from studies of brachiopod textures by Rush and Chafetz (1990) and Wadleigh and Veizer (1991), and with the views expressed by Machel and Burton (1991) and Machel *et al.* (1991), but contrasts with the results of Given and Lohmann (1985) from the Permian El Capitan reef complex of Texas. The last mentioned authors observed that uniformly nonluminescent secondary calcites had the best preserved "marine" isotopic values and that the departure from the original isotopic signal was a direct function of the proportion of luminescent calcite in the sample. Apparently, the early cements from the Upper El Capitan reef are texturally less complex than those from the Sverdrup Basin. The latter show fine and coarse as well

as nonluminescent, luminescent and dull zones coexisting in a complex fashion. This may suggest that diagenetic processes in the two suites of rock differed. Note, however, that the Texan cements were interpreted as dLMC produced in a meteoric closed system. In contrast, most of the Arctic cements are interpreted as hydrothermal and burial-marine neomorphic products (see below). The relationships between textural and geochemical attributes can be particularly complicated if hydrothermal fluids are involved in the neomorphic process (see chapter 5, sequence 2). The partitioning of trace elements, in contrast to O isotopes, is not very sensitive to temperature. Marine cements affected by hydrothermal neomorphism can therefore have textures and chemistry that are similar to "normal" marine cements, but yet have strikingly different $\delta^{18}O$ values.

In summary, the geological, petrological and geochemical data are consistent with the proposition that recrystallization of the early marine (A, HMC) cements to diagenetic calcite has been generally accomplished in pore waters of marine derivation. It must be kept in mind, however, that this statement represents a generalization of a complex natural situation further discussed in chapter 5.

4.5 METEORIC AND LATE CEMENTS - PRIMARY LMC CEMENTS

4.5.1 Meteoric cements

Based on petrographic criteria, meteoric LMC cements have been recognized in carbonates from calcretes, and from the inner and outer shelf (sections 40 and 42; base of 2; top of 2, 3, 4, 35 and 37), respectively. Calcrete cements (mainly MT1) are the product of pure meteoric systems. In contrast, the presumed meteoric cements within marine carbonate sequences (MT1 and MT2) may also inherit marine attributes to a degree that depends on the W/R and/or the distance from the soil-zone at the time of precipitation. Because of the differing origins for calcrete- and for "meteoric" cements from marine carbonates, the factor analysis of the combined population yields composite factors that will serve only as orientation criteria for further discussion (table 4-1 c).

The initial discriminant criteria for the calcrete- and shelf-hosted populations of cements are based on isotope data. In the $\delta^{18}O/\delta^{13}C$ space, these sub-populations plot in dissimilar fields (fig. 4-10 a). The undisputed meteoric cements from calcrete (including MT3) have light $\delta^{18}O$ of about -8.5 ± 1 ‰. This might in part reflect the isotopic composition of the coeval meteoric waters, since increased temperature - due to the surficial origin of these cements - is an unlikely cause. Due to evaporation, the $\delta^{18}O$ could possibly have been increased by 3 ‰ (Lohmann, 1988), giving an approximate minimal value of -11.5 ‰ for the phases precipitated without evaporation effect (fig. 4-10 a). The calcrete cements are also depleted, by some 10 ‰ in ^{13}C, if compared

to the MT2 (and MT1) cements from the shelf sections ("marine facies" in figs. 4-10 a and 4-11 a). This suggests that in the calcrete horizons, the bicarbonate budget has been strongly influenced by soil-derived CO_2. In contrast, the disputed "meteoric" MT2 cements (see 3.3.1) plot on a tangent between the theoretical marine and meteoric end-members in terms of their oxygen, but show a constant marine carbon signal (fig. 4-10 a). The lowest $\delta^{18}O$-values correspond to the theoretical meteoric end-member (about -11.5 ‰) as estimated from the calcrete cements. Sr isotope data for the MT2 cements from section 35 are also consistent with the above interpretation (fig. 4-10 b). The latter cements and those from calcrete profiles contain variable, but mostly radiogenic, values that could reflect the meteoric component. Thus, the MT2 cements from section 35 indeed are a likely product of a meteoric aquifer with its dissolved bicarbonate budget in a phreatic zone buffered by the enclosing host rocks.

The MT2 cements from sections 3 and 4 are not as highly radiogenic, but their $^{87}Sr/^{86}Sr$ are still higher than those of the coeval marine calcites. If one accepts that the cements in calcrete and the MT2 cements in section 35 approximate the composition of calcites that precipitated in equilibrium with local meteoric waters, then the MT2 cements from the basinward sections 3 and 4, if related to meteoric waters, must have formed from solutions that tended towards the marine end-member of a meteoric-marine spectrum (fig. 4-10); they would be a likely product of a mixed meteoric-marine phreatic zone. The meteoric component dominated in section 35, whereas the marine one prevailed in the outer shelf sections 3 and 4; in accord with their geological setting

(cf. 3.3.1). It is entirely possible that precipitation of MT2 cements proceeded concurrently with, or at burial depths only marginally deeper than depth of recrystallization of the early marine cements. This would explain the somewhat comparable trace element chemistry of the MT2 and the early marine cements (figs. 4-11, 4-8, 4-5). On the other hand, evolved marine waters in interaction with recrystallizing marine carbonates could also explain the obtained signal. Pure meteoric waters could not have imprinted the $^{87}Sr/^{86}Sr$ without totally dominating the $\delta^{18}O$ signal. Such a trend is not observed, so the Sr was not entirely derived from reacting marine carbonates. It was either (1) partly contributed by saline waters (evolved marine or diluted brines in burial environment) or (2) by meteoric waters in a high W/R marine-meteoric mixed system.

Based on paleomagnetic reconstructions, the Sverdrup Basin in the Early Permian was at latitudes of 30 ± 5°N (reference in Beauchamp, 1987). At such latitudes, the $\delta^{18}O$ of meteoric waters is usually less than 4 ± 2 ‰ depleted, relative to the coeval marine waters (Anderson and Arthur, 1983). It is therefore puzzling that the inferred pure meteoric signal in cements is as much as 9 ‰ lower than the coeval sea signal (≈ -2 ‰). Perhaps this discrepancy can be partly attributed to the 10 to 25°C higher temperatures of the surficial meteoric cements, compared to the relatively deep water milieu of mud mounds (30 to 40°C). Another alternative is that the signal indicates that the basin was possibly at higher latitudes than suggested by paleomagnetic studies (around 45°N instead of 30°; Beauchamp, 1987). It may be argued that the postulated very light meteoric

waters are only a localized phenomenon, but Scholle *et al.* (1991) obtained similar values for Permian meteoric cements from Greenland (Jameson Land Basin; theoretical paleolatitude of 35°N).

Only a few chemical results are available for MT1 cements from sections 2 and 9, due to their occurrence as thin layers that are very difficult to sample (Appendix). They seem to resemble the data of the MT2 cements in the outer shelf sections, with similar consequences for interpretation of their mode of origin.

4.5.2 Late cements

The genetic classification of cements as "burial" is not a straightforward task. In some cases, petrographic observation undeniably points to a burial origin (association with stylolites, compactional breakage, inclusions of bitumen, etc.). In others, however, no clear criteria for meteoric or burial origin exist. CL patterns can be misleading if interpreted in terms of the redox potential (see chapter 6). Geochemical results can be puzzling as well, because meteoric and burial waters can precipitate cements with similar isotopic attributes (Tucker, 1990; Choquette and James, 1990). Deciphering the nature of late parent waters and their origin can thus be a complex question. In this study, many cements were cautiously grouped under the "late cement" banner. This designation is based on the relative timing of precipitation and on the contrasting habits of the late crystals (inclusion-free, coarse xenotopic calcite vs elongate inclusion-rich marine products).

Factor analysis of the L1 group shows only small communality for all trace elements; these cements have therefore been grouped together with the L2 cements. Two factors explain the variation of chemical and isotopic attributes for the late cements (table 4-1 d). Factor 1, an inverse correlation between Mg-Fe-Mn and C-O isotopes, can be interpreted, at this stage of the discussion, as the result of progressive burial. With increasing depth, and progressive interaction with surrounding rocks, the formation waters become warmer (^{16}O depletion by temperature fractionation), they contain a higher proportion of ^{12}C (thermal cracking of hydrocarbons), and also higher concentrations of Fe, Mn (and Mg) liberated from shaly sequences in the basin. Factor 2, with positive loadings of Mn and $\delta^{18}O$ is enigmatic, but because of the weak loadings and the relatively small impact on the total variation, this uncertainty probably is not significant. Note also that the entire population is dominated by L2 cements, and the statistics therefore relate mostly to this category.

Carbon and oxygen isotopes follow a trend from typical marine values towards increasing depletions for the heavier isotopes (fig. 4-12 a). The observed general depletion are from +6 to +4 ‰ for carbon and from -3 to -12 ‰ for oxygen. The large shift for oxygen isotopes, as opposed to the relatively small one for carbon, could reflect precipitation from relatively cold shallow burial waters for the heavy cements and from progressively warmer burial waters for the lighter ones. The $\delta^{13}C$ comparable to marine ratios might have been buffered by the enclosing rocks or derived from fluids with a carbon signal close to the marine one (see the next chapter for modified regional trends).

In the $\delta^{18}O$-$^{87}Sr/^{86}Sr$ diagram, the strontium isotope ratios range from typically marine to more radiogenic (fig. 4-12 b). Different portions of the basin appear to have differing pathways. The basinward sections 10 and 11 (sequence 2-east) are characterized at first by large gains in ^{87}Sr, with ^{18}O depletion becoming pronounced only for samples with highly radiogenic Sr (trend 1; see also fig. 4-8). The landward sections 28, 27 and 9 define the opposite envelope (trend 2) of rapidly decreasing ^{18}O content, and only slight ^{87}Sr enrichment. Finally, the results for sections 2, 3, 9.5 and 37 define an intermediate trend (3) with more or less equal changes in oxygen and strontium isotopes. For the trend (2), the strontium isotope values are typically marine, confirming that the source of Sr has been the enclosing carbonates. In contrast, diagenetic waters in the outer shelf sections (trend 1) likely inherited their radiogenic component from solutions (burial waters?) that traversed the shaly basinal lithologies (cf. fig. 2-3); the concentration of Sr in freshwater is so low that a very high W/R is required to imprint the $^{87}Sr/^{86}Sr$. Such conditions did not prevail according to the $\delta^{18}O$ signal. The temperature-induced fractionation in the burial environment likely decreased the $\delta^{18}O$ at the ends of the three profiles, producing calcites that are, in some cases, more depleted in ^{18}O than the presumed meteoric cements in calcrete (fig. 4-12 a).

A similar picture emerges from consideration of covariation of isotopes and trace elements. The plot of $\delta^{18}O$ vs Fe contents (fig. 4-13 b) shows comparable fan-shaped dispersal from near-marine values towards depletion in ^{18}O and enrichment in Fe (or Mn, Mg) (table 4-1 d). Thus, increasing burial - causing higher temperatures and lower Eh -

produces progressively more ferroan cements. As for Sr isotopes, outer shelf sections show Fe gains at relatively small changes in $\delta^{18}O$. At the other end of the spectrum, the inner shelf sections show a large ^{18}O depletion (trend 1) accompanied by smaller gains in Fe (trends 2 and 3). A comparable picture emerges also from consideration of Sr/Mn data (fig. 4-13 a), although the basinward progression of sections is not as clear as in the plot of trace elements vs oxygen isotopes. All this could be interpreted as a result of higher salinity brines in basinward sections.

In summary, it seems that the late cementation was possibly the product of three diagenetic systems, resulting from the paleogeographic position of a given section with a deepening shelf profile.

4.6 CATEGORIES OF CALCITE CEMENTS - DISCUSSION

Petrography alone can help to decipher the origin of the broad categories of cements, such as marine versus non-marine or neomorphic versus primary. For the latter, it can sometimes also help to establish whether they are meteoric or burial. The geochemistry becomes important as a subsequent step, when one attempts to (a) discuss the nature of the fluids that altered the metastable marine cements, and (b) categorize the origin of some primary cements.

The geochemical characteristics of the different petrographic types of cements are collated in figures 4-14 and 4-15. The "A" and "H" fields, denoting early marine cements, overlap considerably with the fields for the late, primary calcitic cements (L). This is to be expected to some extent, but if one takes into account the composite nature of these populations in terms of their age and sample locations, the overlap still suggests that recrystallization of A and HCM and precipitation of late calcitic cements proceeded in part simultaneously and in the same diagenetic environments.

Considering first the O/C isotope systematics (fig. 4-14 a), all cements - apart from the MT1 from calcretes - fall within a broad trend, with a large depletion in ^{18}O and a less pronounced decrease in $\delta^{13}C$. In general terms, therefore, the entire population has been formed in an aqueous system that has been rock buffered - had relatively low W/R - with respect to C isotopes. The overall ^{18}O depletion of ~ 14 ‰ can, theoretically, result from increasing proportions of meteoric waters in the diagenetic system, from increasing temperature, or from their combined effect. In the first case, the meteoric end-member would have to be very light; a proposition consistent with the -8 to -11 ‰ values encountered in the meteoric cements (fields C and S). Nevertheless, such large ^{18}O depletions in meteoric waters are not typical of tropical to subtropical hydrologic systems. Ground and surface waters at low latitudes today are usually only 4 ± 2 ‰ depleted in $\delta^{18}O$ relative to seawater (Anderson and Arthur, 1983). Such hydrologic systems, meteoric phreatic to mixed meteoric-marine phreatic, can therefore account for some shift in the observed O/C isotope signal, but they are not responsible for the severely

$\delta^{18}O$ depleted tail. The latter must be a result of increased temperature of diagenetic waters due to progressive burial. This progressive burial and evolution of diagenetic waters is also responsible for the progressively more radiogenic nature of the Sr isotope signal (fig. 4-14 b).

The temperature increase, necessary to explain the entire ^{18}O depletion, is some 10 - 60°C for waters of the meteoric to marine spectrum. With geothermal gradients typical for a rift (60°C km^{-1}) such as the Sverdrup Basin (Beauchamp, 1987) the required burial depth would be about 200 to 1000 m.

The Sr/Mn diagram (fig. 4-15 a) shows that the early cements are strongly depleted in Sr relative to their marine precursors. The recrystallization of marine cements, originally of A and HMC mineralogy, results in dLMC that in terms of trace elements is chemically comparable to the late calcites. The neomorphism must have been accomplished in partially closed systems (low to intermediate W/R) in order to retain some gradient in Sr content between the original A and HMC. With increasing W/R, marine and late cements chemically approach equilibrium with theoretical meteoric or saline waters or both (fig. 4-15). However, each category of cements can be subdivided according to geochemical trends that are specific to paleogeographic settings. These regional diagenetic trends will be discussed in detail in the next chapter.

GEOCHEMICAL MODELS FOR RECRYSTALLIZATION BY METEORIC WATERS

Figure 4-1

Geochemical repartioning during recrystallization of marine carbonates by meteoric waters.

a) Model for diagenetic trace element repartioning proposed by Brand and Veizer (1980). Modified after Lohmann (1988). Boxes represent aragonite (A), high-magnesian calcite (HMC) and low magnesian calcite (L) precursors. Similar trends would be obtained if the carbonates were recrystallized by marine waters.

b) Model for carbon and oxygen isotope covariation. Modified after Lohmann (1988). The circled "R" represents the range of values of the reacting carbonate precursor. Modern calcites can have variable $\delta^{13}C$ and $\delta^{18}O$ values, depending on their distance from the soil-zone and on the intensity of surface evaporation.

In both schemes, letters and numbers represent relative precipitation in time and space. A rock dominated environment can be produced down-stream from the recharge area - or, at a given site - "early" in the history of the diagenetic system.

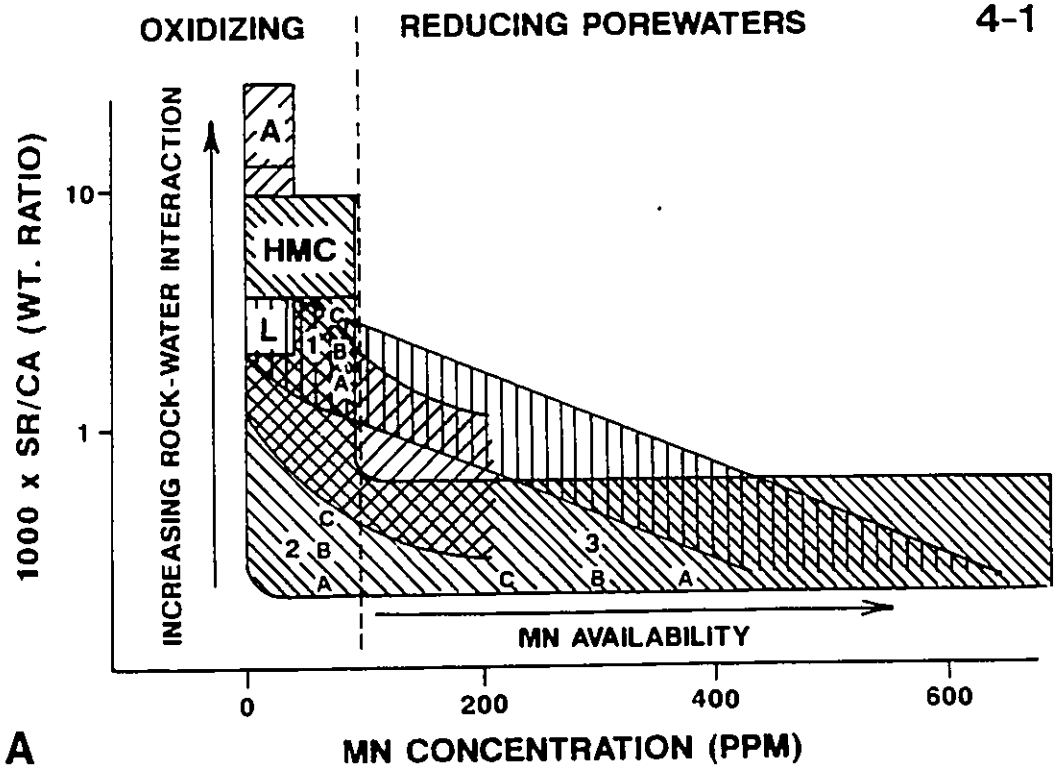
OXIDIZING
REDUCING POREWATERS
1000 x SR/CA (WT. RATIO)
10
1
INCREASING ROCK-WATER INTERACTION
A
HMC
L
1
C
B
A
2
C
B
A
3
C
B
A
MN AVAILABILITY
0
200
400
600
MN CONCENTRATION (PPM)

A

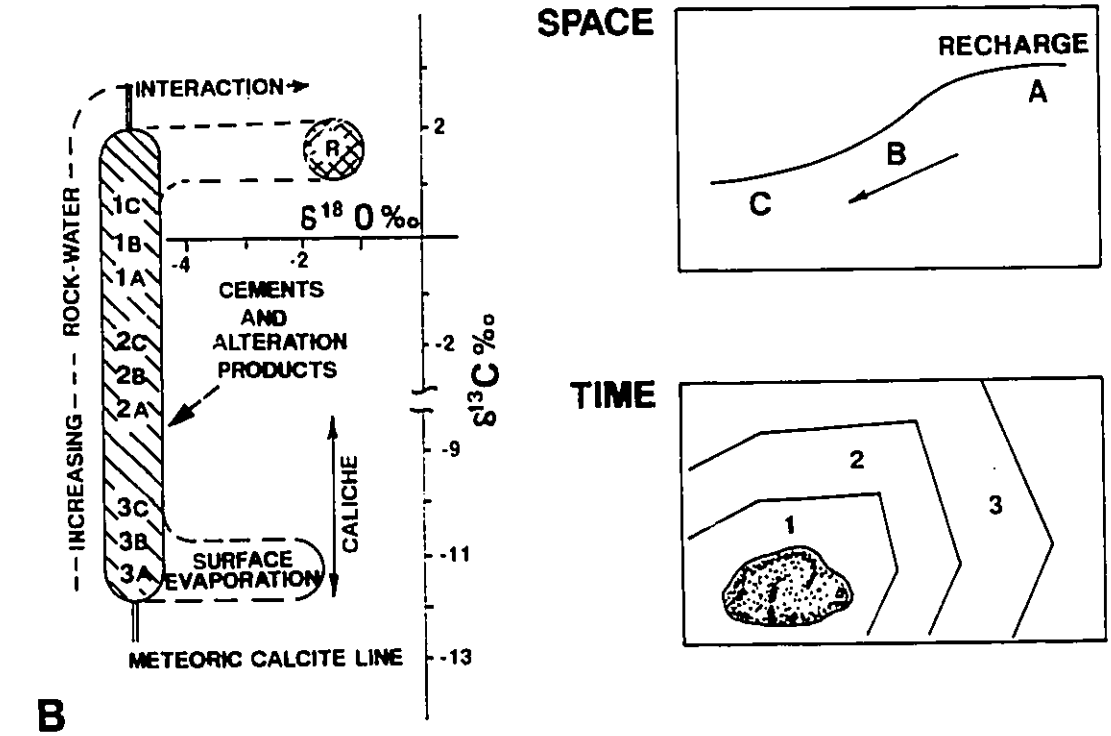
INTERACTION
ROCK-WATER
INCREASING
R
1C
1B
1A
2C
2B
2A
3C
3B
3A
δ18 O‰
-4
-2
CEMENTS
AND
ALTERATION
PRODUCTS
SURFACE
EVAPORATION
CALICHE
METEORIC CALCITE LINE
2
-2
-9
-11
-13
δ13C‰
SPACE
RECHARGE
A
B
C
TIME
1
2
3

B

ISOTOPIC COVARIATIONS BY MASS BALANCE MODELLING

Figure 4-2

a) Covariation of $\delta^{13}C$ and $\delta^{18}O$, predicted by models that simulate sequential *water-rock interaction* (W/R) or mixing of *seawater and freshwater* in a diagenetic system. Freshwater has a $\delta^{18}O$ value of -1 ‰ (SMOW) and a $\delta^{13}C$ value of - 5 ‰ (PDB). For the mixing curve, the total dissolved carbon (TDC) was assumed to be four times that of seawater. The reacting carbonate rock was given a $\delta^{18}O$-value of 2 ‰ and a $\delta^{13}C$ value of 4 ‰ (PDB) assumed temperature was 23°C. N: W/R. Modified after Hanson and Banner (1990).

b) Evolution of $\delta^{18}O$-$^{87}Sr/^{86}Sr$ covariation in a model of water-rock interaction. Initial rock has $\delta^{18}O$ of 1.5 ‰ (PDB), $^{87}Sr/^{86}Sr$ of 0.7076, and Sr-content of 300 ppm. On the freshwater profile, water is assumed to have 0.6 ppm of Sr, 30 ppm of Ca, $^{87}Sr/^{86}Sr$ of 0.7095, and $\delta^{18}O$ of -1 ‰ (SMOW). The two other curves are based on the same Sr/Ca, $\delta^{18}O$ and $^{87}Sr/^{86}Sr$ for freshwater, but the dilute brine contains 90 ppm of Sr and 4500 ppm of Ca, whereas the saline brine has 1200 ppm of Sr and 60000 ppm of Ca. In all cases, the temperature of the reaction was 40°C. In order to produce measurable change in $^{87}Sr/^{86}Sr$ of the stabilizing rock at low W/R, the diagenetic fluid must be saline. Modified after Hanson and Banner (1990).

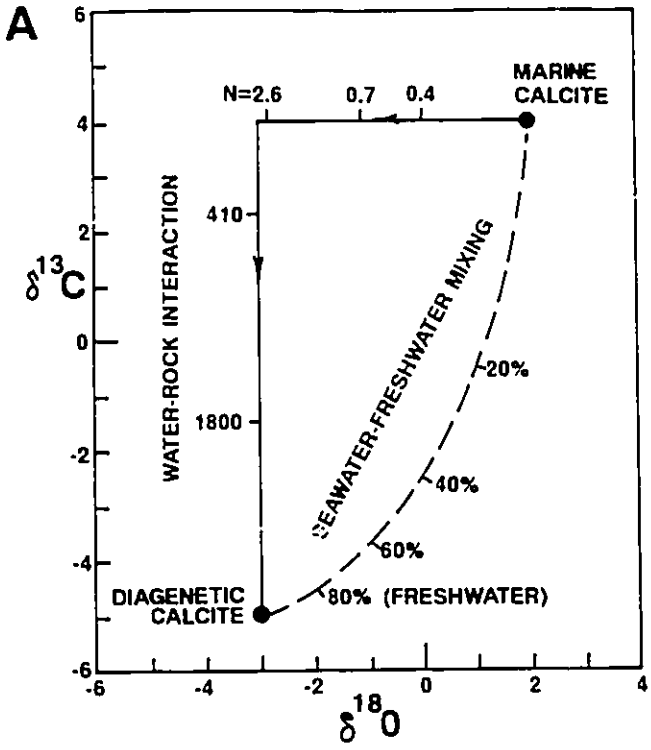
A
MARINE CALCITE
N=2.6
0.7
0.4
410
1800
WATER-ROCK INTERACTION
SEAWATER-FRESHWATER MIXING
20%
40%
60%
80% (FRESHWATER)
DIAGENETIC CALCITE
δ13C
δ18O

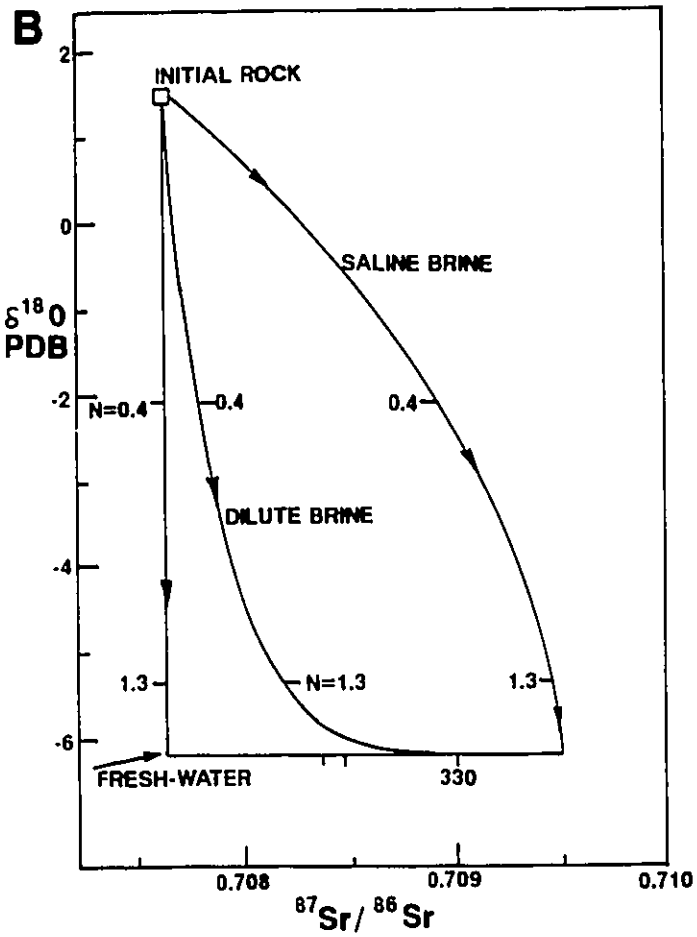
B
INITIAL ROCK
SALINE BRINE
DILUTE BRINE
N=0.4
0.4
0.4
1.3
N=1.3
1.3
FRESH-WATER
330
δ18O PDB
87Sr/86Sr
0.708
0.709
0.710

4-2

STATISTICAL SUMMARY PLOTS - TRACE ELEMENTS

Figure 4-3

a) Mg contents for categories of cements indicated in the legend. The highest and lowest black squares represent the highest and the lowest values, respectively. The center black square is the geometric mean of the population. The empty rectangles represent standard deviations (geometric mean $\pm$ 1σ). Recrystallized HMC and calcitized A are early marine cements, L1 and L2 are late (burial?) cements, and the meteoric cements include cements of the MT2 type.

b) The same for Sr contents.

c) The same for Fe contents.

d) The same for Mn contents.

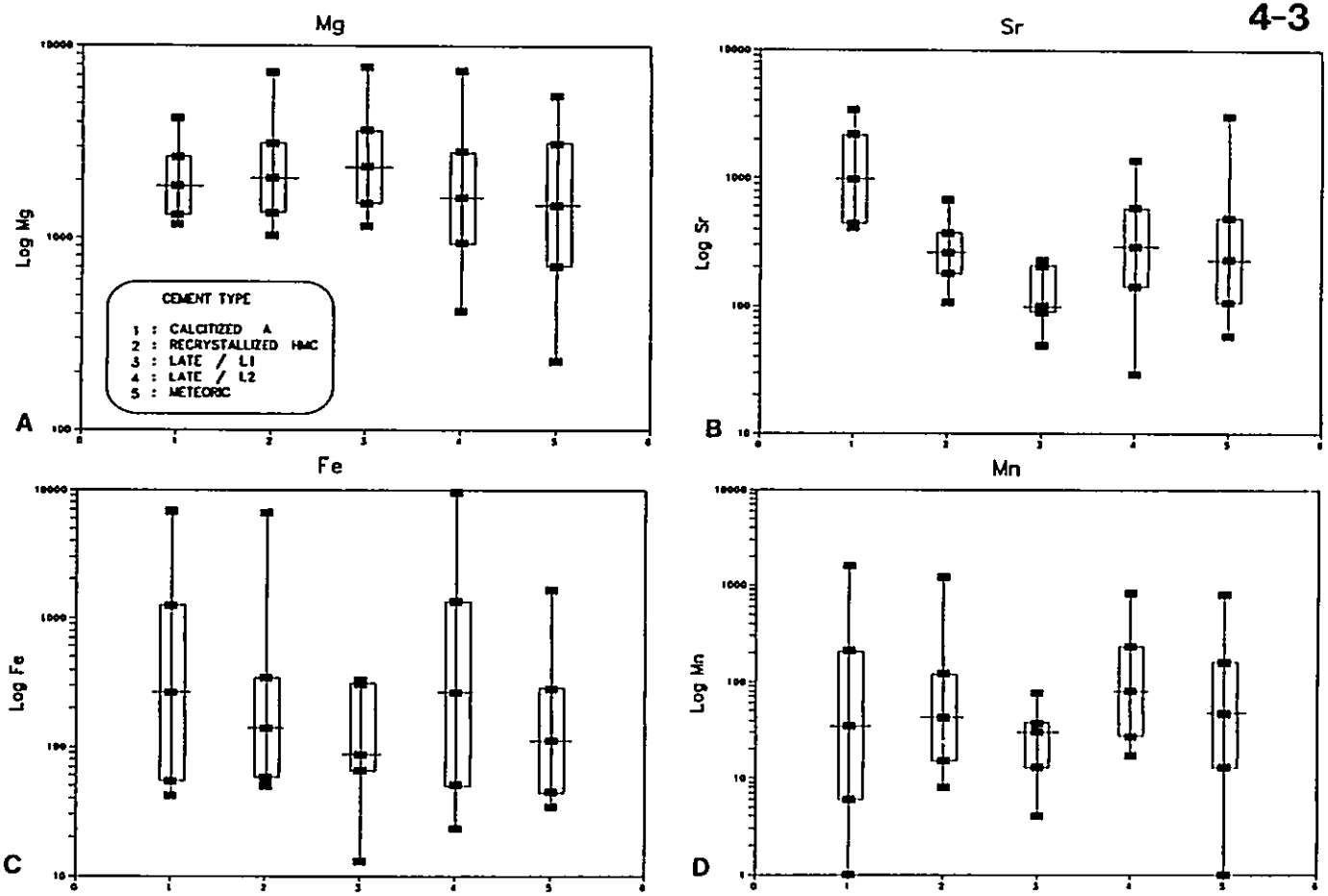
Mg
Log Mg
CEMENT TYPE
1 : CALCITIZED A
2 : RECRYSTALLIZED HMC
3 : LATE / L1
4 : LATE / L2
5 : METEORIC
A
Sr
Log Sr
B
Fe
Log Fe
C
Mn
Log Mn
D

STATISTICAL SUMMARY PLOTS - ISOTOPE RATIOS

Figure 4-4

a) $\delta^{18}O$ values for categories of cements indicated in the legend. The highest and lowest black squares represent the highest and the lowest values, respectively. The center black square is the mean of the population. The empty rectangles represent standard deviations (mean $\pm$ 1σ). Cements as in 4-3a.

b) The same for $\delta^{13}C$ values.

c) The same for $^{87}Sr/^{86}Sr$ (vertical axis).

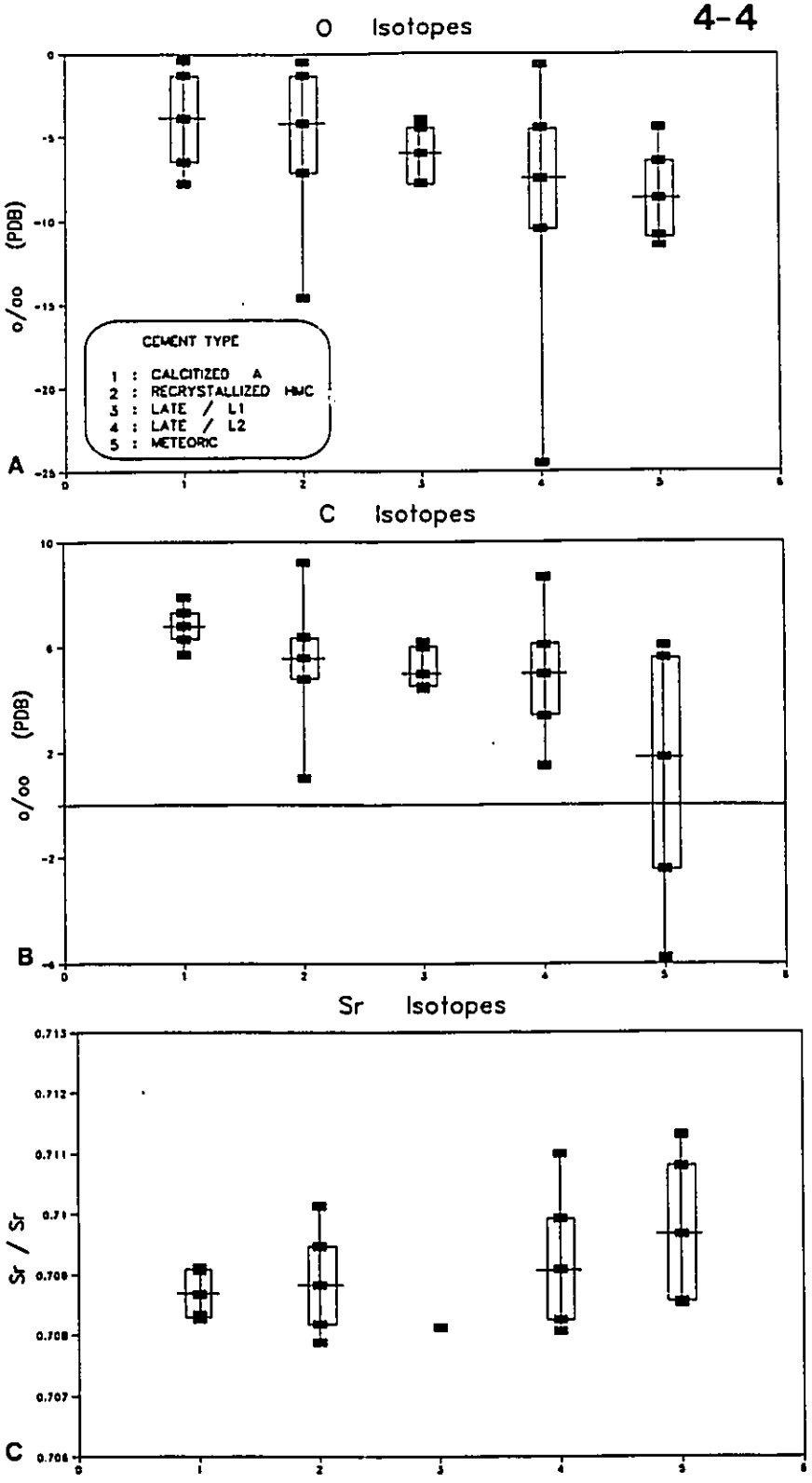
O Isotopes
o/oo (PDB)
CEMENT TYPE
1 : CALCITIZED A
2 : RECRYSTALLIZED HMC
3 : LATE / L1
4 : LATE / L2
5 : METEORIC
A
C Isotopes
o/oo (PDB)
B
Sr Isotopes
Sr / Sr
C

FACTOR ANALYSIS - CATEGORIES OF CEMENTS

TABLE 4-1

Factor analysis of geochemical results for the main categories of cements. The analyses were performed on numerous matrices of raw data comprising trace elements as well as carbon and oxygen isotopes. Strontium isotopes were not included in the statistics because of many missing values.

Matrices were standardized, missing values were handled by pairwise deletion method and correlation matrices were rotated using Varimax rotation method.

N: number of samples in the population. Variable: measured parameter. Factor: factor emerging from the analysis. Est. communality: estimated communality or proportion of the variation for a given parameter that is explained by the analysis. % of variation: percentage of the total variation explained by the given factor(s).

a) Factor analysis for calcitized aragonite. C and O isotopes are not included because of many missing values.

b) Factor analysis for recrystallized HMC.

c) Factor analysis for meteoric cements.

d) Factor analysis for late cements.

TABLE 4-1

a) Calcitized aragonite

Variable/Factor	1	N	Est. communality
Log Fe	0.86	10	0.73
Log Mn	0.97	10	0.94
Log Sr	-0.60	10	0.36
Log Mg	0.89	10	0.79
Eigenvalue	2.83		
% of variation	96		

b) Recrystallized HMC

Variable/Factor	1	2	N	Est. communality
Log Mg	0.69	0.16	51	0.49
Log Sr	0.77	-0.03	51	0.60
Log Fe	0.67	0.27	51	0.53
Log Mn	0.05	0.73	51	0.53
O	0.13	0.70	112	0.50
C	0.16	0.65	112	0.44
Eigenvalue	2.05	1.05		
% of variation	57	29		

c) Meteoric cements

Variable/Factor	1	2	N	Est. communality
Log Mg	0.78	-0.03	63	0.62
Log Sr	-0.26	0.40	63	0.23
Log Mn	0.01	0.19	63	0.03
Log Fe	0.30	0.58	63	0.43
C	0.86	0.04	16	0.74
O	0.07	-0.53	16	0.29
Eigenvalue	1.52	0.82		
% of variation	55	30		

d) Late cements (L1 + L2)

Variable/Factor	1	2	N	Est. communality
Log Fe	0.83	0.26	109	0.75
Log Mn	0.54	0.49	109	0.53
Log Mg	0.43	-0.02	109	0.19
Log Sr	-0.01	0.15	109	0.02
C	-0.70	0.30	107	0.57
O	-0.55	0.48	107	0.53
Eigenvalue	1.94	0.65		
% of variation	63	21		

GEOCHEMICAL RESULTS - CALCITIZED ARAGONITE

Figure 4-5

a) Scatter diagram of Sr vs Mn. The "A" field represents theoretical values for aragonite precipitated in equilibrium with seawater (Veizer, 1983 a). The arrow on the graph points towards increasing degree of equilibrium with diagenetic waters. Theoretical calcite precipitated from meteoric waters would contain high Mn and low Sr (approximately 750 and 200 ppm; Veizer, 1983 a). Brines would produce calcites with Sr-contents that are highly variable (Hanson and Banner, 1990).

b) Scatter diagram of carbon and oxygen isotope data. The plotted values were all obtained for Moscovian samples. The "M" field represents values proposed for brachiopods precipitated in equilibrium with Moscovian seawater by Popp *et al.* (1986 a). The enrichment of cements in ^{13}C relative to this estimate probably reflects the fact that the Sverdrup Sea was, at this time, a semi-restricted water body with elevated $\delta^{13}C$ relative to the open ocean (Beauchamp *et al.*, 1987).

Calcitized Aragonite 4-5 a

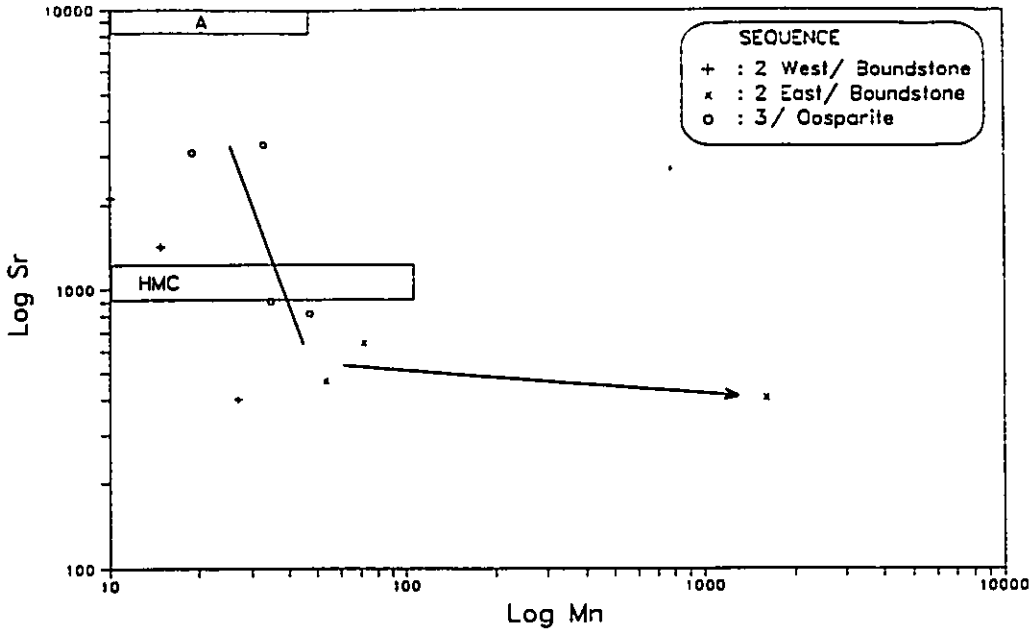

4-5 b

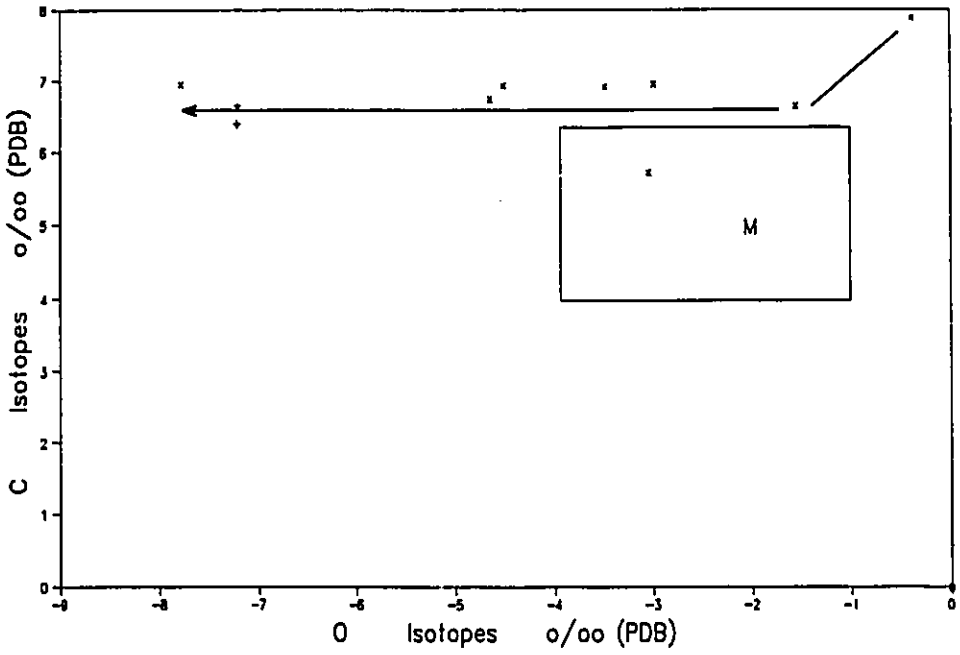

TRAVERSE IN SAMPLE 115620

Figure 4-6

Mg-Sr and Mn-Fe contents are shown for nine point analyses. C and O isotope analyses were performed on marine cements only. Microsamples were taken from the same hand specimen but not from exactly the same portions as trace elements. The types of cements are indicated in the legend and marked on the pictures (A: calcitized aragonite, H: recrystallized HMC, L: late low-Mg calcite). Length of the pictures is 0.75 millimetre.

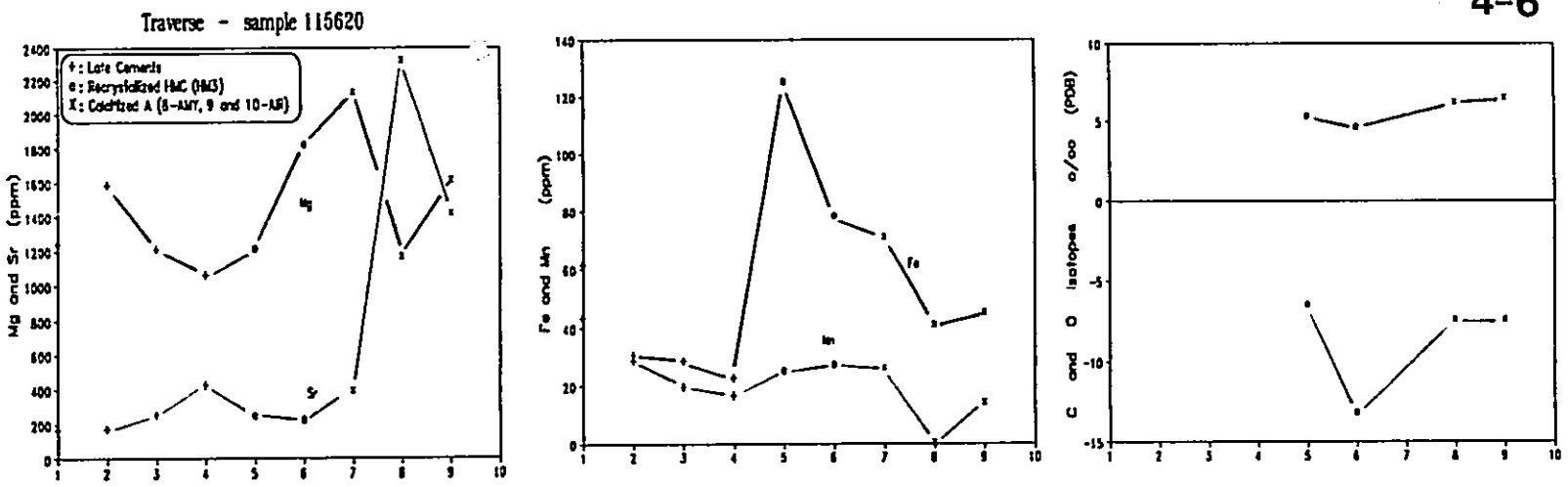
Traverse - sample 115620
+: Late Cements
o: Recrystallized HAC (HA3)
X: Calcitized A (5-AMY, 9 and 10-AB)
Mg and Sr (ppm)
Mg
Sr
Fe and Mn (ppm)
Fe
Mn
C and O Isotopes o/oo (PDB)

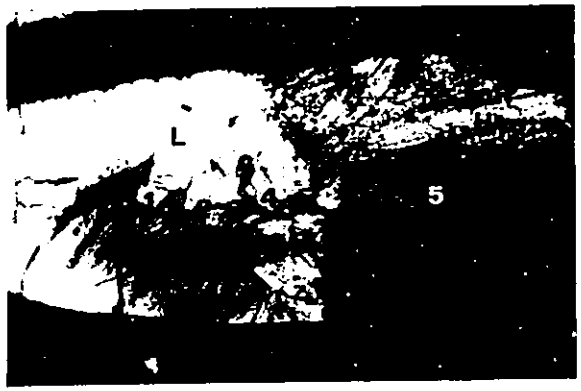
L
5

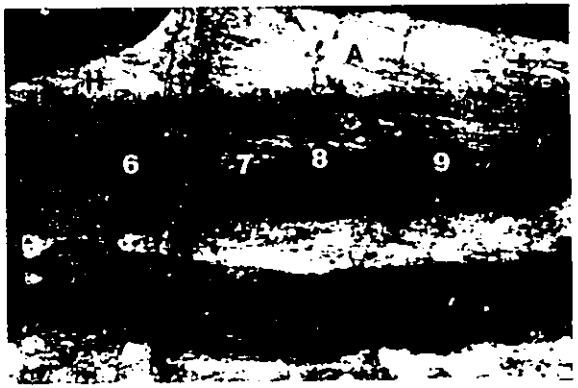
A
6
7
8
9

TRAVERSE IN SAMPLE 171258

Figure 4-7

Mg, Sr, Fe and Mn contents for six point analyses. CL patterns are as indicated in the legend. Pictures of the gold coated sample after the point analyses were performed. Note that the cathodoluminescence is darker than normal because of the coating. Point #7 was rejected because of contamination, as detected by high values for Al, Si and Na. The precise points of analysis are marked by the gold-free spots (numbers 1 to 7). Length of the pictures is 1.5 millimetres.

Traverse – sample 171258

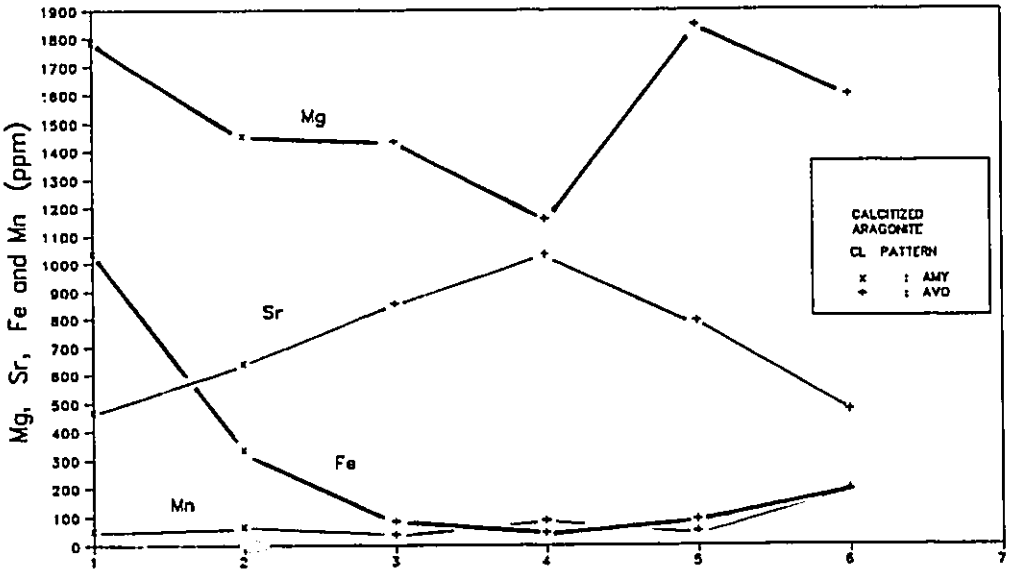

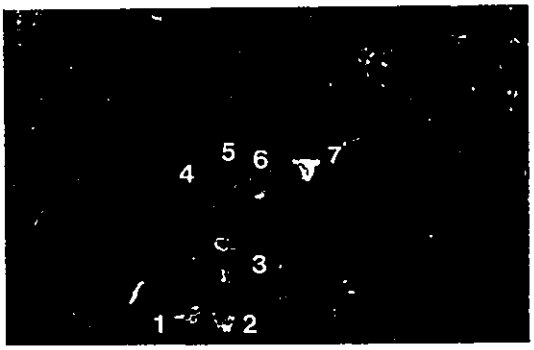

TRACE ELEMENT DIAGRAMS - RECRYSTALLIZED HMC

Figure 4-8

a) Scatter diagram of Mg vs Fe. Symbols indicate location of samples within the particular sequences. The "M" (marine) field represents theoretical values for HMC precipitated in equilibrium with modern seawater (Veizer, 1983 a). Trends (1) and (2) as discussed in the text.

b) Scatter diagram of Sr vs Mn. Legend as for a. A and HMC fields represent theoretical values for aragonite and HMC, precipitated in equilibrium with seawater (Veizer, 1983 a). Trends (1) and (2) as discussed in text.

Recrystallized HMC 4-8 a

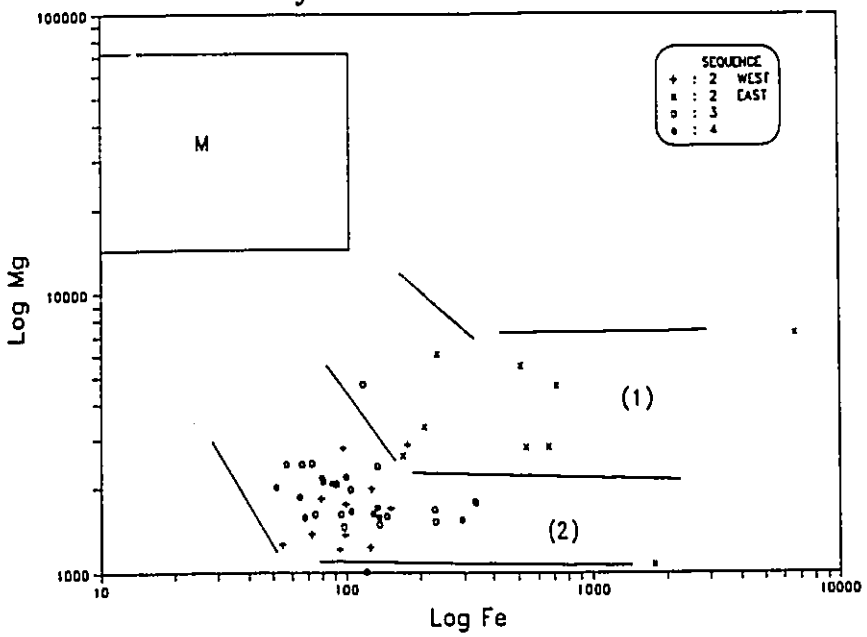

4-8 b

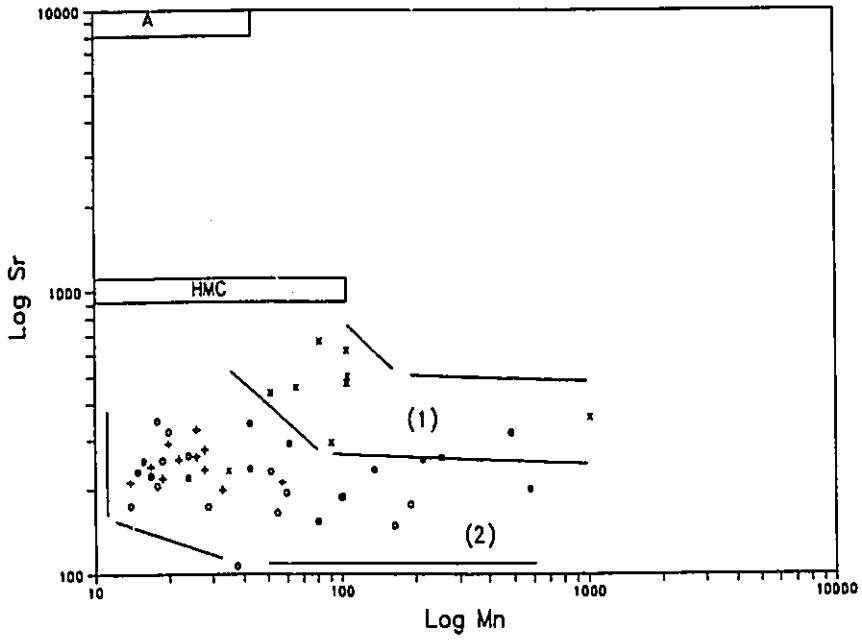

ISOTOPE RESULTS - RECRYSTALLIZED HMC

Figure 4-9

a) Scatter diagram of $\delta^{13}C$ vs $\delta^{18}O$. Location of samples within sequences as in the legend. M: marine field based on the values proposed by Popp *et al.* (1986 a) for the time interval from Moscovian (Late Carboniferous) to the Artinskian (Early Permian).

b) Scatter diagram of $\delta^{18}O$ vs $^{87}Sr/^{86}Sr$. Legend as for a. M: marine field based on the results from Popp *et al.* (1986 a, b). 0.0001 was added to their values for Sr isotopes (NBS-987: 0.71014) in order to adjust them to Bochum values (NBS-987: 0.71024). Trends (1) and (2) as discussed in the text.

Recrystallized HMC 4-9 a

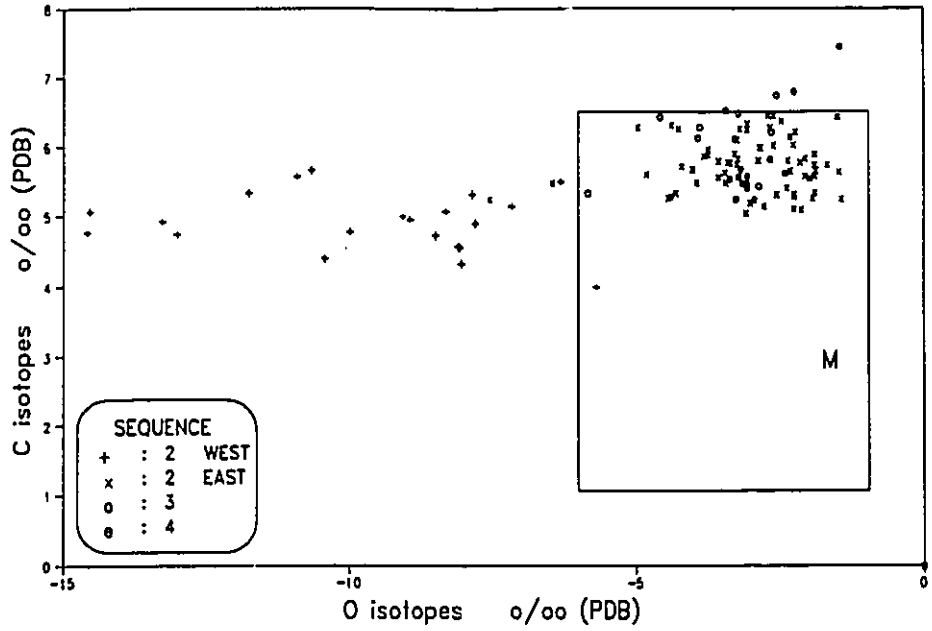

4-9 b

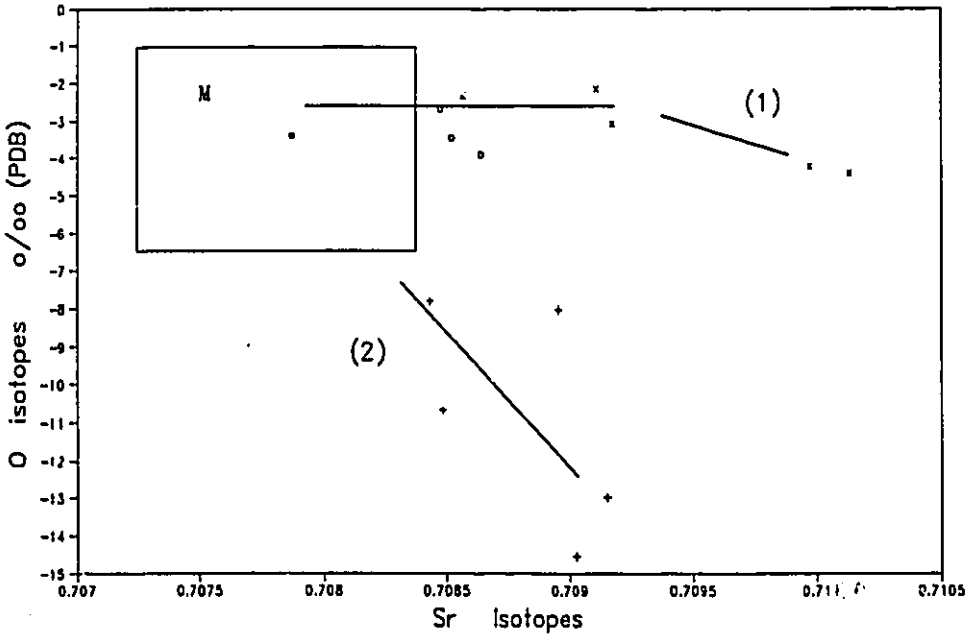

COMPARISON OF TEXTURAL AND ISOTOPIC PRESERVATION IN RECRYSTALLIZED HMC

Table 4-2

The degree of textural preservation increases from HM1-HM2a to HM2b, to HM3-HM4. H:highest value, M:mean, L:lowest value, n:number of analyses. The first row excludes the hydrothermal samples, whereas the two rows marked by stars include them.

	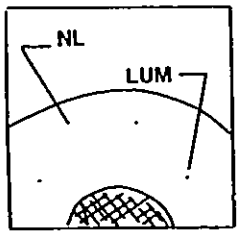 HM1	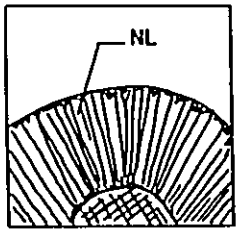 HM2a	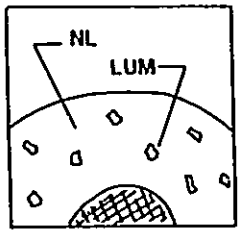 HM2b	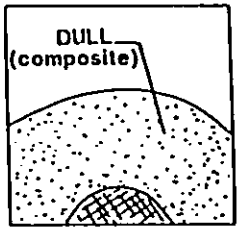 HM3	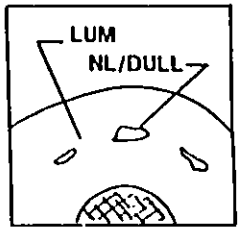 HM4
$\delta^{18}O$, $\delta^{13}C$ H M L n	 -1.5; 6.8 -2.9; 5.8 -6.4; 5.1 19	 -1.9; 6.8 -3.0; 5.9 -4.9; 5.3 14	 -1.7; 6.5 -3.1; 5.8 -5.8; 5.1 25	 -2.4; 9.2 -3.8; 5.9 -7.5; 5.2 17	 -1.4; 7.5 -2.8; 5.6 -4.4; 5.1 15
*M L n	-3.5; 5.8 -10.9; 4 22	-3.4; 5.8 -8.9; 5 15	-4.8; 5.5 -10.7; 4.3 36	-4.8; 5.8 -14.6; 4.8 20	
*$^{87}Sr/^{86}Sr$ H M L n	 0.70911 0.70872 0.70847 3	 0.71013 0.70965 0.70917 2	 0.70997 0.70873 0.70788 6	 0.70915 0.70884 0.70852 3	

Table 4-2

*Including data from section 37.

ISOTOPIC RESULTS - METEORIC CEMENTS

Figure 4-10

a) Scatter diagram of $\delta^{13}C$ vs $\delta^{18}O$. Location and nature of samples are given in the legend. M: marine field as for figure 4-9 a. W/R: water to rock ratio.

b) Scatter diagram of $\delta^{18}O$ vs $^{87}Sr/^{86}Sr$. Legend as for a. M: marine field as for figure 4-9 b. The arrow shows the possible effect of evaporation.

Meteoric Cements

4-10 a

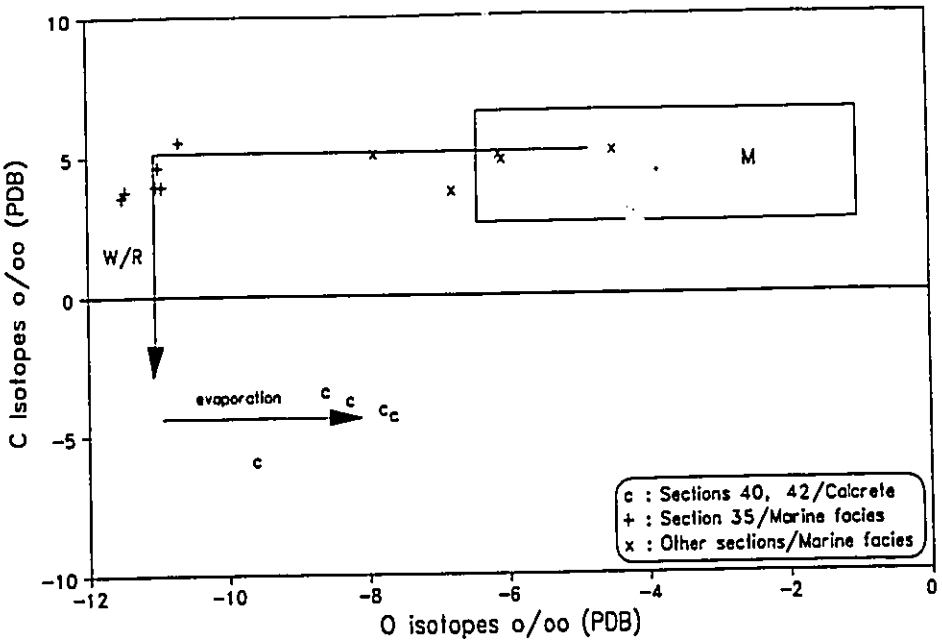

4-10 b

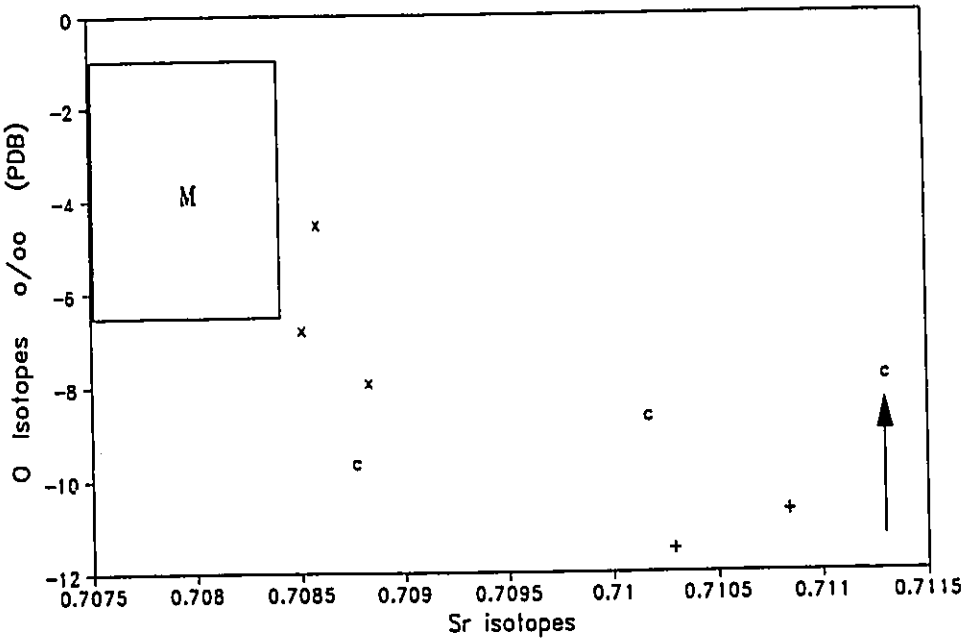

TRACE ELEMENT DIAGRAMS - METEORIC CEMENTS

Figure 4-11

a) Scatter diagram of Sr vs Mg. Type of samples and location as indicated in the legend. M: marine field as for figure 4-8.

b) Scatter diagram of Mg vs Fe. Legend as in a. M: marine field as for figure 4-8 a.

Meteoric Cements 4-11 a

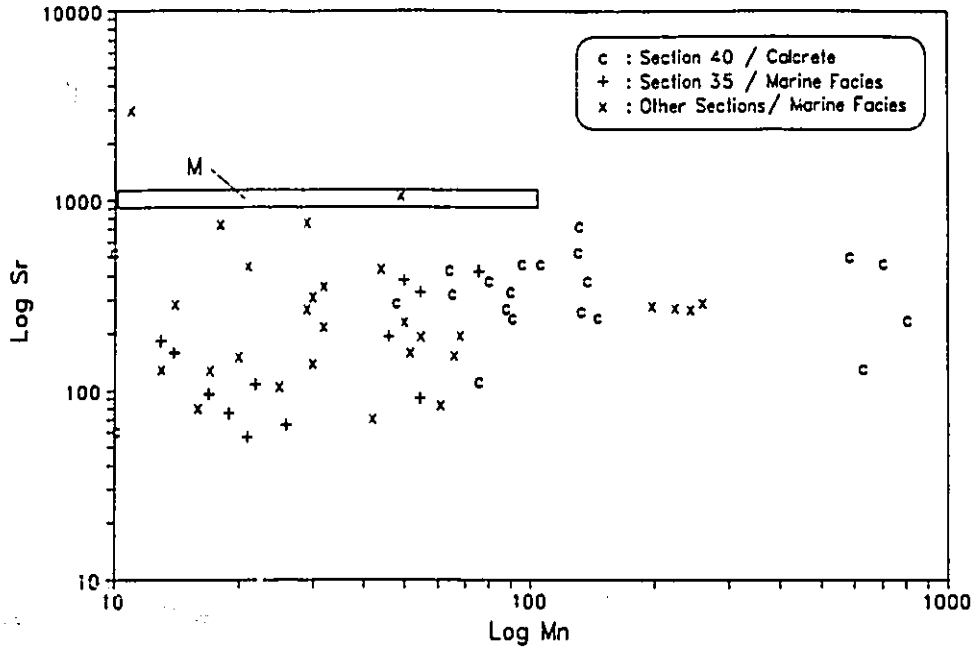

4-11 b

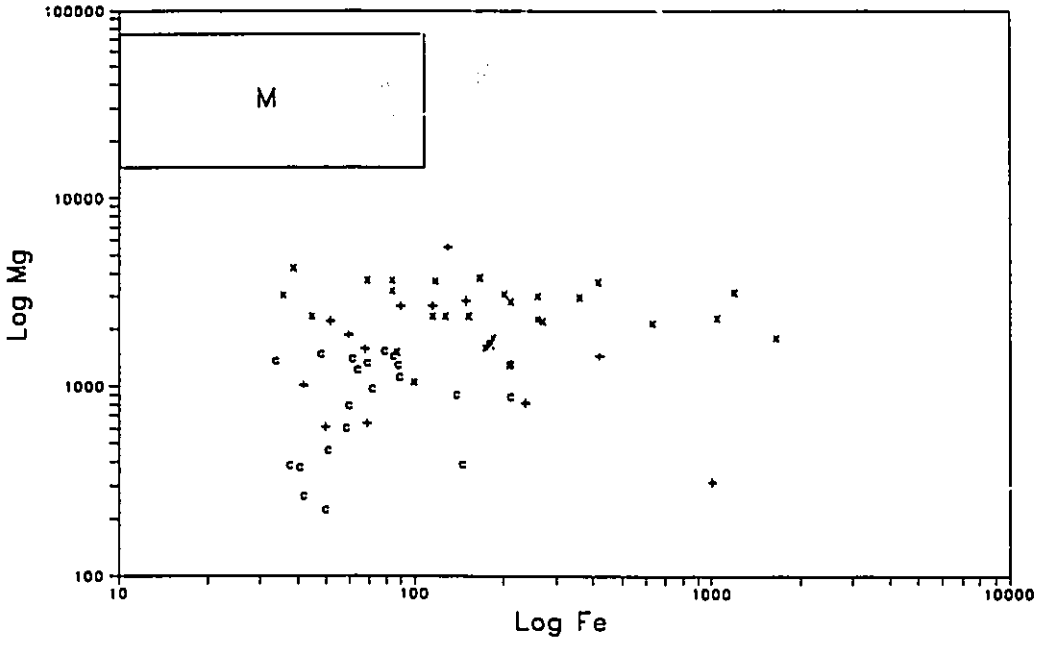

ISOTOPIC RESULTS - LATE CEMENTS

Figure 4-12

a) Scatter diagram of $\delta^{13}C$ vs $\delta^{18}O$. The types of cements as in the legend. Samples are from all three sequences. The most depleted value was obtained on a cement filling a late fracture. This isolated value will not be shown on the subsequent graphs. M: marine field as for figure 4-9 a. C: field based on results from meteoric cements from calcrete (sections 40 and 42).

b) Scatter diagram of $\delta^{18}O$ vs $^{87}Sr/^{86}Sr$ for L2 cements. Numbers on the diagram indicate the sections from which the samples originate. M: marine field as for figure 4-9 b. Trends (1), (2) and (3) as discussed in text.

Late cements 4-12 a

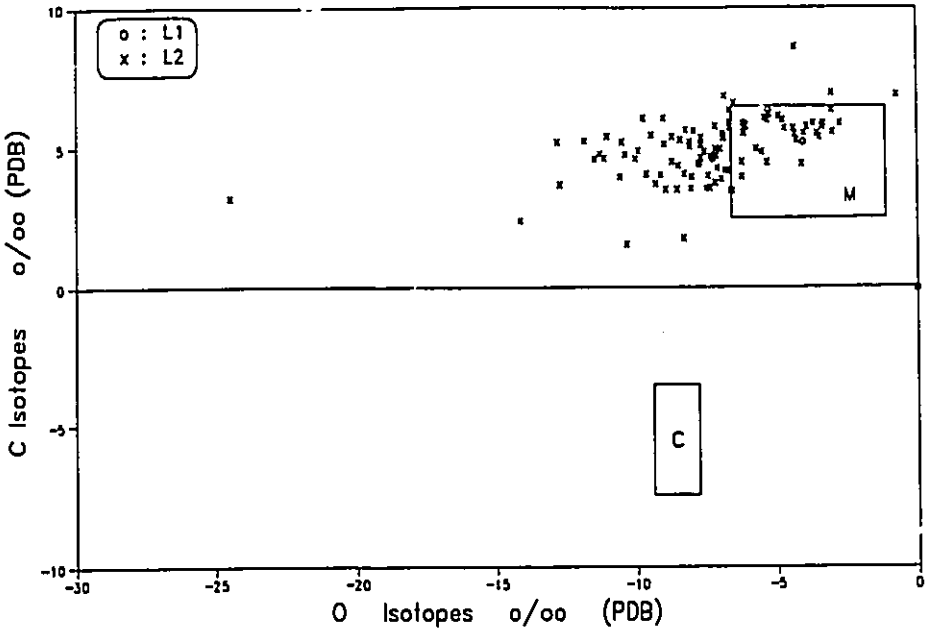

4-12 b

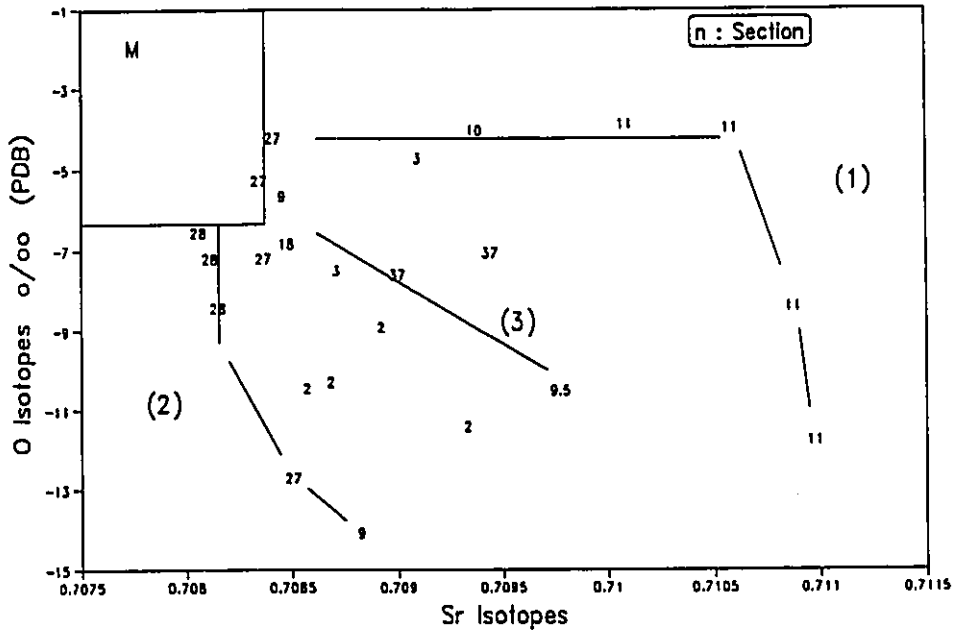

TRACE ELEMENT - LATE CEMENTS

Figure 4-13

a) Scatter diagram of Sr vs Mn. M: marine field as for figures 4-8 b. Many samples have Sr-concentrations within the marine field, while many others are significantly depleted in Sr. Numbers represent the sections from which the samples originate.
b) Scatter diagram of $\delta^{18}O$ vs Fe. M: marine field as for figures 4-8 a and 4-9 a. Numbers represent sections from which the samples originate. Trends (1), (2) and (3) as discussed in the text.

Late cements 4-13 a

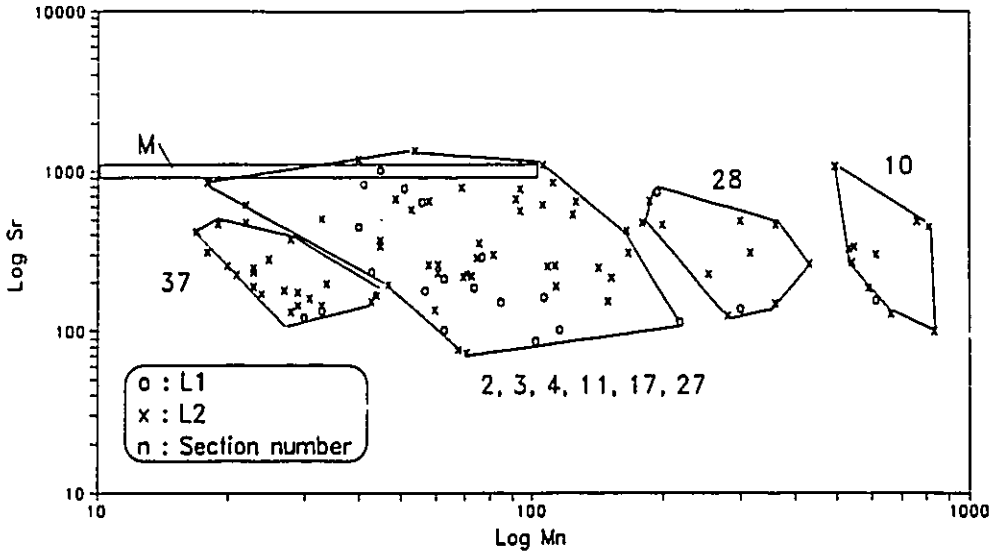

4-13 b

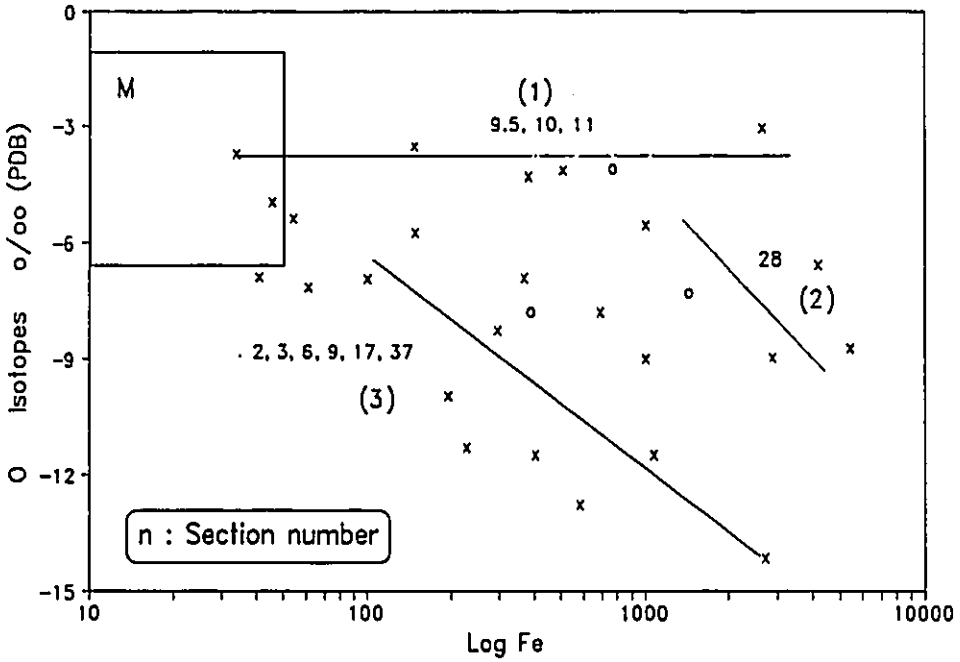

SUMMARY PLOTS OF ISOTOPIC RESULTS

Figure 4-14

a) $\delta^{13}C$-$\delta^{18}O$ diagram. Cement types in the fields as indicated by the legend. M: marine field as for figure 4-9 a. Recrystallized HMC cements are divided into two populations (H fields), with low $\delta^{18}O$ for section 37 ("hydrothermal" - see chapter 5) and high $\delta^{18}O$ for the other sections. Meteoric cements from shelf facies are identified by (1) for sections 3 and 4, and by (2) for section 35.

b) $\delta^{18}O$-$^{87}Sr/^{86}Sr$ diagram. M: marine field based on brachiopods ranging in age from Moscovian to Artinskian (Popp *et al.*, 1986 a, b). A and HMC are not distinguished because of their complete overlap (field "E").

Summary Plots

4-14 a

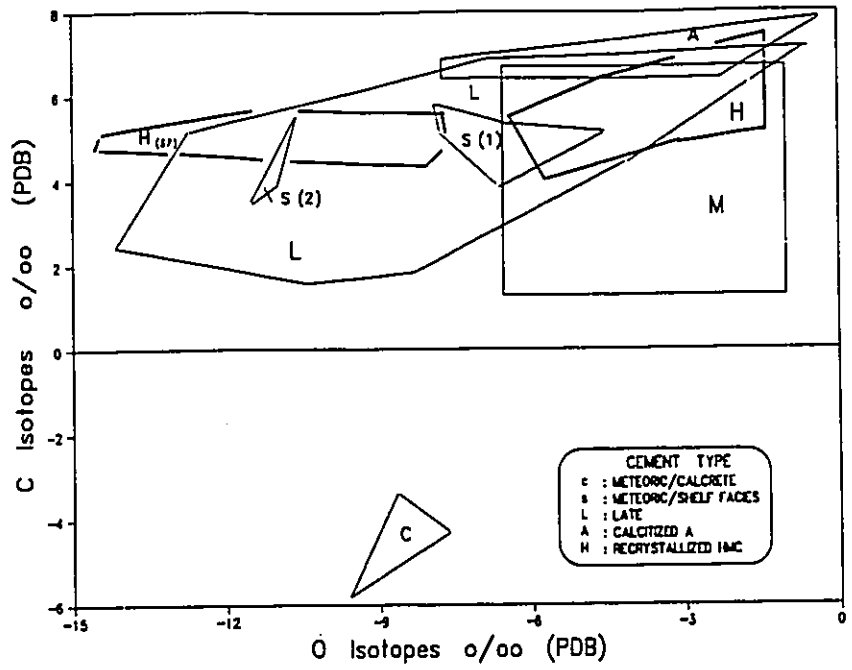

4-14 b

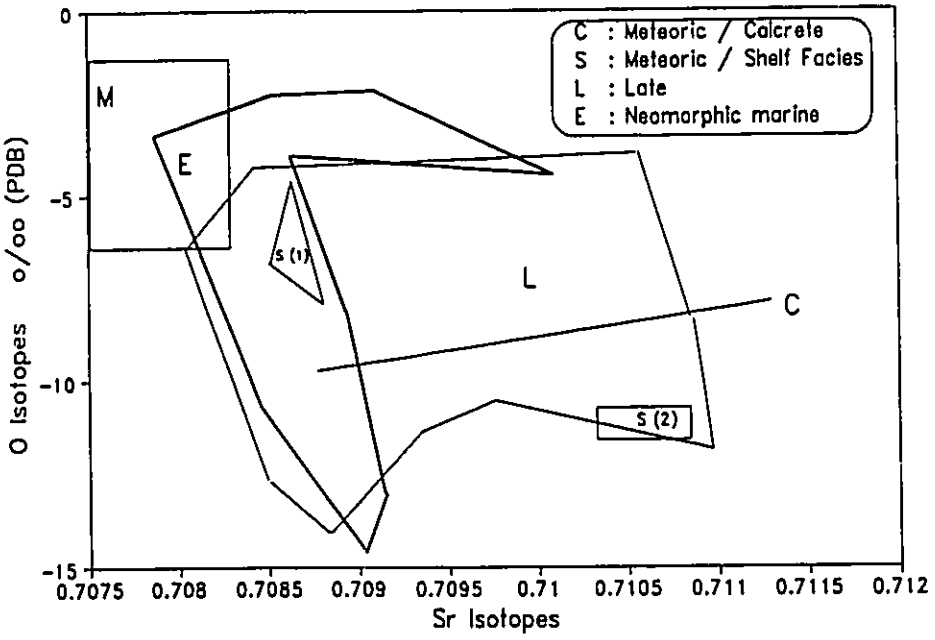

SUMMARY PLOTS FOR TRACE ELEMENTS

Figure 4-15

a) Sr-Mn summary plot. HM and MA fields are for theoretical calcite and aragonite precipitated in equilibrium with seawater (Veizer, 1983 a). Fields for cement types as indicated in the legend.

b) Mg-Fe summary plot. S(1) and S(2): meteoric cements from shelf facies of sections 2, 3 and 4, and 35, respectively. Other explanations as in a).

Summary Plots 4-15 a

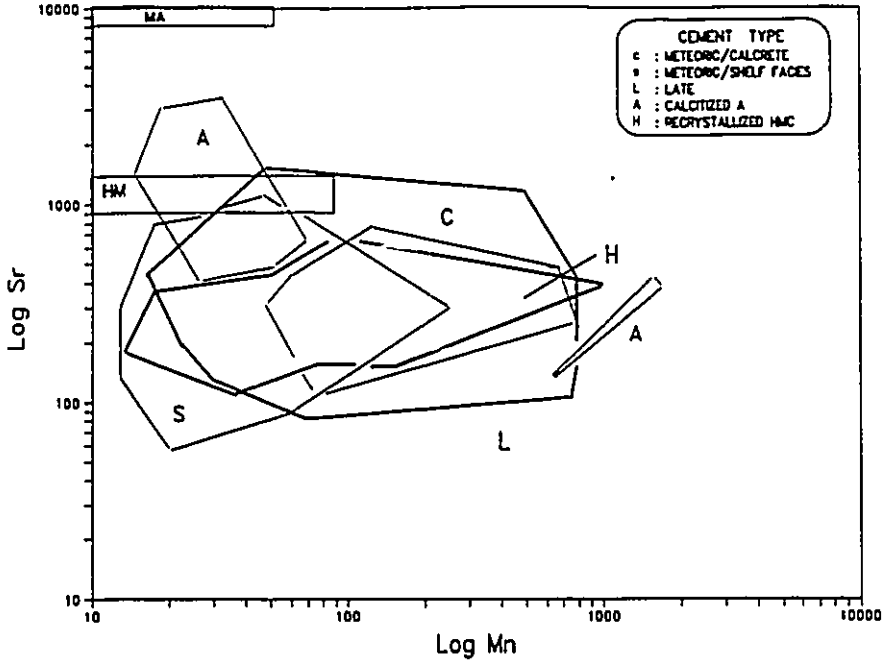

4-15 b

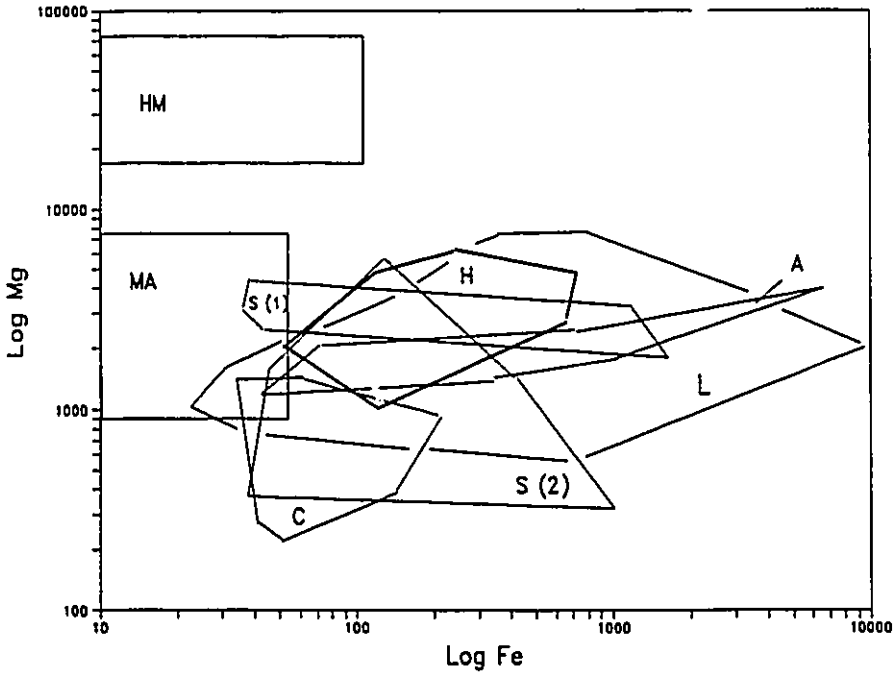

5. DIAGENETIC EVOLUTION OF CARBONATE SEQUENCES 2 AND 3

Sea level fluctuations and tectonic pulses that influence the migration of diagenetic fluids may be reflected in the diagenetic evolution of carbonate sequences, and this information can help to elucidate the geologic evolution of the basin.

In the following discussion, the geochemical results for sequences 2 and 3 (and 4), which by themselves may represent third order fluctuations, in the sense of sequence stratigraphy concepts, are treated as two distinct populations. The paleoenvironments in which the cements formed ranged from land based calcrete (section 40) to basin centre (sections 9.5 to 10) for sequence 2, from near-shore (sections 28 and 9) to shelf margin (sections 35, 2, 3 and 4) for sequence 3, and from calcrete (section 42) to near-shore (section 30) and shelf margin (sections 27, 17 and 18) for sequence 4 (fig. 2-3 b).

5.1 DIAGENESIS OF SEQUENCE 2

Cements in this sequence were sampled mainly from the mud mounds at the shelf edge and slope, and to a lesser degree from the Moscovian calcrete. The former are from two distant areas, western Axel Heiberg Island (Nansen Formation, section 37) and northern Ellesmere Island to the east (Hare Fiord and Otto Fiord Formations, sections 9.5, 11 and 10, respectively; fig. 2-3 a). Eastern sections 9.5 and 11 were subsequently drowned and covered by basinal fine clastic and carbonate sediments of the Hare Fiord

Formation, whereas the western area was covered by shelf edge carbonates (fig. 2-3b). Early marine cements are uniformly distributed in both areas, but the nature of diagenetic fluids may have been different in response to differences in tectono-stratigraphic settings.

5.1.1 Geochemistry of cements

The overall geochemical trends for cements of sequence 2, from early marine to late cements, are the progressive depletions in ^{18}O, ^{13}C and Sr concomitant with enrichment in Mn, Fe, Mg and ^{87}Sr, although the overlap of data is considerable. The early marine cements of the western region (section 37) are significantly impoverished in Mn, Fe, Sr, ^{18}O, ^{13}C and ^{87}Sr compared to their counterparts in the east (figs. 5-1, 5-2). Furthermore, each sampled section has its own pattern within the overall trend, no matter whether the early or the late cements are considered. Because of the east-west dichotomy in the geochemical attributes of early cements, the two areas will be discussed separately.

Isotopic composition

The stabilized marine cements of the eastern area have oxygen and carbon isotope signals mostly comparable to theoretical $CaCO_3$ precipitated in equilibrium with Moscovian seawater (fig. 5-1 a), but their Sr isotopes are somewhat more radiogenic (fig. 4-9 b). These cements were obtained from platform-margin mud mounds that were drowned during a rapid transgression by deeper, and colder, seawater. The carbonates

were then covered by the basinal fine clastic and carbonate sediments of the Hare Fiord Formation, and the subsequent burial diagenesis likely progressed without any role being played by the surficial meteoric waters. Final stabilization of marine components has then been completed during burial, at slightly higher temperatures, as indicated by the slight ^{18}O depletion and its covariation with radiogenic Sr (fig. 4-9 b). Since the early marine and the late cements overlap within the "marine" field (fig. 5-1 a), it is probable that stabilization of marine cement and late cementation already commenced in the marine realm *stricto sensu*, or at very shallow burial depths (Walter and Burton, 1990; Hesse, 1990). Stabilization of marine cements was completed at a depth of a few hundreds of metres, but the precipitation of late cements could have continued to depths of ~ 1.2 km, assuming that the geothermal gradient was about 60°C km^{-1} and that the parent waters were of marine deviation. This scenario could explain the general depletion in ^{18}O, the relatively constant ^{13}C and the radiogenic $^{87}Sr/^{86}Sr$ values in the cements (figs. 5-1 a, 4-9 b, 4-12 b).

The Middle Moscovian marine cements from *western Axel-Heiberg Island* (section 37) are texturally identical to those from the eastern area. The only visible differences are that they contain sulphate pseudomorphs that cross-cut ghosts after cement fibres and needles (fig. 3-12 d and e) and that they are associated with a singular dark yellow coarse calcite that is present as a minor phase. In comparison to the eastern area, the oxygen isotope ratios of the early marine cements from section 37 are much lower (fig. 5-1 b). The single sample of a peculiar, coarse, dark yellow calcite that preceded

the late cements is strongly depleted in ^{18}O and somewhat in ^{13}C (-21.5 and 3.1 ‰). Based on petrography, precipitation of this peculiar cement could have been coeval with recrystallization of the early cements.

The observed large ^{18}O-depletion in early marine cements can hardly be attributed to recrystallization in diagenetic environments dominated by meteoric waters. Moscovian meteoric waters were not more depleted in ^{18}O than the parent solutions of the calcrete cements. Yet, even taking into account the possible ^{18}O enrichment due to evaporation, these calcretes are heavier than many of the marine cements (fig. 5-1 b). The ^{18}O depletion must therefore be a consequence of higher temperatures. If these temperatures were simply a function of burial, the recrystallization of these early cements would have had to proceed at a greater depth - about 1 km - than the precipitation of the late cements, because the latter have heavier oxygen values (fig. 5-1 b). This would demand rapid subsidence followed by uplift. Geologically, this is an unlikely scenario. A more conceivable proposition is that hydrothermal fluids that precipitated the anomalous yellow calcite also caused the recrystallization of the early marine cements at shallow burial depth. These waters may or may not have been impoverished in ^{18}O (and ^{13}C) relative to the eastern ones, but they had higher temperatures. If these hydrothermal waters were brines, the resulting ^{18}O enrichment would have had to be counteracted by their still warmer nature, but this alternative is not supported by the moderate $^{87}Sr/^{86}Sr$ values (fig. 4-9 b). Assuming that the hydrothermal waters had an isotopic composition close to seawater, and utilizing the equation of Friedman and O'Neil

(1977), the calculated temperature of precipitation would have been ≈ 180°C. The shallow burial nature of these waters is also supported by the strontium isotopic ratios in the early cements that range from near-marine values of 0.70833 to 0.70895 (fig. 4-9 b). This postulated hydrothermal activity must have ceased prior to significant burial, and the precipitation of late cements must have proceeded at temperatures that were in accord with the regional geothermal gradients.

The pseudomorphs of sulphate postdate the marine cements at Axel Heiberg Island. Relics of sulphates are non existent in the succeeding burial cements or in the marine cements from the eastern area. This sulphatization could therefore relate to the same hydrothermal event. The assertion of hydrothermal circulation in the vicinity of section 37 is in accord with field observations. Syn-sedimentary faults do exist nearby, and the base of section 37 is massively dolomitized (B. Beauchamp, pers. comm., 1989). This suggests that hydrothermal recrystallization occurred during the rifting stage of the Basin, at a time of ubiquitous volcanic activity (Beauchamp, pers. comm, 1990).

Trace element composition

The above isotopic dichotomy of early cements is not just a question of the degree of alteration, because trace element trends (and Sr isotopes) indicate that the degree of alteration would have to increase west to east (figs. 5-2 c, d, 4-9 b), whereas the oxygen and carbon isotopes suggest a decrease. This apparent discrepancy could be the result of differing responses to temperature by various tracers. Whereas the fractionation of

oxygen, and to a minor degree of carbon, are strongly temperature dependent, the partitioning of other tracers is relatively insensitive to this variable. The western early cements contain only tens to hundreds of ppm of Fe and Mn, but the eastern ones have values ranging from tens to thousands of ppm (fig. 5-2). If, as suggested in the former section, warm hydrothermal solutions have been involved in recrystallization of western samples, the aquifer may have had relatively high Eh, resulting in the low Fe and Mn concentrations (fig. 5-2 c, d). In contrast, the basinward eastern sections may have been stabilized in more reducing waters that derived their Mn, Fe and ^{87}Sr from interactions with shaly lithologies (fig. 5-2 a, b).

The trace element patterns for late cements in the eastern area are similar to those of the marine cements, indicating comparable assertions for the chemical nature of diagenetic waters. Late cements, in general, show a Sr and Fe-Mn-Mg anticorrelation.

5.1.2 Summary

Marine cements (neomorphosed A and HMC) are very abundant in the Moscovian mounds of the Sverdrup Basin. Their "best preserved" isotopic signals compare well with results from brachiopods of comparable age from other localities (Popp *et al.*, 1986 a and b). However, the carbon signal in the Sverdrup Basin is distinctly enriched in ^{13}C. Recrystallization of the early cements was accomplished in at least two distinct diagenetic regimes: hydrothermal and burial. The western region of the Moscovian basin was affected by upward migration of oxygenated hot waters. As a

result, the early marine cements are depleted in ^{18}O relative to burial cements. This suggests that the presumed hydrothermal activ1ity must have ceased prior to significant burial, since the $\delta^{18}O$ signature of late cements from section 37 does not stand out from the rest of the data for late cements from other sections. The eastern region underwent normal and gradual burial diagenesis in a system that was characterized by progressively more reducing conditions.

5.2 DIAGENESIS OF SEQUENCES 3 AND 4

5.2.1 Stratigraphy of sequence 3

Cements for sequence 3 were sampled from the landward edge of the basin (section 28) as well as from the basinward shelf and shelf margin of the carbonate belt (sections 35, 9, 4, 3 and 2). Carbonates in sequence 3 form numerous fourth- to fifth-order cycles (Kendall and Schlager, 1981), many topped by strata with leached components and other meteoric features, particularly in the landward sections (Beauchamp, 1987). Section 28, deposited during a regressive phase, contains only inner shelf cycles. In contrast, section 2, deposited during a transgressive phase, starts with inner shelf cycles at the base and evolves upwards into outer shelf cycles. Section 35, from Axel-Heiberg Island, differs somewhat from other comparable sections (fig. 2-3 b) in that marine cements are rare and too thin to be sampled for isotopic analysis. Note that the sampled interval is located 235 metres under a discordance. Another

exceptional feature of this section is that it contains abundant cements with a mosaic fabric and with multilayered zoned texture under CL (fig. 3-12 c). These cements were interpreted as possibly of meteoric origin (see 4.6.1). In thin sections, marine cements show dissolution and corrosion features that chronologically precede the precipitation of the above cited presumed meteoric cements. Since the top of section 35 was eroded away during the Early Artinskian (fig. 2-3 b), this area, and perhaps other parts of the outer shelf, have been uplifted into the meteoric zone during or prior to Early Artinskian. Similar "meteoric" cements have been observed also as late precipitates in section 37 of the subjacent sequence 2, where they postdate all other diagenetic phases (figs. 3-12 d, e; 5-2 c, d). If the meteoric cements of sections 35 and 37 were genetically related and coeval, then the final occlusion of pore space in section 37 might have been achieved in the Artinskian.

5.2.2 Geochemistry of cements - sequence 3

Samples of marine cements originate from the resistant hemicycles of the outer shelf (sections 2 and 3), whereas the late cements have been collected across the entire shelf (sections 28, 9, 4, 3 and 2).

The overall geochemical trends for marine and late cements in sequence 3 follow faithfully the classical model of diagenetic repartitioning, no matter whether considered as a group or treated as separate populations. Depletions in Mg, Sr, ^{18}O and ^{13}C are accompanied by enrichments in Mn, Fe and ^{87}Sr (figs. 5-3, 5-4).

Marine cements

The summary of all oxygen and carbon isotope data for cements is given in figure 5-3 a. As illustrated in this summary, the originally marine cements (recrystallized HMC cements sampled at the top of sections 2 and 3) approach in their oxygen isotopic composition the values that would be expected for carbonate phases in equilibrium with the Assellian seawater, although the majority of cements are somewhat depleted in ^{18}O. The depletion was caused by the recrystallization of HMC cements into dLMC, either during cyclical exposure of sediments to an environment dominated by meteoric or mixed meteoric-marine waters, or during burial, by saline waters at higher temperatures. Their strontium isotopes are more radiogenic than the proposed coeval marine signal (fig. 5-3 b). Usually, for recrystallized calcite, oxygen isotopes attain equilibrium with freshwater at W/R three orders of magnitude lower than strontium isotopes. The covariation on the $\delta^{18}O$-$^{87}Sr/^{86}Sr$ diagram could suggest therefore that mixed or saline waters were responsible for the recrystallization, because alteration of the original marine $^{87}Sr/^{86}Sr$ by pure freshwaters would have required a very high W/R. Such assumption is at odds with the fact that the $\delta^{18}O$ values are some 4 - 7 ‰ heavier than the proposed meteoric signal (fig. 5-3). Moreover, the recrystallized early cements show corrosion and partial dissolution features, which usually imply meteoric or mixed water influence. Thus, the petrographic observations and the isotopic results are not decisive; recrystallization was accomplished either by mixed or saline waters. Both interpretations fit with trace element data.

Late cements

Isotopically, the late cements span the entire domain from marine to meteoric cements in $\delta^{18}O$, but with a larger spread in $\delta^{13}C$. Outer shelf sections 2 and 3 are characterized mostly by ^{18}O depletion, whereas sections 9 and 28, towards the basin margin, and some samples from the outer shelf sections, are depleted in ^{12}C as well (fig. 5-3 a). The outer shelf samples also have a concomitant increase in ^{87}Sr, whereas this is mostly not the case for inner shelf late cements (fig. 5-3 b). It may be tempting to explain these regional differences by an interaction of the intervening burial waters with the ^{87}Sr-rich shaly lithologies in the basin for the outer shelf sections, as opposed to mostly carbonates in the inner shelf settings. Additionally, the landward sections that mostly comprise inner shelf cycles were exposed to meteoric conditions. This may have enabled an influx of meteoric waters into the pores, resulting in a regional meteoric to marine (saline) gradient in the phreatic and deeper burial ground water system. The ^{12}C-enriched signal could presumably be inherited from soil-derived CO_2, while the Sr isotopes would have been buffered by the enclosing carbonates.

The trace element composition of the late cements shows somewhat comparable trends, but modified in detail. Firstly, the highest Sr concentrations are of the order of 1300 ± 100 ppm, as opposed to only 350 ppm in marine cements, and the lowest values are less than 100 ppm (fig. 5-4 a). These Sr concentrations suggest that the late diagenetic waters have had variable Sr/Ca ratios, covering the entire span from high seawater-like to low ratios, the latter comparable to that of meteoric waters. Secondly,

the cements from the landward sections, particularly section 28, have higher Mn and Fe concentrations at a given level of Sr and Mg than their outer shelf counterparts (fig. 5-4 a, b), perhaps attesting to a somewhat greater contribution of the meteoric component (or lower Eh) of the diagenetic waters.

The exposure of sequence 3 sediments to the influx of meteoric waters into the aquifer at this "late stage" (?) of diagenesis, resulting in a "freshening" of its shallower portions may have been facilitated by sea level fluctuations that have been typical at the time of deposition. The impact of such fluctuations would have been more pronounced in the landward inner shelf cycles than in their outer shelf counterparts. Overall, the composition of the "late" diagenetic waters during lithification of this sequence likely oscillated between meteoric, mixed meteoric-marine and saline waters.

5.2.3 Summary - sequence 3

In sequence 3, petrographic criteria and geological considerations suggest three main diagenetic steps. Firstly, precipitation of HMC marine cements took place. Secondly, in the case of section 35, exposure to meteoric environment, probably during late Sakmarian sea level drop, resulted in partial dissolution of these HMC cements as well as in precipitation of the proposed meteoric cements (MT2) within a phreatic environment. In the case of the other sections, cyclical exposure to a meteoric environment resulted in the dissolution of marine components mainly at the top of inner shelf cycles and in sparse precipitation of meteoric (?) cements (MT2 of sections 3 and

4). Finally, partial recrystallization of the original marine components into dLMC was probably constrained to the same diagenetic system as was the incipient precipitation of late cements. It is likely that this system was characterized by lateral as well as depth variations imposed by hydrodynamic meteoric influx and sea level fluctuations. The precipitation of late cements continued in the progressively deeper burial zone.

5.2.4 Notes on the diagenesis of sequence 4

Cements from sections 17 and 18 are from the Raanes mud mounds that were deposited during a major transgression. In contrast, samples from section 27 are from younger sponge-bryozoan mounds on the Great Bear Cape Peninsula that were formed during the most drastic regression in the history of the Sverdrup Basin (Beauchamp and Henderson, in progress). This regression led to the partial erosion of section 30 at the margin of the basin that yielded numerous brachiopods for this project. These were studied by cathodoluminescence petrography and the nonluminescent samples selected for isotopic investigations. Complementary SEM or trace element criteria have not been employed. In this sequence, marine cements were only of HMC mineralogy. They were abundant in sections 17 and 18, but in section 27 they were too thin for conventional isotopic work.

The geochemical attributes of marine cements from sections 17 and 18 faithfully follow the burial model for diagenetic repartitioning, with depletion in ^{18}O, Mg and Sr and enrichment in Mn, Fe and ^{87}Sr (fig. 5-4 c; trend 2 in figs. 4-8, 4-9). In late cements

(sections 17, 18, 27), a gradual depletion in ^{18}O, ^{13}C and Sr, and a progressive enrichment in ^{87}Sr, Fe and Mn were also observed (figs. 5-4 c, 4-10 b, 4-12 b).

In contrast to the clustered marine cements, brachiopods from sections 30, 29 and 27 show $\delta^{18}O$ and $\delta^{13}C$ values varying by 2 and 3 ‰ respectively (fig. 5-4 c). This spread for brachiopods can be explained either by vital effect, or by alteration of the isotopic signal. The most depleted specimens, being from the landward sections 30 and 29, possibly underwent partial meteoric resetting during the Kungurian regression.

5.3 DIAGENESIS OF CARBONATE SEQUENCES 2 AND 3 - SUMMARY

5.3.1 Recrystallization of marine cements

The present study shows that meteoric waters are not the only media promoting recrystallization of shelf edge carbonates. Hydrothermal, burial and possibly marine waters could have fostered stabilization as well. The hydrothermal and burial stabilization resulted in marked ^{18}O depletion caused by increased temperature (sequence 2), whereas only a slightly altered marine signal resulted from bottom marine water recrystallization (sequence 2, eastern area). The meteoric pathway that follows the classical repartitioning trend for tracers, with little variations in $\delta^{18}O$ and a significant decrease in $\delta^{13}C$, may have been of some importance for sequences 3 and 4 (see brachiopods), but a more detailed study is required for more definitive conclusions (see

chapter 9). Except for the short lived hydrothermal system, all major stabilization pathways, or parent water systems, merged gradually into the late diagenetic realm (fig. 5-5). The early stabilizing and the very shallow burial waters responsible for precipitation of late cements appear to have been of similar character and origin.

5.3.2 Diagenetic inventory of calcite cements from the Sverdrup Basin

Reconciliation of petrography, geochemistry and stratigraphy arises in genetic classification of Carboniferous and Permian calcite cements of the Sverdrup Basin (table 5-1). The sedimentary environment from which the samples were taken, the habits of the cements, their CL patterns (as described in chapter 3) and the possible parental waters (as discussed in chapters 4 and 5) are summarized for the entire population of specimens studied. These inferred systems of cementation - or diagenetic environments - are suggested to be responsible for the total stabilization and lithification of sequences. This diagenetic inventory can contribute to the elaboration of the geologic history of the basin.

5.3.3 Basin history

During the deposition and stabilization of sequence 2, the area was in a semi-arid climatic belt (Beauchamp, 1987). Aragonite (A) and HMC precursors were both recognized in Bashkirian and Moscovian sections. The gigantic aragonite botryoids perhaps suggest that the water salinity was high and that the basin was at times somewhat restricted. Tectonically, the area was involved in extensional movements and

rifting that commonly led to plutonism and volcanism and to related hydrothermal activity. The latter induced incipient recrystallization of cements in the western portion of the basin (figs. 5-5, 5-6 a, 5-7 a). In contrast, local drowning of the shelf in the east led in some cases to early marine recrystallization of the unstable phases (figs. 5-5, 5-6 b, 5-7 b). In both areas, normal burial cementation followed the early events.

The quantity of marine cements in sequence 3 diminished, and aragonite cements disappeared in the mud mounds, but were still produced in the shallow water facies (oosparite). The basin was perpetually connected with the western ocean (Beauchamp, 1987). Occasional meteoric exposure resulted from multiple, short term, fourth- to fifth-order fluctuations of sea level, that may have recrystallized some HMC cements but the bulk were likely recrystallized during the formation of "late" (shallow burial) cements (figs. 5-5, 5-6 c, 5-7 c; also see section 5.2). Meteoric cementation possibly affected late Sakmarian patch reefs on Axel Heiberg Island (section 35) as a result of the major sea level drop in the very Early Asselian.

In sequence 4, the Upper Sakmarian-Lower Artinskian shelf sections underwent normal meteoric to mixed meteoric/marine diagenesis. Marine cements were composed exclusively of HMC and were relatively abundant. However, this was not the case for the Artinskian bryozoan-sponge mounds that contain only thin layers of isopachous cements. The sequence was probably exposed to meteoric waters at the time of the

drastic sea level drop in the early Kungurian, as suggested by the relatively low isotopic ratios of brachiopods from the landward sections.

The Upper Bashkirian and Lower Moscovian (sequence 2) were characterized by oscillations of hypersaline to saline conditions (Nassichuk and Davies, 1980) in a restricted to slightly open sea. During Moscovian time, the Sverdrup Basin was connected to the ocean by a northwest passage, and marine conditions were less saline. This paleogeographic evolution was coincident with a northward drift of the Sverdrup Basin, from 10° North in the Early Moscovian to higher latitudes in the Middle Artinskian (sequence 4). This resulted in a climatic change, from an arid and hot climate in the Late Carboniferous to a colder one and glaciation at the end of the Permian. A decrease in salinity and in temperature of seawater may have been the reason for the transition from an assemblage of A-HMC to HMC cements.

5.3.4 Porosity evolution

Taking into account the diagenetic evolution discussed above, a rough percentage of meteoric components in parent waters of the studied cements has been estimated for each section (table 5-1). The inferred rough estimates of $\delta^{18}O$ values were utilized to evaluate the temperature of precipitation for the late cements. This temperature is expected to be lower or at most equal to the maximal temperatures reached by the ambient portions of the basin.

The estimated temperatures suggest that precipitation of late cements generally occurred before the sections reached their maximum burial depth, the latter recorded by other temperature indices (table 5-2). This resulted in the reduction of primary porosity, from 10-20 to 0 %. The highest temperatures have been obtained for the northern sections (37, 9.5 and 11), which underwent maximal thermal alteration. Assuming a geothermal gradient of 60°C km^{-1}, the maximal depth of precipitation of late cements would have been about one kilometre.

5.4 ECONOMIC POTENTIAL

The carbonate sequences of the Sverdrup Basin represent good prospects for discovery of Mississippi Valley Type lead-zinc deposits. They form a sediment pile that was deposited during Upper Palaeozoic intracratonic rifting and was further affected by the mid-Tertiary Eurekian orogeny that produced mountain ranges on the eastern side of the basin, and deep subsidence on its western extremity; a progression shared by numerous MVT districts, such as Pine Point, Gays River, Southern Missouri, etc. In these examples, platformal carbonate sequences were traversed by basinal brines during carbonate lithification, with the timing of the actual hydrothermal event varying from one district to another. The advocated hot waters that may have stabilized the early cements in section 37, likely represent a manifestation of such a hydrothermal activity. The fact that the event occurred early in the diagenetic history is a good omen, since the primary

porosity was still high and the permeability and reservoir quality good. Another indication of metallogenic promise is the occurrence of massive dolostones distributed along the presumably syn-sedimentary faults (Beauchamp, pers. comm., 1989). Brine migration through the partially consolidated outer shelf sediments, or along faults in the basin centre, could have resulted in base metal deposition of the MVT or SEDEX types. SEDEX deposits could have been produced by waters that would have traversed through the fine clastic sediments of the central portion of the basin.

As already pointed out by Utting *et al.* (1989), the Upper Paleozoic strata that are today within the oil window are the platform facies along the southern and southeastern margins of the basin. The now overmature basinal shales are potential source rocks. In particular, the shelf carbonates on Devon Island (Grinnel Peninsula) could be a potential reservoir, provided that oil migration and trapping took place before the primary pore space was occluded, that is before 0.5 to 1 kilometre of burial.

$\delta^{13}C$-$\delta^{18}O$ DIAGRAMS - SEQUENCE 2

Figure 5-1

$\delta^{13}C$-$\delta^{18}O$ fields for recrystallized HMC, calcitized A and late cements.

a) In the eastern region, the population of cements is from sections 11, 10 and 9.5. Marine field "M" is based on Moscovian brachiopods (Popp *et al.*, 1986 a). b: brachiopod from section 10. A and H fields overlap considerably, but the upper part of the field contains exclusively A samples.

b) In the western region, the calcrete cements are from section 40, and all the other cements are from section 37. Explanations as in a).

Eastern Region 5-1 a

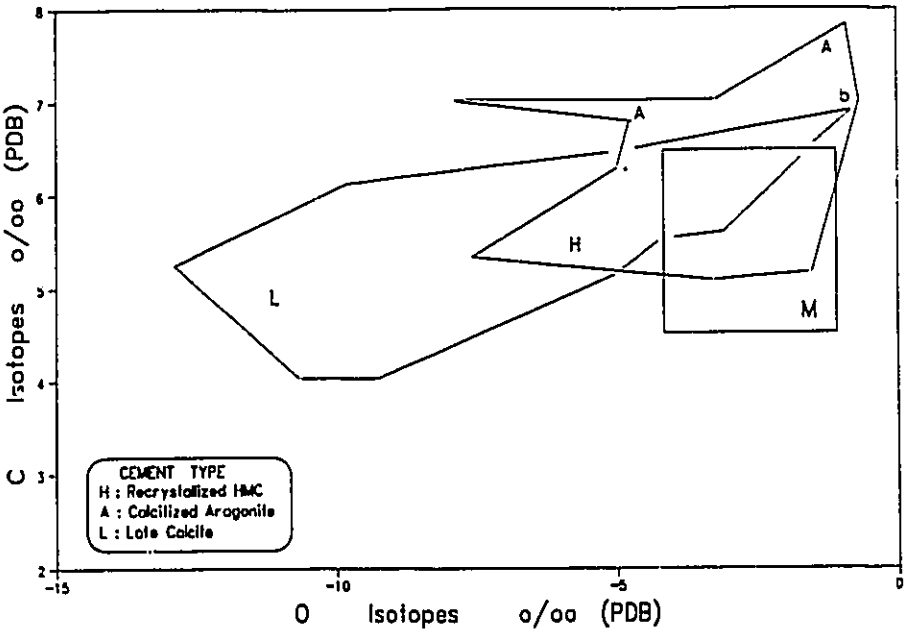

Western Region 5-1 b

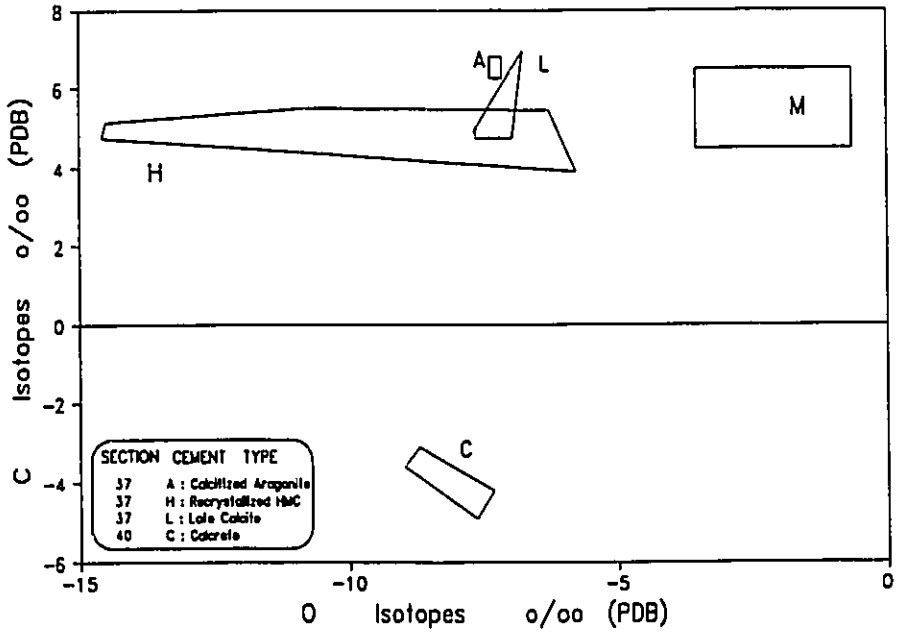

TRACE ELEMENT DIAGRAMS - SEQUENCE 2

Figure 5-2

a) Sr-Mn diagram for the eastern region. Cement types and sections as indicated in the legend. A and HMC fields are theoretical values for these phases in equilibrium with seawater (Veizer, 1983 a).

b) Mg-Fe diagram for the western region. Legend as in a).

c) Sr-Mn diagram for the western region (section 37). Cement types as indicated in the legend. A and HMC fields are theoretical values for these phases in equilibrium with seawater (Veizer, 1983 a).

d) Mg-Fe diagram for the western region. Legend as in c).

Eastern Region 5-2 a

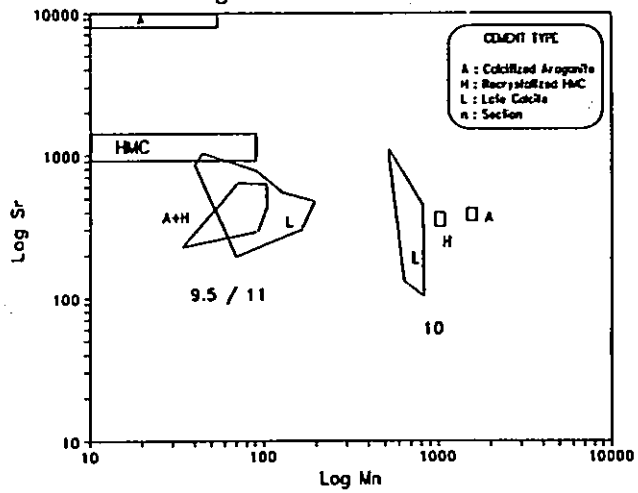

Eastern Region 5-2 b

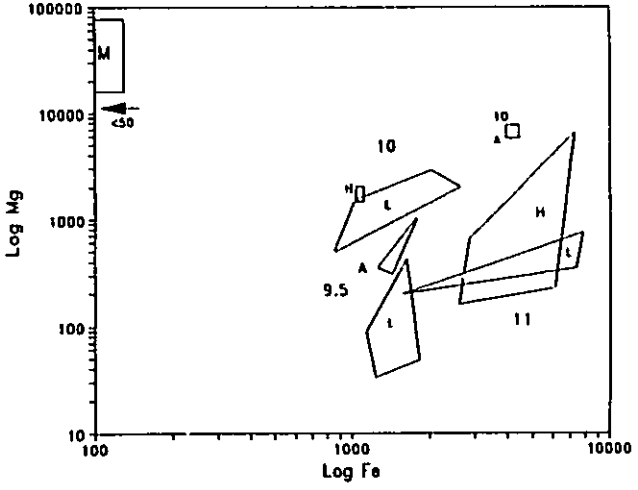

Western Region 5-2 c

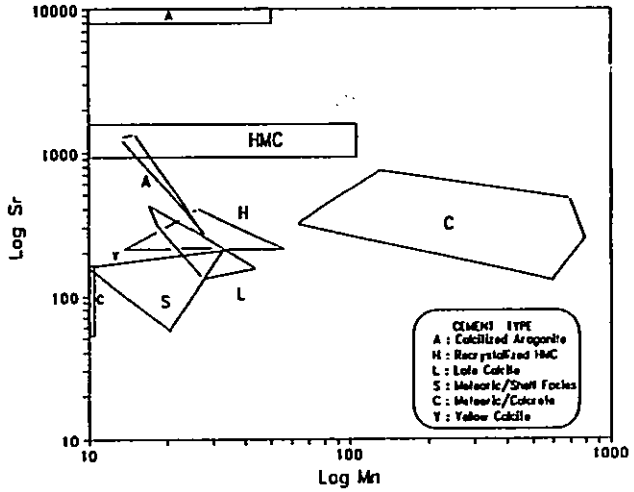

Western Region 5-2 d

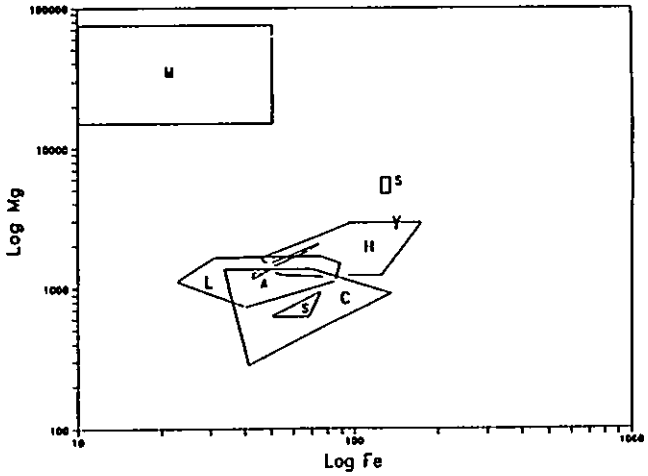

ISOTOPIC RESULTS - SEQUENCE 3

Figure 5-3

a) $\delta^{13}C$-$\delta^{18}O$ diagram. Marine field (M) for carbonates in equilibrium with Asselian-Sakmarian seawater is based on brachiopods (Popp *et al.*, 1986 a).

b) $\delta^{18}O$-$^{87}Sr/^{86}Sr$ diagram. Marine field (M) for carbonates in equilibrium with Asselian-Sakmarian seawater is based on brachiopods (Popp *et al.*, 1986 a, b). Small cases represent data.

Sequence 3

5-3 a

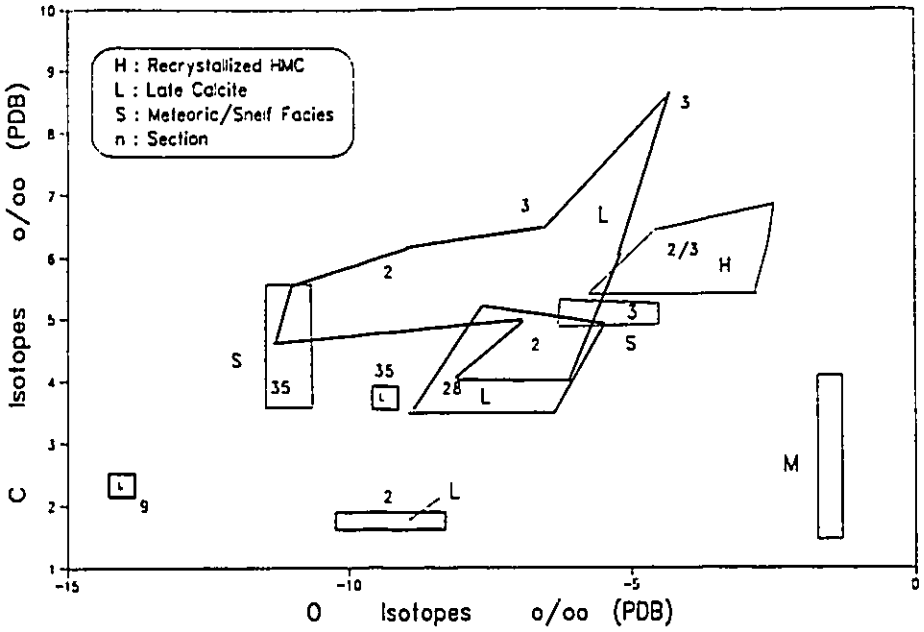

5-3 b

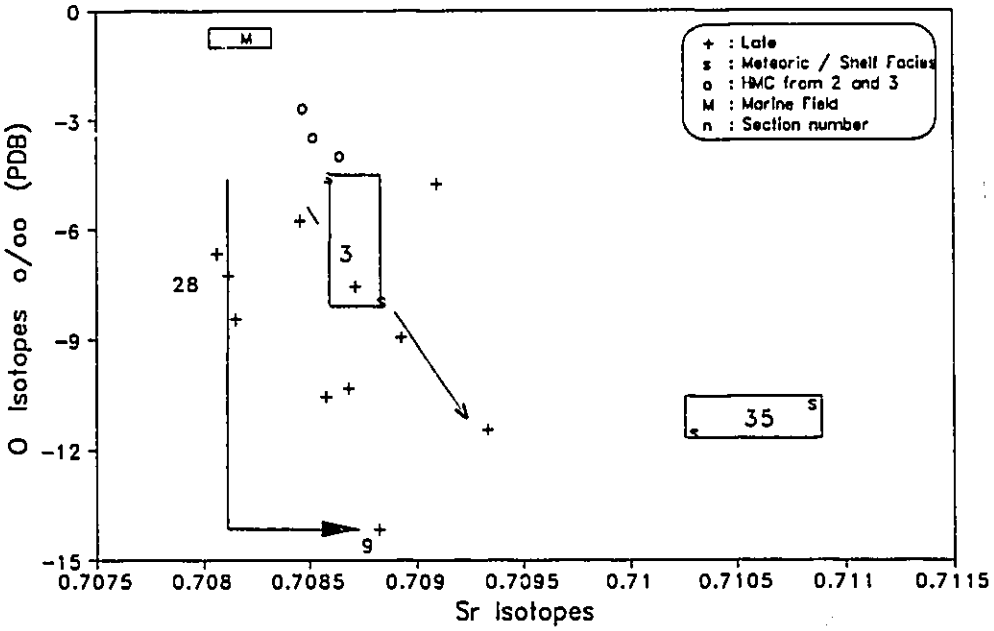

GEOCHEMICAL RESULTS - SEQUENCES 3 AND 4

Figure 5-4

a) Sr-Mn diagram for late cements only. Marine field (M) for calcite in equilibrium with seawater (Veizer, 1983 a). HM: recrystallized HMC of sequence 3.

b) Mg-Fe diagram for the late cements only. HM: results for recrystallized HMC of sequence 3.

c) $\delta^{13}C$-$\delta^{18}O$ diagram for SEQUENCE 4. Marine field (M) based on Artinskian North-American brachiopods (Popp *et al.*, 1986 a). H: marine cements (HMC), L: late cements, B: brachiopods, C: calcrete cements.

Late Cements/Sections 28, 9, 3, and 2/5-4a

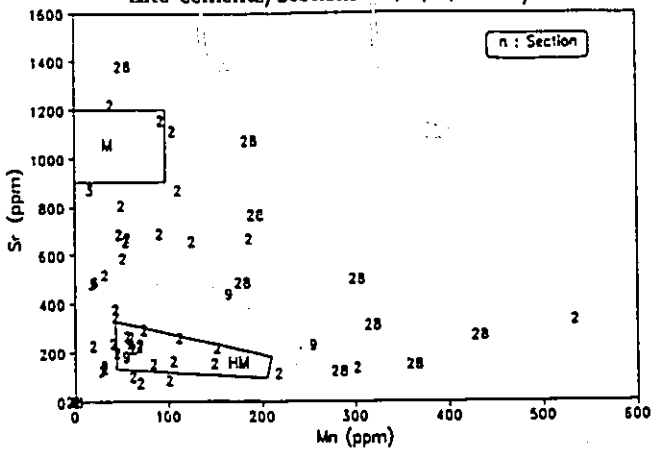

5-4 b

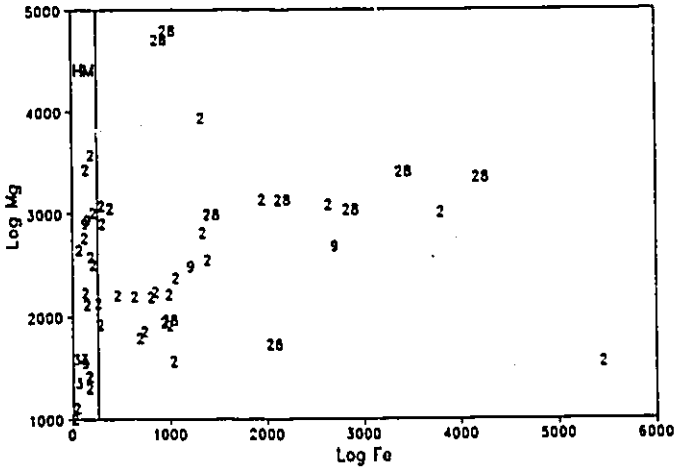

Sequence 4

5-4 c

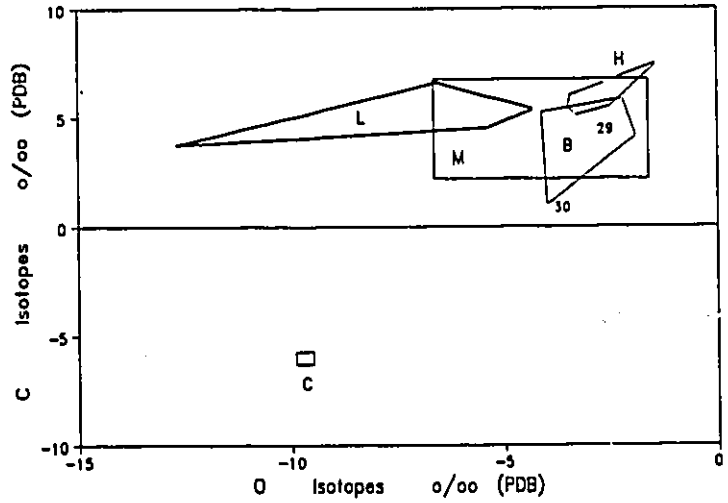

GEOCHEMICAL TRENDS - SUMMARY

Figure 5-5

a) $\delta^{13}C$-$\delta^{18}O$ diagram illustrating the idealized geochemical trends in sequences 2 and 3 and their interpretation. Passage from marine (1) to burial (saline) waters (2) is accomplished progressively with time (trends A, B and D; eg. sequence 2, section 11). Mixed meteoric-marine waters likely induced the trend (F) in landward sections, whereas both saline (2) or mixed meteoric-marine waters (3) could be responsible for the trends (B and E) observed in the basinward sections of sequence 3. The theoretical (T) meteoric (M) water (W) line (L) is inferred from the study of meteoric cements (shelf and calcrete environments; sections 35, 40 and 42; trend 4). The arrow shows the possible fractionation induced by surface evaporation in the calcrete (C) cements. The $\delta^{18}O$-value of -11.5 ‰ appears to be extremely low in comparison to the marine signal. Although there is no definite explanation for this yet, Scholle *et al.* (1991) have found similar values (-8 to -12 ‰) in Permian meteoric cements from east Greenland (bryozoan-algal mud mounds, Jameson Land Basin). The geochemical attributes of section 37 (sequence 2, west) are represented trend 5. A: aragonite. Red: early marine cements, green: late cements, yellow: meteoric cements

b) Same for $\delta^{18}O$-$^{87}Sr/^{86}Sr$ diagram.

c) Same for Sr-Mn diagram.

Geochemical Trends

5-5 a

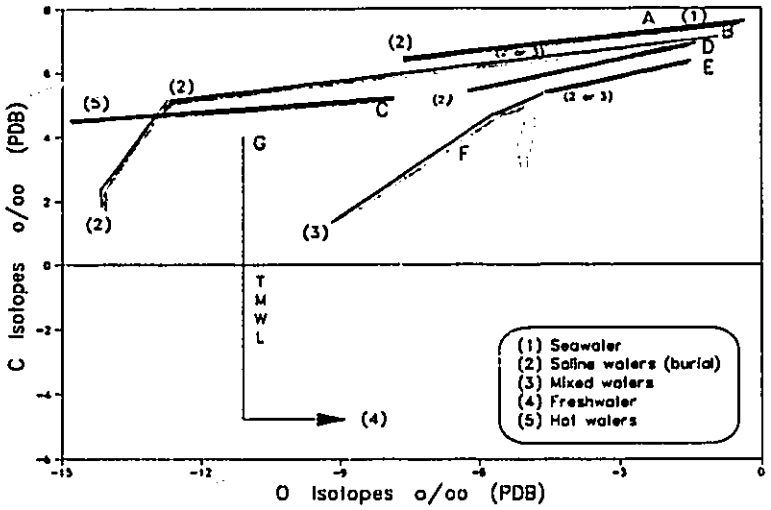

5-5 b

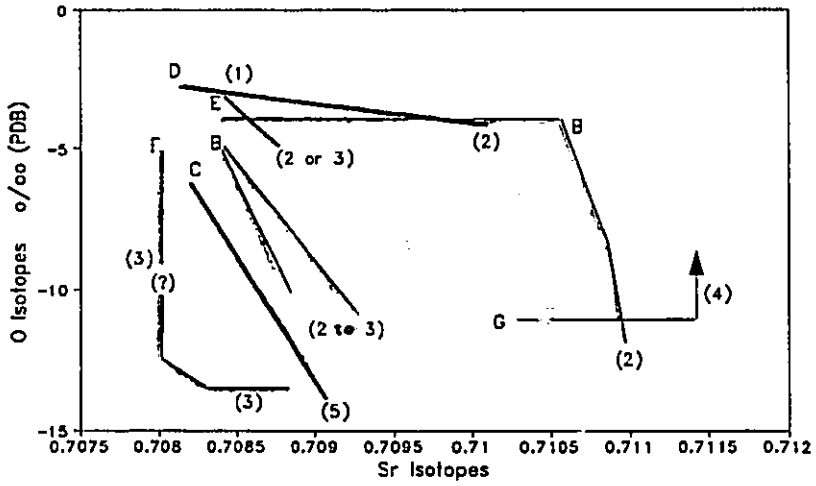

5-5 c

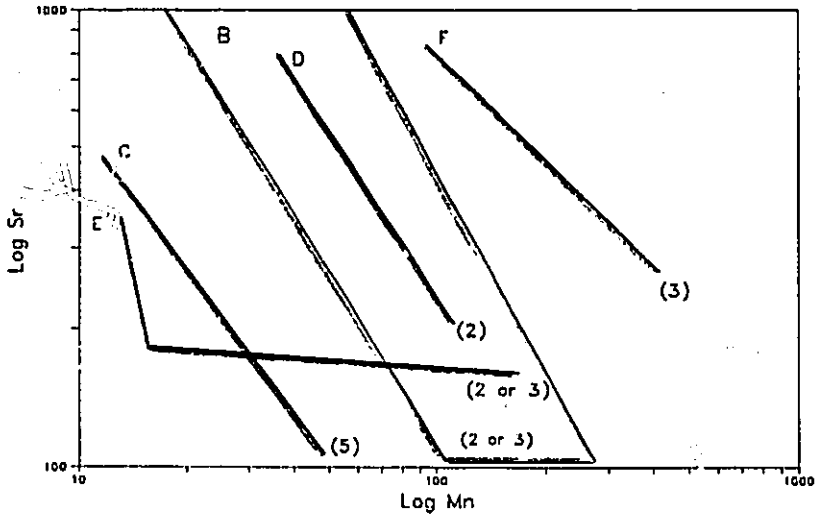

DIAGENETIC INVENTORY OF CALCITE CEMENTS FROM THE SVERDRUP BASIN

Table 5-1

The inventory of calcite cements from the Sverdrup Basin, of their possible parent waters, and their suggested diagenetic environments. The latter are proposed to be responsible for the total stabilization and lithification of the three studied sequences.

TABLE 5-1

SEDIMENTARY ENVIRONMENT	CEMENT TYPE		POSSIBLE PARENT WATERS	DIAGENETIC ENVIRONMENT
	LM	CL		
Outer shelf/mud mounds	Botryoidal (acicular ghosts, dLMC)	AIR/AVO/AFN/ AMD/AMY	Primary cement: A+HMC/ marine waters	
Inner shelf/oosparite grainstone	Tangential oolitic (oolite ghosts, dLMC)	AOO	Neomorphic cement: dLMC/ - marine cold (?) - marine-derived saline waters (basinal) - hydrothermal waters - meteoric and mixed waters	From marine to: - marine (cold) phreatic (?) - shallow burial
Outer shelf/mud mounds	Fibrous isopachous	HM1 HM2 HM3 HM4		- marine hydrothermal (?) - mixed or meteoric phreatic
	Rhombohedral	HMRH		
Calcrete + inner shelf	Anhedral equant in mosaic (LMC)	MT1 (in cases meniscus fabric?)	Meteoric waters	- Meteoric (calcrete) - Meteoric vadose and phreatic (shelf facies)
Inner shelf Outer shelf	Equant in mosaic (LMC)	MT2	Meteoric to mixed waters	- Phreatic meteoric and mixed
Shelf	Stubby to bladed (LMC)	L1	Marine-derived (saline) waters	- Shallow burial
Shelf	Xenomorphic (poikilotopic) in mosaic (LMC)	L2	Mixed meteoric-marine/saline waters	- phreatic mixed

DIAGENETIC MODELS

Figure 5-6

a) Model proposed for the western region of sequence 2. The carbonate sediments were likely stabilized by hydrothermal waters. These waters were possibly channelled by a nearby fault. The succeeding late cements were produced during subsequent precipitation in the phreatic zone of the regional aquifer.

b) Model proposed for the eastern region of sequence 2. After drowning of a portion of the eastern shelf (reason unclear), cold waters invaded the residual pore space and possibly caused partial recrystallization of the unstable phases. Saline waters recrystallized most of the early cements and precipitated the late cements during progressive burial without any influence by surficial meteoric waters.

c) Model proposed for sequence 3. Pore waters of the inner and outer shelf were cyclically affected by meteoric and mixed waters as a result of fourth- to fifth-order sea level fluctuations. Relative positions of sections are illustrated in the inset.

A-Sequence-2
Western Region

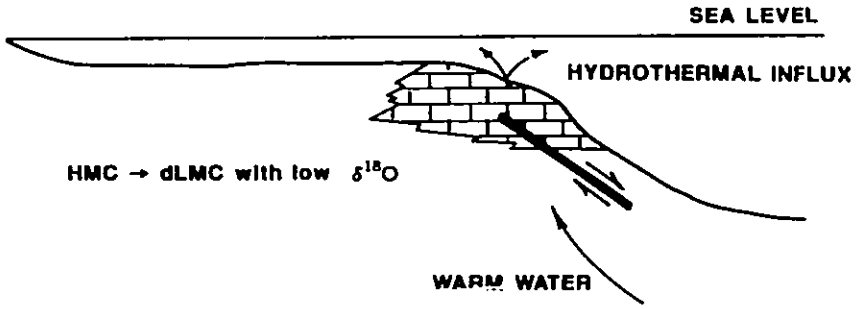

B-Sequence-2
Eastern Region

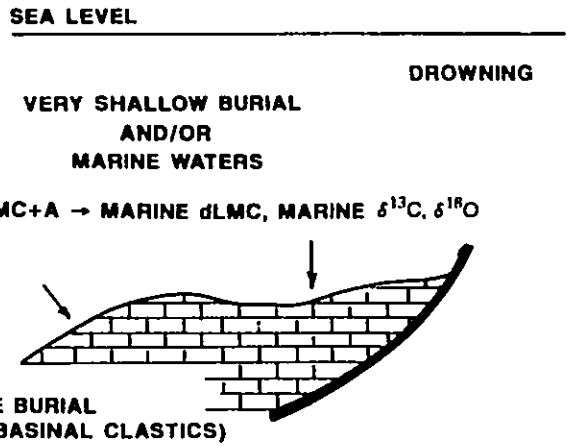

C-Sequence-3

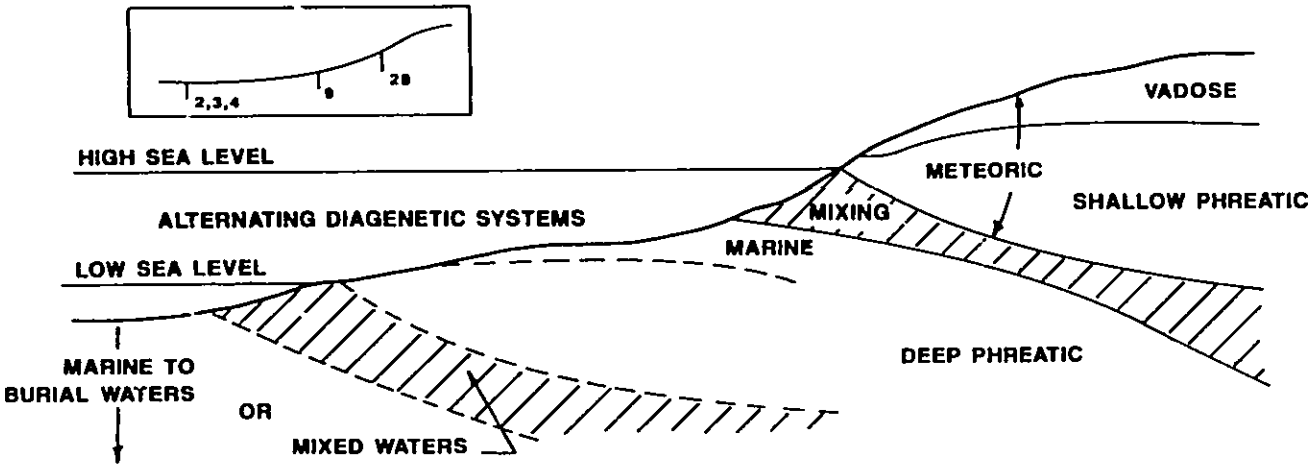

IDEALIZED DIAGENETIC SUCCESSIONS

Figure 5-7

a) Succession produced by "normal" diagenetic sequence - from marine to burial systems (no meteoric influence; e.g. section 11, sequence 2). 1- Marine cementation (HM), 2- shallow to deeper burial cementation (L1+L2) along with stabilization of early marine cements, 3- Microfracturing and stylolitization contemporaneous with some L2.

b) Succession produced by hydrothermal influx - Paragenetic evolution from marine to hydrothermal, to normal burial (e.g. section 37, sequence 2). 1- Marine cementation (HM), 2- recrystallization by hydrothermal influx, precipitation of sulfate (?), 3- burial cementation, 4- dissolution of sulfate, 5- meteoric cementation. Steps 4 and 5 are not illustrated on the sketch.

c) Succession produced in meteoric environment - marine to meteoric systems (e.g. section 35, sequence 3). 1- Marine cementation (HM), 2- corrosion and recrystallization of early marine cements, 3- precipitation of meteoric calcite (MT2), 4- burial cementation.

IDEALIZED DIAGENETIC SEQUENCES

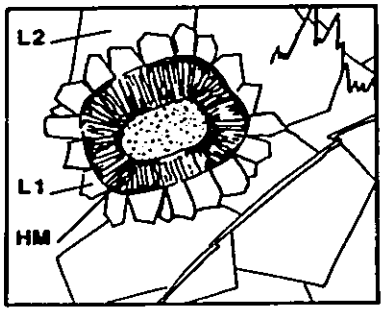

A

PROGRESSIVE BURIAL DIAGENESIS

	$\delta^{18}O$	$\delta^{13}C$	$^{87}Sr/^{86}Sr$
HM	-6 to -1	+4 to +8	0.7085 to 0.7090
L1 + L2	-16 to -3	+4 to +6	0.7085 to 0.7095

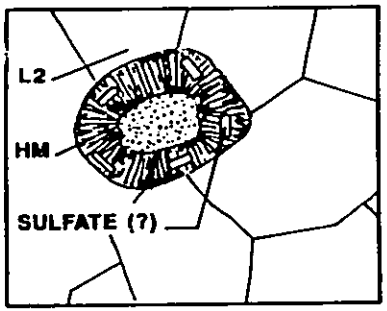

B

HYDROTHERMAL INFLUX

HM (hydrothermal recrystallization)	-15 to -7	+4 to +5	0.7084 0.7091
L2	-7 to -5	+5 to +7	0.7095

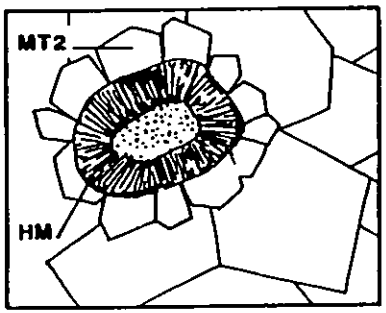

C

METEORIC DIAGENESIS

(HM)			
MT2	-15	+ 4 to +5	0.7103
L2	-8	+3 to +4	0.7090

APPROXIMATE TEMPERATURE OF LATE CEMENTATION

Table 5-2

Calculation of the possible temperature of precipitation of the late cement. The calculation was based on the assumption that the $\delta^{18}O$ values of the "late" parent waters varied from entirely meteoric to entirely marine. The respective proportion of these waters was estimated according to the diagenetic history discussed in chapters 4 and 5. For instance, in section 42 the late parent waters were probably 100 % meteoric, with $\delta^{18}O$ taken as -12.6 ‰ (SMOW). For section 2, two alternatives were taken because in some cases the proportion of meteoric waters was perhaps 50 % and the $\delta^{18}O$ intermediate between the marine and the meteoric end members ((-2.5 ‰ + -11 ‰) ÷ 2 = -6.75 ‰). In other cases, the meteoric proportion was probably 0 %. The calculated temperatures are compared to those obtained by Utting *et al.* (1989) utilizing the Conodont Alteration Index (CAI).

Note that if the parent waters were more saline than inferred here, the estimated temperatures of precipitation would increase. Nevertheless, the possible depth of precipitation would still remain relatively shallow. This is the important conclusion of this exercise.

TABLE 5-2

Seq. #	Section this study	Late cement (‰ PDB) lowest $\delta^{18}O$	% of meteoric components in parent waters[1]	Water $\delta^{18}O$ (SMOW)	T (°C) Craig (1965)[2]	Utting et al. (1989) CAI	Utting et al. (1989) T (°C)
4	27	-13.0	50 or	-7.0	47	1.0	50-80
		-13.0	100	-12.6	19		
	17 and 18	-7.0	0	-1.5	44	1.5/1.0	50-140
	42	-21.7	100	-12.6	66	perhaps 1.5	50-90
3	28	-9.0	50	-6.75	27	1.0	50-80
	2	-11.3	0 or	-2.5	64	2.0/3.5	60-200
		-8.5	50	-6.75	25		
2	37	-7.5	0	-1	50	4.5	300-900
	9.5	-10.5	0	-1	69	4/5	190-480
	11	-13.0	0	-1	86	4/5	190-480

[1] The $\delta^{18}O$ relative to SMOW for meteoric and marine end members are estimated to be: -12.6, -1.5; -11, -2.5; and -11 and -1‰ for sequences 4, 3 and 2, respectively. The percentages of meteoric components are guessed from the inferred diagenetic history of the sections (see "Basin History", 5.4.2.).

[2] $T^{\circ}(C) = 16.9 - 4.2\,(\delta^{18}O_{cal\ (PDB)} - \delta^{18}O_{wat\ (SMOW)}) + 0.13\,(\delta^{18}O_{cal\ (PDB)} - \delta^{18}O_{wat\ (SMOW)})^2$

6. ISOTOPIC COMPOSITION OF THE SVERDRUP SEAWATER

For the studied time span, Late Carboniferous to Early Permian, a compilation of published data illustrates that the isotopic signal for the coeval seawater is not well constrained (fig. 6-1).

Considerations of the systematics of alteration for isotopic signals during diagenesis suggest that the "best estimates" for the isotopic composition of the Sverdrup Seawater should be based on marine cements (calcitized A and recrystallized HMC) with the heaviest $\delta^{18}O$ and $\delta^{13}C$ and the least radiogenic $^{87}Sr/^{86}Sr$. A few brachiopods that were analyzed during this study are shown for comparative purposes. These brachiopods were selected for isotopic studies on the basis of their nonluminescent pattern. Only the "best" specimens were compiled.

Compared to the published data, the Late Paleozoic oxygen and carbon isotopic signals for the Sverdrup seawater appear to be monotonous and at times slightly enriched in ^{18}O and ^{13}C. In contrast, the ^{87}Sr-content declines with time (table 6-1 and fig. 6-1). The overall $\delta^{13}C$ signal is marginally enriched in ^{13}C relative to the values proposed by Popp *et al.* (1986 a) and up to 3 ‰ relative to Brand (1989 a). Beauchamp *et al.* (1987) suggested that the heavy $\delta^{13}C$ typical of the Sverdrup Basin resulted from a massive sequestering of ^{12}C-rich organic matter into fine sediments within the basin as well as from high evaporation in a semi-arid to arid climate. The best values for $\delta^{18}O$ compare well with the results of Popp *et al.* (1986 a), but diverge considerably (-1 to +5.5 ‰) from

the Moscovian results of Brand (1989 a). One could argue that the samples of Brand (1989 a) were of open marine variety, whereas the Moscovian Sverdrup Basin represented a partially enclosed water body with enhanced salinity and temperature. Yet, even these environmental considerations could hardly explain the isotopic discrepancies. Any increase in $\delta^{18}O$ due to enhanced salinity within the Sverdrup Basin would be counteracted by higher temperatures. Also, carbon isotope fractionation due to salinity and temperature is relatively minor and, within realistic scenarios, can hardly account for the observed shifts of about 4 ‰. Note that the heaviest specimens in Popp *et al.* (1986 a) and the "best" cements in the present study yield comparable results. This suggests that the Moscovian estimates of Brand (1989 a) perhaps were in part based on altered samples.

The observed strontium isotope trend is somewhat more radiogenic than the results obtained by Popp *et al.* (1986 b), but of similar shape (Table 6-1; fig. 6-1). These higher ratios likely signify that the studied marine components have been affected somewhat by ^{87}Sr-rich diagenetic waters.

Recrystallization of marine cements by saline burial waters could produce neomorphic dLMC, with $\delta^{18}O$ values even higher than the marine precursor, provided that the salinity is high enough to counteract the effect of temperature. In the same train of thought, recrystallization by cold marine waters could produce phases with heavier $\delta^{18}O$ values as well.

ISOTOPIC ESTIMATES OF SVERDRUP SEA COMPOSITION

Table 6-1

The estimates of marine signals for sequence 2 (Lower to Upper Moscovian), sequence 3 (Asselian) and sequence 4 (Artinskian). These are based on the heaviest results for the $\delta^{18}O$ and $\delta^{13}C$, the least radiogenic values for $^{87}Sr/^{86}Sr$ measurements in marine cements of original A and HMC mineralogy, and complemented by measurements on coeval brachiopods (B). If, instead of a single sample, the mean of the 5 or 10 heaviest samples is utilized for this evaluation, the marine signal departs only slightly from the suggested values.

TABLE 6-1

AGE	SAMPLE	$\delta^{18}O$ (PDB) ‰	$\delta^{13}C$ ‰	$^{87}Sr/^{86}Sr$
Artinskian	HMC	-1.4	+7.5	0.70787
	B	-1.8	+4.1	
Asselian	HMC	-2.5	+6.8	0.70847
	A west			0.70833
Upper	HMC west			0.70843
Moscovian	A east	-0.4	+7.9	0.70856
	HMC east	-1.5	+6.7	0.70857
Lower	B	-0.5	+7.0	
Moscovian	A	-3.0	+7.0	0.70911

UPPER CARBONIFEROUS TO EARLY PERMIAN SEAWATER COMPOSITION

Figure 6-1

Marine $\delta^{18}O$, $\delta^{13}C$ and $^{87}Sr/^{86}Sr$ temporal variations during the studied time span. Literature estimates are compared with the estimates obtained in this study.

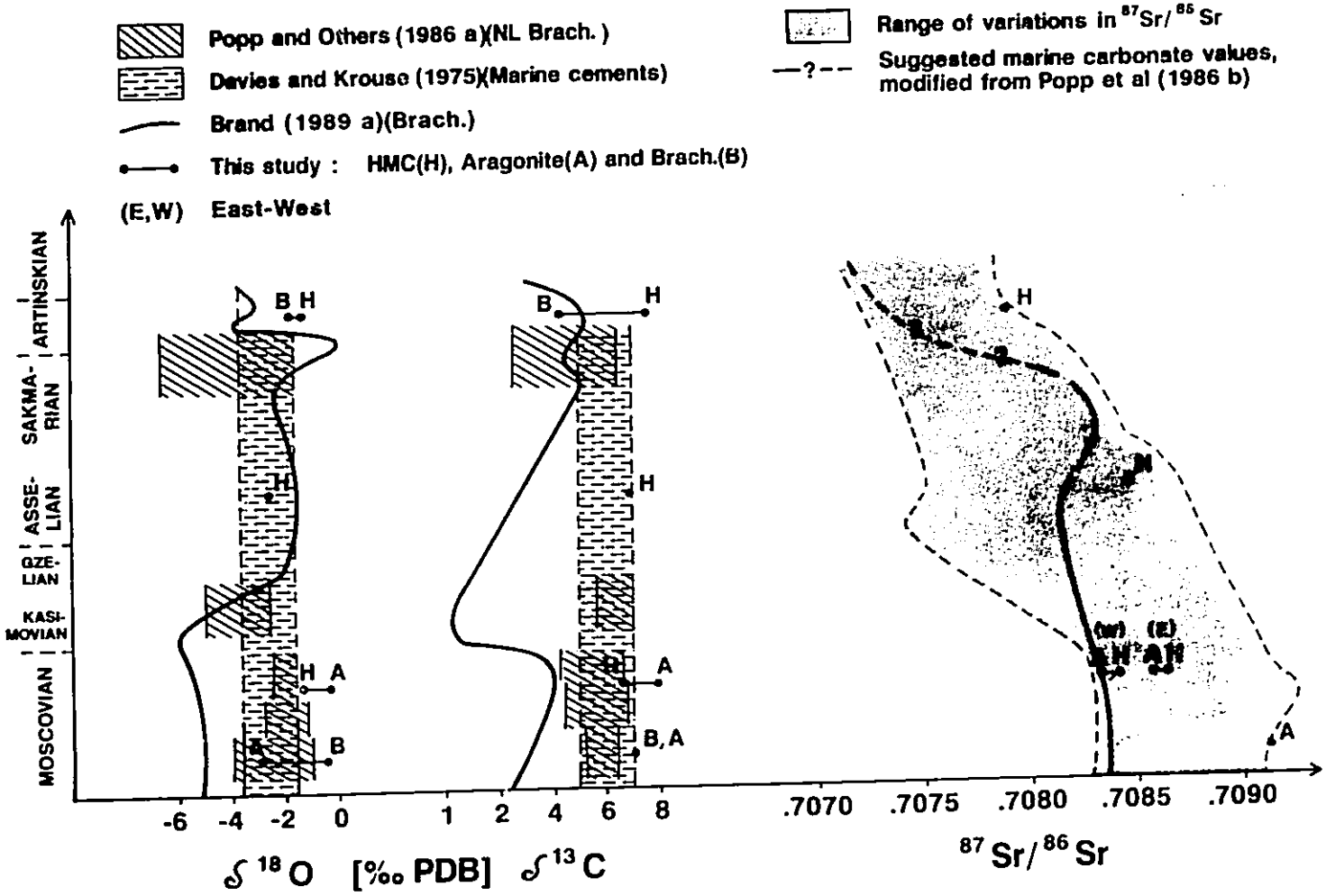
Popp and Others (1986 a)(NL Brach.)
Davies and Krouse (1975)(Marine cements)
Brand (1989 a)(Brach.)
This study : HMC(H), Aragonite(A) and Brach.(B)
(E,W) East-West
Range of variations in 87Sr/86Sr
Suggested marine carbonate values, modified from Popp et al (1986 b)
MOSCOVIAN
KASI-MOVIAN
GZE-LIAN
ASSE-LIAN
SAKMA-RIAN
ARTINSKIAN
-6 -4 -2 0 1 2 4 6 8
δ 18O [‰ PDB] δ 13C
.7070 .7075 .7080 .7085 .7090
87Sr/86Sr

7. THE CHEMISTRY OF CATHODOLUMINESCENCE ZONES IN CALCITE

The petrography of carbonate cements today is based on the combination of criteria from studies by light microscope, cathode-luminoscope, fluoroscope, SEM, and staining. In particular, the CL is a useful tool for deciphering the details of crystal growth. The entire concept of cement stratigraphy is based on this approach. Furthermore, the absence of luminescence, or uniform cathodoluminescence patterns are popularly considered to signify good preservation of the cements, while blotchy or composite CL patterns are attributed to recrystallization (Meyers, 1978; Given and Lohmann, 1985). The causes of CL intensity are, however, complex, although many researchers believe that it reflects the nature of chemical "impurities" (*e.g.* Meyers, 1974; Amieux, 1981; Reed and Grover; 1983). The consensus attributes CL intensity to the Mn/Fe ratios, a supposition based mostly on electron probe results, that is on data frequently falling near the detection limit of the technique. In this study, SIMS was employed to test the above assertions.

7.1 TYPES OF CATHODOLUMINESCENCE IN CALCITE

The intensities of luminescence in calcite are usually grouped into four categories: nonluminescent (dead or black), very dull, dull (brown) and luminescent (bright yellow or orange). Within a single crystal, numerous CL zones can alternate in either a regular or a sporadic way, commonly revealing features that are not

discernible by light microscopy (LM). CL is a routine tool in studies of petrography and diagenesis of carbonates, frequently utilized for cement "stratigraphy" and correlated on a basin wide scale. It is therefore essential to understand the reasons for luminescent zoning.

In theory, emission of luminescence from excited calcite crystals is produced either by defects, sector zoning, trace elements, or by a combination of these causes (Amieux, 1982; Miller, 1988; Machel *et al.* 1991). The control of luminescence by trace elements results from a combination of activation, sensitization and quenching. Activators (Mn^{2+}, Pb^{2+}, Cu^{2+}, Zn^{2+}, Ag^{+}, Bi^{+} and Mg^{2+}?) are trace elements that have outer electrons undergoing energy transitions when excited by an incident electron beam. The excited electrons emit energy as luminescent radiation when returning to their original energy level. Sensitizers (Pb^{2+}, Ce^{2+} and Ce^{4+}) absorb some of the energy and, by electron transfer, totally or partially transmit it to activators. In doing so, they increase the net intensity of the luminescence without changing the wavelength. Finally, quenchers (Fe^{2+}, Ni^{2+} and Co^{2+}) absorb energy without emitting radiation, their electrons returning to stable state by non radiative transition. This suppresses the activator and sensitizer effects, leading to a lower intensity of luminescence.

For the last fifteen years, Mn and Fe were commonly regarded as the main activator and quencher for calcite. This dogmatic simplification led to the popular

perception that luminescence and redox state of the diagenetic environment are directly related (Amieux, 1982; Reed and Grover, 1983; Meyers, 1978; Barnaby and Rimstidt, 1989; Emery and Dickson, 1989; and others). In reality, the causes of luminescence have never been well documented. The suggested roles of Fe and Mn as the main controls of luminescence in calcite needs testing.

Previous studies directly dealt with the chemistry of luminescence from well separated CL zones in natural or artificial carbonates using an electron probe (Fairchild, 1983; ten Have and Heijnen, 1985; Hemming, *et al.*, 1989). Only a few studies applied new analytical techniques that have higher sensitivity and thus the ability to measure point concentrations of trace elements at the levels typical for natural carbonates (Mason, 1987; Fraser *et al.*, 1989). The purpose of the present ion probe study was to measure the concentrations of Fe (possible quencher), Mn and Mg (possible activators), and Ce (possible sensitizer) in luminescent, non-luminescent and dull zones of natural calcites. Considering that the detection limits for Fe and Mn by SIMS are approximately 10 ppm, the ion microprobe resolution capabilities are superior to those achieved by electron probes (detection limits were 375 and 350 ppm for Dorobek, 1987; 200 and 100 ppm for Hemming *et al.*, 1989).

The study is based on 111 spot analyses of visually identified uniform CL zones (31 NL, 58 Dull and 22 Lum). Spots that overlapped two or more adjacent zones were excluded. Most, but not all, marine cements were ignored in this discussion

because of their composite CL nature. The investigated CL zones are developed in A, MT, L1 and L2 cements that originated in marine, marine to meteoric phreatic, and calcretic diagenetic environments (see chapters 3, 4 and 5).

7.2 RESULTS

Factor analysis of all luminescent zones yields 2 factors that control their CL intensities and chemical composition (table 7-1). Factor 1, with positive loadings of Fe, Ce, Mg and Mn, shows their sympathetic behaviour in diagenetic systems, related to the fact that they all have several redox states and that their partition coefficients $D_{calcite/water}$ exceed unity (Ce is unknown). The second factor shows the positive loadings by luminescence and Mn. Considering the low communality (proportion of variation in CL explained by both factors) for luminescence, the statistical importance of this factor is minimal. In other words, the statistics accumulated here can explain very little of the variations in CL intensity.

The Fe-Mn scatterplot (fig. 7-1) illustrates only that it is possible to delineate three chemical domains. Domain 1 comprises only the dull zones and domain 2 only the luminescent ones. Domain 3, which covers the range where most natural calcites occur, can harbor any of the above as well as nonluminescent zones. Dull luminescence, likely due to efficient quenching, occurs at Fe concentrations that

exceed 1000 to 1500 ppm (domain 1). Below this Fe threshold, luminescence is activated at Mn contents above some 225 ppm (domain 2). At Mn and Fe concentrations below 225 and 1000 ppm, respectively, nonluminescent, luminescent and dull zones can occur randomly (domain 3).

The effect of the possible activators (Mn and Mg) and sensitizer (Ce) is possibly cumulative. However, a plot of Fe vs Ce+Mg+Mn did not reveal any more consistent picture than the one already discussed, and only two chemical domains were recognizable: dull, with Fe content in excess of 1400 ppm, and an undifferentiated one below this value.

Following the hypothetical relationship between luminescence and redox conditions (Barnaby and Rimstidt, 1989), dull cements should have precipitated under reducing conditions and luminescent ones in more oxygenated environments. The above results for domain 3 (fig. 7-1) however show that the relationship of the redox sensitive Fe-Mn pair is not the sole control of cathodoluminescence zoning. As proposed by other workers, other activators, sensitizers and quenchers (Pb^{+2}, several REE, Cu^{2+}, Zn^{2+}, Ag^{+}, Bi^{+}; Pb^{2+}; Ce^{2+}, Ce^{4+}, several REE; Ni^{2+}, Co^{2+}; Machel, 1985) or other centres of luminescence (lattice imperfections; Amieux, 1982; Miller, 1988; Machel and Burton, 1991) ought to influence the actual cathodoluminescence emitted in this domain (3). The only clear limit that emerges from this study is the Fe-threshold of 1000 to 1500 ppm that separates the dull area from the luminescent and

undifferentiated domains (fig. 7-1). This threshold is comparable to the 1600 ppm threshold that was advocated by Mason (1987).

CHEMISTRY OF CATHODOLUMINESCENCE - FACTOR ANALYSIS

Table 7-1

Conditions of analysis as in table 4-1. CL intensity was visually evaluated (4: luminescent, 3: dull, 2: very dull, 1: nonluminescent) and used as a variable for statistical analysis.

Fe-Mn CATHODOLUMINESCENCE DOMAINS

Figure 7-1

Fe-Mn diagram showing the dull (1), luminescent (2) and undifferentiated (3) domains for calcite in cathodoluminescence.

TABLE 7-1

Chemistry of CL

Variable/Factor	1	2	N	Est. communality
Log Mg	0.47	-0.15	111	0.25
Log Sr	0.66	0.27	111	0.50
Log Fe	0.82	0.27	111	0.74
Log Mn	0.43	0.67	111	0.64
CL Intensity	-0.04	0.59	111	0.36
Eigenvalue	1.88	0.60		
% of variation	76	24		

Cathodoluminescence domains 7-1

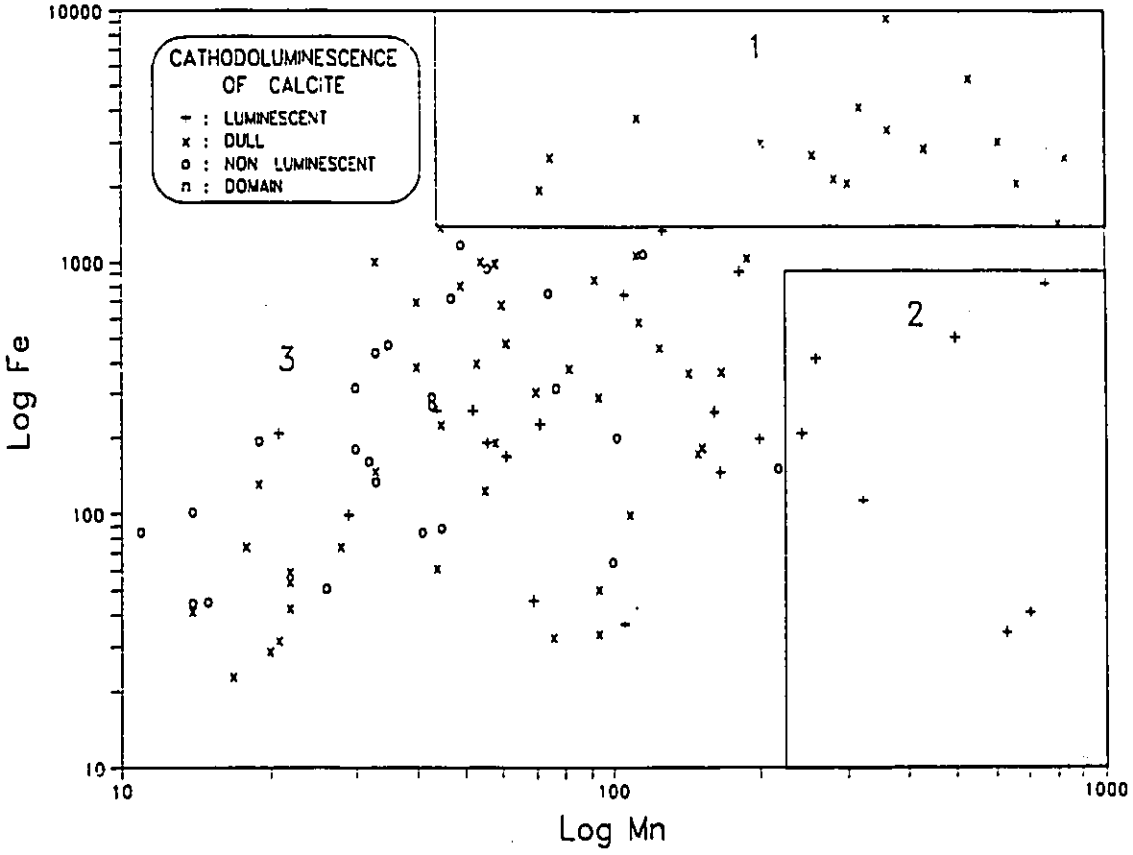

8. CONTRIBUTIONS OF THIS STUDY

This study dealt with numerous aspects of carbonate diagenesis, and its main contributions are summarized below.

Categorization of cements

On the basis of petrography, calcite cements sampled in the Upper Paleozoic carbonate sequences 2, 3 and 4 of the Sverdrup Basin were separated into two large groups: neomorphic and primary. The neomorphic cements were interpreted as successors after original HMC and A marine precursors, whereas the primary cements were precipitated directly as low-Mg calcites. The latter were subdivided into meteoric (MT1, MT2 and MT3) and late (L1 and L2) cements.

Regardless of age or location, the broad petrographic categories of cements have distinctive, although overlapping, geochemical attributes. Successors to marine aragonitic cements have Sr contents frequently in excess of 1000 ppm, whereas the remaining types of cements have mean contents of about 250 ppm. The most notable features are, however, the conspicuous depletions in ^{18}O and ^{13}C and the significant enrichment in ^{87}Sr from early marine to late and to meteoric cements. Geochemical attributes ($\delta^{18}O$, $\delta^{13}C$, $^{87}Sr/^{86}Sr$, Mg, Sr, Fe and Mn) agree with the petrographic categorization of cements. Three broad categories have been distinguished: marine (neomorphic after A- and HMC-precursors), meteoric (from calcrete and very shallow shelf) and late (marine phreatic and burial *stricto sensu*).

Early cements

In CL, six recrystallization patterns were recognized in the stabilized former A-cements: four *in situ* dissolution-reprecipitation products (AIR, AFN, AMY and AOO) and two apparent "whole-sale" dissolution-reprecipitation products (AMD and AVO). Five patterns (HM1, HM2, HM3, HM4 and HMRH) were distinguished in former HMC-cements. These complex patterns and their relationships suggest that their diagenetic stabilization has been accomplished via multiple microenvironments, at diverse W/R, and probably involved more than one dissolution-reprecipitation step.

For the marine neomorphic cements, the CL patterns - stages of textural preservation - do not correlate with isotopic preservation. Many texturally well preserved cements show clearly altered isotopic signatures and *vice versa*.

Meteoric cements

The meteoric cements from calcretes have typical meteoric signals ($\delta^{18}O$ and $\delta^{13}C$ of -8.5 and -4.5 ‰ and $^{87}Sr/^{86}Sr$ of 0.7102), whereas the shelf facies "MT2" cements have marine $\delta^{13}C$-values but their $\delta^{18}O$-cover a range between theoretical marine and meteoric end-members (from -4.5 to -10.5 ‰). The calcrete cements represent "pure" meteoric products whereas the MT2 cements could have been formed in a mixed marine-meteoric environment. The isotopic values obtained from calcrete (after correction for evaporation) and from the depleted end-member of the MT2 cements,

both with $\delta^{18}O$ of about -11 ‰ (PDB), reflect the composition of the coeval meteoric water.

Late cements

The category of "late cements" is defined on the basis of the relative timing of precipitation and intentionally ignores the possible diagenetic environments, because the cements could have precipitated from many types of diagenetic waters.

Most of the late cements precipitated in very shallow burial, even phreatic marine, or possibly mixed phreatic meteoric-marine environments. Only a low percentage of the population has undeniable "burial" petrographic and geochemical attributes. But even these "burial" cements likely occluded the remaining pore space before one kilometre of burial was attained.

Trace elements

For trace element investigations, the Secondary Ion Mass Spectrometry technique was applied. This constitutes a precedent in the study of cement geochemistry. The daily measurement of standards gave a precision of 12, 6, 6 and 6 % for Mg, Fe, Mn and Sr, respectively.

Diagenesis of the studied sequences

In sequence 2, the western region of the Moscovian basin was affected by upward migration of oxygenated hot brines. This presumed hydrothermal activity was responsible for stabilization of marine cements that are markedly depleted in ^{18}O. In contrast, the eastern region underwent normal and gradual burial diagenesis.

In sequence 3, petrographic criteria and geological considerations suggest that the precipitation of early marine cements of HMC mineralogy was followed by cyclic, and probably partial, exposure to the meteoric diagenetic realm that perhaps resulted in partial dissolution and recrystallization in sections 9, 28 and 35, and precipitation of meteoric cements in section 35. In sections 2, 3 and 4, dissolution and recrystallization were produced either by mixed meteoric-marine or saline waters. The late cements probably formed in mixed phreatic (meteoric-saline waters) and shallow burial (saline waters) environments; a land to basin chemical gradient in the diagenetic waters is suggested by greater proportions of meteoric components in the landward sections.

In sequence 4, recrystallized HMC cements are tightly grouped in the $\delta^{13}C$-$\delta^{18}O$ diagram. In contrast, the associated brachiopods showed a broader range of results. These are non luminescent brachiopods which have been partially isotopically reset in meteoric waters during the drastic seawater regression in the Early Kungurian.

As indicated above, meteoric waters are not the only fluids that promote recrystallization of shelf edge carbonates. Hydrothermal, cold marine (?), phreatic marine and burial waters probably fostered stabilization of the marine cements studied herein.

Isotopic signals of Sverdrup seawater

Through the studied time span, the "best" $\delta^{18}O$ and $\delta^{13}C$ results for cements indicate that the Sverdrup seawater signal remained relatively constant. It falls within the range of previously published data, although at their heavy end-member. On the other hand, Sr isotopes are more radiogenic than the published values that were obtained from brachiopods. These higher ratios likely signify that the studied marine components have been somewhat affected by ^{87}Sr-rich waters. Nevertheless, the trend agrees with the global evolution from more radiogenic values in the Moscovian to less radiogenic ones in the Artinskian.

The best results obtained for nonluminescent brachiopods in this study compare well with the results for cements. As discussed earlier, both ancient brachiopods and marine cements can only give "best" estimates of the isotopic composition of the ancient marine waters.

Chemistry of cathodoluminescence zones in calcite

In the Fe-Mn space, an Fe-threshold of 1000 to 1500 ppm separates the dull domain from the luminescent and undifferentiated ones. Below this threshold, calcite luminescence is activated at Mn concentrations of some 225 ppm (luminescent domain). However, at Fe and Mn concentrations below these thresholds, the type of luminescence is independent of chemical attributes. The existence of this undifferentiated domain implies that the redox sensitive Fe-Mn pair is not the sole control on CL zoning.

These results, along with the isotopic data obtained for the CL patterns in neomorphic calcites, reveal that the relationship between CL textures and geochemical attributes is not straightforward. Although it would be better to avoid the interpretation of CL in terms of chemistry, the luminoscope remains a useful petrographic tool.

9. RESEARCH PERSPECTIVE IN THE SVERDRUP BASIN

This study establishes a framework on which numerous specific projects could be based. As the studied area was too large for a single Ph.D. project, and the sampling was limited by the cost and logistics of field work in the Canadian Arctic, new studies with tighter regional coverage would be useful for detailing the diagenetic history of carbonate sequences in the Sverdrup Basin.

As suggested earlier, hydrothermal activity was likely active during the deposition of sequence 2. This activity could have been responsible for the massive dolomitization that is observed along the faults; this hypothesis requires further testing. Brine migration through permeable massive carbonates could have resulted in MVT or SEDEX deposits. Consequently, delineation of the regional extent of this hydrothermal anomaly is of importance for exploration.

The suggested influence of fourth- to fifth-order cycles related to sequence stratigraphy on late cementation could be verified on a tighter scale, utilizing the numerous cycles that extend from the inner to the outer shelf. In addition, the categorization of parent fluids for late cements could be greatly improved by fluid inclusion studies.

The models suggested as explanations of the covariation of tracers could be further tested by numerical modelling. This could lead to rejection or improvement of the models.

With new discoveries of mud mounds (Beauchamp *et al.* 1991), it is now possible to fill some gaps in the isotopic curves for seawater of the Sverdrup basin. The detailed signal could be based on the parallel investigation of brachiopods and early marine cements.

REFERENCES

ADAMS, A.E., SCHOFIELD, K. (1983). Recent submarine aragonite, magnesium calcite and hematite cements in gravel from Islay, Scotland. Journal Sedimentary Petrology, v.53, p.417-421.

AISSAOUI, D.M. (1985). Botryoidal aragonite and its diagenesis. Sedimentology, v.32, p.345-361.

AISSAOUI, D.M. (1988). Magnesian calcite cements and their diagenesis: dissolution and dolomitization, Mururoa Atoll. Sedimentology, v.35, p.821-841.

AL-AASM, I., VEIZER, J. (1986a). Diagenetic stabilization of aragonite and Low-Mg calcite, I. Trace elements in Rudists. Journal Sedimentary Petrology, v.56, p.138-152.

AL-AASM, I., VEIZER, J. (1986b). Diagenetic stabilization of aragonite and Low-Mg calcite, II. Stable Isotopes in Rudists. Journal Sedimentary Petrology, v.56, p.763-770.

AMIEUX, P. (1982). La cathodoluminescence: méthode d'étude sédimentologique des carbonates. Bulletin des centres de recherche exploration-production. Elf-Aquitaine, v.6, p.437-483.

ANDERSON, T.F., ARTHUR, M.A. (1983). Stable isotopes of oxygen and carbon and their application to sedimentologic and paleoenvironmental problems. In "Stable Isotopes in Sedimentary Rocks", Society of Economic Paleontologists and Mineralogists (SEPM), short course no. 10, Dallas 1983, chap. 1.

ASSERETO, R., FOLK, R.L. (1980). Diagenetic fabric of aragonite, calcite, and dolomite in an ancient peritidal-spelean environment: Triassic Calcare Rosso, Lombardia, Italy. Journal Sedimentary Petrology, v.50, p.371-394.

BANNER, J.L., HANSON, G.H. (1990). Calculation of simultaneous isotopic trace element variations during water-rock interaction with applications to carbonate diagenesis. Geochimica et Cosmochimica Acta, v.54, p.3123-3137.

BARBIN, V., RAMSEYER, K., DEBENAY, J.P., SCHEIN, E., ROUX, M., DECROUEZ, D. (1991). Cathodoluminescence of Recent biogenic carbonates: an environmental and ontogenic fingerprint. Geological Magazine, v.128, p.19-26.

BEAUCHAMP, B. (1987). Stratigraphy and facies analysis of the Upper Carboniferous to Lower Permian Canyon Fiord, Belcher Channel and Nansen Formations, Southwestern Ellesmere Island. Unpublished Ph.D. thesis, University of Calgary, Alberta, 370 p.

BEAUCHAMP, B., OLDERSHAW, A.E., KROUSE, R. (1987). Upper Carboniferous to Upper Permian ^{12}C-enriched primary carbonates in the Sverdrup Basin, Canadian Arctic: comparisons to coeval western north american occan margins. Chemical Geology, v.65, p.391-413.

BEAUCHAMP, B. (1989 a). Lower Permian (Artinskian) Sponge-Bryozoan Buildups, Southwestern Ellesmere Island, Canadian Arctic Archipelago. In Reefs, Canada and adjacent areas, edited by H.H.J. Geldsetzer, N.P. James and G.E. Tebbut, Canadian Society of Petroleum Geologists, Memoir 13, p.575-584.

BEAUCHAMP, B. (1989 b). Lower Permian (Sakmarian) *Tubiphytes*-Bryozoan Buildup, Southwestern Ellesmere Island, Canadian Arctic Archipelago. In Reefs, Canada and adjacent areas, edited by H.H.J. Geldsetzer, N.P. James and G.E. Tebbut, Canadian Society of Petroleum Geologists, Memoir 13, p.585-589.

BEAUCHAMP, B., DAVIES, G.R., NASSICHUK, W.W. (1989 a). Upper Carboniferous to Lower Permian Palaeoaplysina-Phylloid Algal Buildups, Canadian Arctic Archipelago. In Reefs, Canada and adjacent areas, edited by H.H.J. Geldsetzer, N.P. James and G.E. Tebbut, Canadian Society of Petroleum Geologists, Memoir 13, p.590-599.

BEAUCHAMP, B., HARRISON, J.C., HENDERSON, C.M. (1989 b). Upper Paleozoic stratigraphy and basin analysis of the Sverdrup Basin, Canadian Arctic Archipelago: Part 1, time frame and tectonic evolution. In Current Research, Part G, Geological Survey of Canada, Paper 89-1G, p.105-113.

BEAUCHAMP, B., HARRISON, J.C., HENDERSON, C.M. (1989 c). Upper Paleozoic stratigraphy and basin analysis of the Sverdrup Basin, Canadian Arctic Archipelago: Part 2, transgressive-regressive sequences. In Current Research, Part G, Geological Survey of Canada, Paper 89-1G, p.115-124.

BEAUCHAMP, B. OLCHOWY, B., HENDERSON, C.M. (1991). A newly recognized Lower Permian reef tract, west-central Ellesmere Island, Arctic Archipelago. Current Research, Part B, Paper 91-1B, p. 23-32.

BEAUCHAMP, B., HENDERSON, C.M. (In press). The LOwer Permian (Artinskian) Raanes, Great Bear Cape and Trappers Cove Formations: three new stratigraphic units of the Sverdrup Basin, Canadian Arctic. Geological Survey of Canada Bulletin.

BEAUCHAMP, B. (In prep.). Carboniferous and Permian reefs of Sverdrup Basin, Canadian Arctic: an aid to Barents Sea exploration.

BRAND, U. (1989 a). Biogeochemistry of Late Paleozoic North America brachiopods and secular variation of seawater composition. Biogeochemistry, V.7, p.159-193.

BRAND, U. (1989 b). Aragonite-calcite transformation based on Pennsylvanian molluscs. Geological Society America Bulletin, v.101, p.377-390.

BRAND, U., VEIZER, J. (1980). Chemical diagenesis of a multicomponent carbonate system - 1: Trace elements: Journal Sedimentary Petrology, v.51, p.987-998.

BUCHBINDER, L.G., FRIEDMAN, G.M. (1980). Vadose, phreatic and marine diagenesis of Pleistocene-Holocene carbonates in a borehole: Mediterranean coast of Israel. Journal Sedimentary Petrology, v.50, p.395-408.

BUDD, D.A., LAND, L.S. (1990). Geochemical imprint of meteoric diagenesis in Holocene ooid sands, Schooner Cays, Bahamas: Correlation of calcite cement geochemistry with extant groundwaters. Journal Sedimentary Petrology, v.60, p.361-378.

BUHL, D., NEUSER, R.D., RICHTER, D.K., RIEDEL, D., ROBERTS, B., STRAUSS, H., VEIZER, J. (1991). Nature and nurture: environmental isotope story of the River Rhine. Naturwissenschaften, in press.

BURKE, W.K., DENISON, R.E., HETHERINGTON, E.A., KOEPNICK, R.B., NELSON, H.F., OTTO, J.B. (1982). Variation of seawater $^{87}Sr/^{86}Sr$ throughout Phanerozoic time. Geology, v.10, p.516-519.

CHOQUETTE, P.W., JAMES, N.P. (1987). The deep burial environment. Diagenesis #12. Diagenesis in limestones. Geoscience Canada, v.14, p.3-35.

CONIGLIO, M. (1989). Neomorphism and cementation in ancient deep-water limestones, Cow Head Group (Cambro-Ordovician) western Newfoundland, Canada. Sedimentary Geology, v.65, p.15-33.

DAVIES, G.R. (1977). Former magnesian calcite and aragonite submarine cements in Upper Paleozoic reefs of the Canadian Arctic: a summary. Geology, v.5, p.11-15.

DAVIES, G.R., KROUSE, H.R. (1987). Carbon and oxygen isotopic composition of late paleozoic calcite cements, Canadian Arctic Archipelago - preliminary results and interpretation. In Current Research , Part B, Geological Survey of Canada, Paper 75-1, p.215-220.

DAVIES, G.R., NASSICHUK, W.W. (1980). Stratigraphy and sedimentation of the Otto Fiord Formation - a major Mississipian-Pensylvanian evaporite of subaqueaous origin in the Canadian Arctic Archipelago. Geological Survey of Canada, Bulletin 286, 87 p.

DAVIES,G.R., NASSICHUK, W.W. (1990). Submarine cements and fabrics in Carboniferous to Lower Permian, reefal, shelf margin and slope carbonates, Northwestern Ellesmere Island, Canadian Arctic Archipelago. Geological Survey of Canada, bulletin 399, 77 p.

DAVIES, G.R., NASSICHUK, W.W., BEAUCHAMP, B. (1989). Upper Carboniferous "Waulsortian" Reefs, Canadian Arctic Archipelago. In Reefs, Canada and adjacent areas, edited by H.H.J. Geldsetzer, N.P. James and G.E. Tebbut, Canadian Society of Petroleum Geologists, Memoir 13, p.658-666.

DAVIES, G.R., RICHARDS, B.C., BEAUCHAMP, B., NASSICHUK, W.W. (1989). Carboniferous and Permian Reefs in Canada and adjacent areas. In Reefs, Canada and adjacent areas, edited by H.H.J. Geldsetzer, N.P. James and G.E. Tebbut, Canadian Society of Petroleum Geologists, Memoir 13, p.565-574.

EMERY, D., DICKSON, J.A.D. (1989). A syndepositional meteoric phreatic lens in the Middle Jurassic Lincolnshire limestone, England, U.K. Sedimentary Geology, v.65, p.273-284.

FOLK, R.L. (1965). Some aspects of recrystallisation in ancient limestones. In "Dolomitization and limestone diagenesis", edited by L.C. Pray et R.C. Murray. Society Economic Paleontologists Mineralogists, Special Publication No.13, p.14-48.

FOLK, R.L. (1974). The natural history of crystalline calcium carbonate: effect of magnesium content and salinity. Journal Sedimentary Petrology, v.44, p.40-53.

FOWLER, A.D. (1990). Oscillatory zoning in mineral growth: possible period doubling due to non-linear growth dynamics. Geological Association Canada, annual meeting, Vancouver, program with abstracts, v.15, p.A40.

FRIEDMAN, G.M. (1964). Early diagenesis and lithification in carbonate sediments. Journal Sedimentary Petrology, v.34, p.777-813.

FRYKMAN, P. (1986). Diagenesis of Silurian bioherms in the Klinteberg Formation, Gotland, Sweden. In "Reef Diagenesis", edited by J.H. Schroeder and B.H. Purser, Springer-Verlag, p.399-423.

GELDSETZER, H.H.J, JAMES, N.P., TEBBUTT, G.E. (1988). Reefs, Canada and adjacent areas. Memoir 13, Canadian Society Petroleum Geologists, 775 p.

GIVEN, R.K., LOHMANN, K.C. (1985). Derivation of the original isotopic composition of Permian marine cements. Journal Sedimentary Petrology, v.55, p.430-439.

GROVER, G. Jr. READ, J.F. (1983). Paleoaquifer and deep burial related cements defined by regional cathodoluminescent patterns, Middle Ordovician carbonates, Virginia. American Association Petroleum Geologists Bulletin, v.67, p.1275-1303.

HECKEL, P.H. (1983). Diagenetic model for carbonate rocks in Midcontinent Pennsylvanian eustatic cyclothems. Journal Sedimentary Petrology, v.53, p.733-759.

HESSE, R. (1990). Early diagenetic pore water/sediment interaction: modern offshore basins. In "Diagenesis", edited by I.A. Morrow and D.W. Morrow, Geoscience Canada, reprint series #4, p.227-316.

HORBURY, A.D., ADAMS, A.E. (1989). Meteoric phreatic diagenesis in cyclic late Dinantian carbonates, northwest England. Sedimentary Geology, v.65, p.319-344.

HURLEY, N.F., LOHMANN, K.C. (1989). Diagenesis of Devonian reefal carbonates in the Oscar Range, Canning Basin, Western Australia. Journal Sedimentary Petrology, v.59, p.127-146.

JAMES, N.P., CHOQUETTE, P.W. (1990). The Sea Floor Diagenetic Environment. In "Diagenesis", edited by I.A. Morrow and D.W. Morrow, Geoscience Canada, reprint series #4, p.13-34.

JAMES, N.P., GINSBURG, R.N. (1979). The seaward margin of Belize Barrier and atoll reefs. International Association of Sedimentologists, Special Publication number 3, 191 p.

KENDALL, A.C. (1985). Radiaxial fibrous calcite: a reappraisal. In "Carbonate cements" edited by N. Schneidermann and P.M. Harris, Society Economic Paleontologists and Mineralogists, Special Publication No.36, p.59-78.

KENDALL, C.G.St.C., SCHLAGER, W. (1981). Carbonates and relative changes in sea level. Marine Geology, v.44, p.181-212.

KERANS, C., HURLEY, N.F., PLAYFORD, P.E. (1986). Marine diagenesis in Devonian reef complexes of the Canning Basin, Western Australia. In "Reef Diagenesis", edited by J.H. Schroeder and B.H. Purser, Springer-Verlag, p.357-380.

LAND, L.S. (1967). Diagenesis of skeletal carbonates. Journal Sedimentary Petrology, v.37, p.914-930.

LEE, M.R., HARWOOD, G.M. (1989). Dolomite calcitization and cement zonation related to uplift of the Raisby Formation (Zechstein carbonate), Northeast England. Sedimentary Geology, v.65, p.285-305.

LOHMANN, K.C. (1983). Discriminating types of carbonate cements and porosity through geochemistry. In "New ideas and methods for exploration for carbonate reservoirs", Short Course, American Association Petroleum Geologists Annual Meeting, Dallas, Texas.

LOHMANN, K.C. (1988). Geochemical patterns of meteoric diagenetic systems. In "Paleokarst", edited by N.P. James and P.W. Choquette. Springer-Verlag, pp.58-80.

LOHMANN, K.C., MEYERS, W.J. (1977). Microdolomite inclusions in cloudy prismatic calcites: a proposed criterion for former High-Magnesium Calcites. Journal Sedimentary Petrology, v.47, p.1075-1088.

LONGMAN, M.W. (1980). Carbonate diagenetic textures from nearsurface diagenetic environments. Bulletin American Association Petroleum Geologists, v.64, p.461-486.

MACHEL, H. (1985). Cathodoluminescence in calcite and dolomite and its chemical interpretation. Geoscience Canada, v.12, p.139-147.

MACHEL, H. (1986). Early lithification, dolomitization, and anhydritization of Upper Devonian Nisku Buildups, Subsurface of Alberta, Canada. In "Reef Diagenesis", edited by J.H. Schroeder and B.H. Purser, Springer-Verlag, p.336-356.

MACHEL, H. (1987). Saddle dolomite as a by-product of chemical compaction and thermochemical sulfate reduction. Geology, v.15, p.936-940.

MACHEL, H. (1989). Relationship between sulphate reduction and oxidation of organic compounds to carbonate diagenesis, hydrocarbon accumulations, salt domes, and metal sulphide deposits. Carbonates and Evaporites, v.4, p.137-151.

MACHEL, H., BURTON, E.A. (1991). Factors governing cathodoluminescence in calcite and dolomite, and their implications for studies of carbonate diagenesis. In Luminescence Microscopy: Quantitative and Qualitative Aspects, edited by C.E. Barker and D.C. Kopp, SEPM Short course no.25, p.37-57.

MACHEL, H., MASON, R.A., MARIANO, A.N., MUCCI, A. (1991). Causes and emission of luminescence in calcite and dolomite. In Luminescence Microscopy: Quantitative and Qualitative Aspects, edited by C.E. Barker and D.C. Kopp, SEPM Short course no.25, p.9-25.

MACINTYRE, I.G. (1977). Distribution of submarine cements in a modern Caribbean fringing reef, Galeta Point, Panama. Journal Sedimentary Petrology, v.47, p.503-516.

MACQUEEN, R.W., GHENT, E.D. (1970). Electron microprobe study of magnesium distribution in some Mississippian echinoderm limestones from western Canada. Canadian Journal Earth Sciences, v.7, p.1308-1316.

MANHEIM, F.T., SAYLES, F.L. (1974). Composition and origin of interstitial waters of marine sediments, based on deep sea drill cores. In "The Sea", edited by E. D. Goldgerg, Marine Chemistry, v.5, John Wiley & Sons, p.527-568.

MASON, R.A. (1987). Ion microprobe analysis of trace elements in calcite with an application to the cathodoluminescence zonation of limestone cements from the lower carboniferous of South Wales, U.K. Chemical Geology, v.64, p.209-224.

MAZZULO, S.J. (1980). Calcite pseudospar replacive of marine acicular aragonite, and implications for aragonite cement diagenesis. Journal Sedimentary Petrology, v.50, p.409-422.

MEYERS, W.J. (1974). Carbonate cement stratigraphy of the Lake Valley Formation (Mississippian) Sacramento mountains, New Mexico. Journal Sedimentary Petrology, v.44, p.837-861.

MEYERS, W.J. (1978). Carbonate cements: their regional distribution and interpretation in Mississippian limestones of southwestern New Mexico. Sedimentology, v.25, p.371-400.

MEYERS, W.J., LOHMANN, K.C. (1985). Isotope geochemistry of regionally extensive calcite cement zones and marine components in Mississippian limestones, New Mexico. In "Carbonate cements" edited by N. Schneidermann and P.M. Harris, Society Economic Paleontologists and Mineralogists, Special Publication No.36, p.223-239.

MEYERS, W.J. (1989). Trace element and isotope geochemistry of zoned calcite cements, Lake Valley Formation (Mississippian, New Mexico): insights from water-rock interaction modelling. Sedimentary Geology, v.65, p.355-370.

MILLER, J. (1988). Cathodoluminescence microscopy. In "Techniques in Sedimentology", edited by M. Tucker, Blackwell Scientific Publications, p.174-190.

MIRSAL, I.A., ZANKL, H. (1979). Petrography and geochemistry of pore-filling cements in fossil reefs. Geologie Rundschau, v.68, p.920-951.

MORIN, J., BEAUCHAMP, B. DESROCHERS, A. (1991). Preliminary results and interpretations of Early Permian cyclic shelf sedimentation, west-central Ellesmere Island, Arctic Archipelago. Current Research, Part B, Paper 91-1B, p. 71-81.

MUCCI, A., CANUEL, R., SHAOJUN, Z. (1989). The solubility of calcite and aragonite in sulfate-free seawater and the seeded growth kinetics and composition of the precipitates at 25 C. Chemical Geology, v.74, p.309-320.

NELSON, W.A., READ, J.F. (1990). Updip to downdip cementation and dolomitization patterns in a Mississippian aquifer, Appalachians. Journal Sedimentary Petrology, v.60, p.379-396.

NEUGEBAUER, J. (1974). Some aspects of cementation in chalk. In "Pelagic Sediments: on land and under sea", edited by K.J. Hsu and H.C. Jenkins. Special Publications of the International Association of Sedimentologists, No.1, pp.149-176.

PIERSON, B.J., SHINN, E.A. (1985). Cement distribution and carbonate mineral stabilization in Pleistocene limestones of Hogsty Reef, Bahamas. In "Carbonate cements" edited by N. Schneidermann and P.M. Harris, Society Economic Paleontologists and Mineralogists, Special Publication No.36, p.153-168.

POPP, B., ANDERSON, T.F., SANDBERG, P.A. (1986). Brachiopods as indicators of original isotopic compositions in some Paleozoic limestones. Geological Society America Bulletin, v.97, p.1262-1269.

REED, S.J.B. (1989). Ion microprobe analysis - a review of geological applications. Mineralogical Magazine, v.53, p.3-24.

RICHTER, D.K. (1983). Calcareous ooids: a synopsis. In "Coated grains", edited by T. Peryt, Heidelberg, Springer-Verlag, p.71-99.

ROBERSON, K.E. (1989). Meteoric diagenesis. In "The fabric of cements in Paleozoic limestones", edited by K.R. Walker, Geological Society America, a short course/workshop, St-Louis. Studies in Geology, #20, University of Tennessee, Knoxville, p.54-65.

RUSH, P.F., CHAFETZ, H.S. (1990). Fabric-retentive, nonluminescent brachiopods as indicators of original $\delta^{13}C$ and $\delta^{18}O$ composition: a test. Journal Sedimentary Petrology, v.60, p.968-981.

SALLER, A.H. (1986). Radiaxial Calcite in Lower Miocene Strata, Subsurface Enewetak Atoll. Journal Sedimentary Petrology, v.56, p.743-762.

SANBERG, P.A. (1983). An oscillating trend in Phanerozoic non-skeletal carbonate mineralogy. Nature, v.305, p.19-22.

SANDBERG, P.A. (1985). Aragonite cements and their occurrence in ancient limestone. In "Carbonate cements" edited by N. Schneidermann and P.M. Harris, Society Economic Paleontologists and Mineralogists, Special Publication No.36, p.33-58.

SAVARD, M., BEAUCHAMP, B., VEIZER, J. (1990 a). Petrography of silica in Upper Paleozoic carbonates of the Sverdrup Basin, Canadian Arctic. In Current Research, Part D, Geological Survey of Canada, paper 90-1D p.101-109.

SAVARD, M., BEAUCHAMP, B., VEIZER, J., KROUSE, H.R. (1990 b). Methane-derived carbonate cements in ancient cold-seep communities, Canadian Arctic Archipelago. Geological association of Canada, Program with abstracts, v.15, p.A117.

SAVARD, M., BOURQUE, P.-A. (1989). Diagenetic evolution of a Late Silurian reef platform, Gaspé Basin, Quebec, based on cathodoluminescence petrography. Canadian Journal Earth Sciences, v.26, p.791-806.

SAVARD, M. (1986). Pétrographie en cathodoluminescence et evolution diagénétique d'une plate-forme calcaire, Silurien Supérieur, Gaspésie (Québec). Master's thesis, Laval University, Québec, 59 p.

SCHOLLE, P.A., ARTHUR, M.A., EKDALE, A.A. (1983). Pelagic environment. In "Carbonate depositional environments", edited by P.A. Scholle, D.G. Bebout and C.H. Moore, American Association of Petroleum Geologists, Memoir 33, p.619-692.

SCHOLLE, P.A., STEMMERICK, L. ULMER, D.S. (1991). Diagenetic history and hydrocarbon potential of Upper Permian carbonate buildups, Wegener Halvo Area, Jameson Land Basin, East Greenland. American Association Petroleum Geologists Bulletin, v.75, p.701-725.

SCHROEDER, J.H. (1972). Fabrics and sequences of submarine carbonate cements in Holocene Bermuda Cup Reefs. Geologische Rundschau, v.61, p.708-730.

SCOTT, E., HENDERSON, C.M., BEAUCHAMP, B. (1991). Field investigations of Artinskian (Lower Permian) strata, west-central Ellesmere Island, Arctic Archipelago. Current Research, Part B, Paper 91-1B, p. 81-93.

SHINN, E.A. (1969). Submarine lithification of Holocene carbonate sediments in the Persian Gulf. Sedimentology, v.12, p.109-144.

SWART, P.K., (1990). Calibration of the ion microprobe for quantitative determination of strontium, iron, manganese and magnesium in carbonate minerals. Analytical Chemistry v.62, p.722-728.

THERIAULT, P., BEAUCHAMP, B. (1991). Preliminary interpretation of the depositional history and tectonic significance of the Carboniferous to Permian Canyon Fiord Formation, west-central Ellesmere Island, Arctic Archipelago. Current Research, Part B, Paper 91-1B, p. 93-104.

TOWE, K.M., HEMLEBEN, C. (1976). Diagenesis of magnesian calcite: evidence from miliolacean foraminifera: Geology, v.4 p.337-339.

TUCKER, M.E., HOLLINGWORTH, N.T.J. (1986). The Upper Reef Complex (EZ1) of North East England: Diagenesis in a marine to evaporitic setting. In "Reef Diagenesis", edited by J.H. Schroeder and B.H. Purser, Springer-Verlag, p.270-289.

UTTING, J., GOODARZI,F., DOUGHERTY,B.J., HENDERSON,C.M. (1989). Thermal maturity of Carboniferous and Permian rocks of the Sverdrup Basin, Canadian Arctic Archipelago. Geological Survey of Canada, Paper 89-19.

VEIZER, J. (1983 a). Chemical diagenesis of carbonates: theory and application of trace element technique. In Stable isotopes in sedimentary geology, Society Economic Paleontologists Mineralogists, Short Course No.10, Chap. 3.

VEIZER, J. (1983 b). Trace elements and isotopes in sedimentary carbonates. In Carbonates: mineralogy and chemistry, Mineralogical Society America, Reviews in Mineralogy, v.11, p.265-300.

VEIZER, J. (1989). Strontium isotopes in Seawater through time. Annual Reviews Earth Planetary Sciences, v.17, p.141-167.

VEIZER, J., FRITZ, P., JONES, B. (1986). Geochemistry of brachiopods: oxygen and carbon isotopic records of Paleozoic oceans. Geochimica Cosmochimica Acta, v.50, p.1679-1696.

VEIZER, J., HINTON, R.W., CLAYTON, R.N., LERMAN, A. (1987). Chemical Diagenesis of Carbonates in thin-sections: ion microprobe as a trace elements tool. Chemical Geology, v.64, p.225-237.

VEIZER, J., HOEFS, J. (1976). The nature of $^{18}O/^{16}O$ and $^{13}C/^{12}C$ secular trends in sedimentary carbonate rocks. Geochimica Cosmochimica Acta, v.40, p.1387-1395.

VIDETICH, P.E. (1985). Electron microprobe study of Mg distribution in Recent Mg calcites and recrystallized equivalents from the Pleistocene and Tertiary. Journal Sedimentary Petrology, v.55, p.421-429.

WADLEIGH, M., VEIZER, J. (1991). $^{18}O/^{16}O$ and $^{13}C/^{12}C$ in Lower Paleozoic brachiopods: isotopic evolution of sea water. Unpublished manuscript.

WALTER, L.M., BURTON, E.A. (1990). Dissolution of Recent platform carbonate sediments in marine pore fluids. American Journal Science, v.290, p.601-643.

WILKINSON, B.H., JANECKE, S.U., BRETT, C.B. (1982). Low-magnesian calcite marine cement in Middle Ordovician hardgrounds from Kirkfield, Ontario. Journal Sedimentary Petrology, v.52, p.47-57.

WILKINSON, B.H., BUCZYNSKI, C., OWEN, R.M. (1984). Chemical control of carbonate phases: implications from Upper Pennsylvanian calcite-aragonite ooids of Southeastern Kansas. Journal Sedimentary Petrology, v.54, p.932-947.

WILSON, J.L. (1975). Carbonate Facies in Geologic History. Springer-Verlag, 549 p.

APPENDIX - GEOCHEMICAL RESULTS

Sample numbers are from official GSC notation. The location and stratigraphic position of the samples are as indicated for the sections on figure 2-3. CL Patterns are as described in chapter 3. Trace elements are in ppm. Stable isotopes are given in o/oo relative to PDB. Samples designated by "*" were utilized for studies of the chemistry of cathodoluminescence in calcite (chapter 6). MCC: miccrocodium. By: Bryozoan; Brach: brachiopod; Crin: crinoid; VD: very dull; Fa: void fill in former aragonite; L: luminescent; NL: nonluminescent; X: more than one luminescence microzone sampled; F: fracture; MET: associated with meteoric features. Numbers in CL pattern indicate the percentage of the components sampled. YC: yellow calcite. n.d.: not detected.

CALCITIZED ARAGONITE

The following CL patterns were recognized in dLMC with botryoidal fabric, within which ghosts of needles are commonly visible.

Irregular pattern (AIR) - Nonluminescent elongated irregular calcite crystals aligned parallel to the axis of former needles, but with crystal boundaries overstepping the original crystal limits (fig. 3-4 a).

Fine needle pattern (AFN) - Luminescent and dull needle-like fine zones (2 to 10 micrometres wide) developed successively after the nonluminescent irregular pattern (fig. 3-4 b). The dull and luminescent calcite seems to have replaced the nonluminescent one. This chronology is supported also by the observation that luminescent and dull calcites occlude voids that are lined at the periphery by nonluminescent calcite (see void patterns below).

Mold pattern (AMD) - Nonluminescent and luminescent elongated calcite crystals that are laterally restricted by molds of the former aragonite needles (fig. 3-4 c, d, 3-5 d). The molds are 20 to 50 micrometres wide and 2 to 3 centimetres long.

Microcrystal pattern (AMY) - Composite texture made of dot-like nonluminescent and luminescent microzones (with an average diameter of 0.01 mm) and of films of dull overgrowths (fig. 3-5 b). Some samples show only dull calcite.

Void patterns (AVO) - Regular luminescent and dull calcite overgrowths on nonluminescent calcite. These luminescent and dull portions represent typical layers grown in dissolution voids (fig. 3-3 b, g, h, 3-4 b, e).

The following CL pattern was recognized in oosparite.

Tangential-oolitic calcite (AOO) - Nonluminescent microspar that forms the banded cortex of oolites (200 micrometres in diameter). It contrasts with the fill of the oomoldic cavities that are occluded exclusively by dull xenomorphic spar.

RECRYSTALLIZED HMC

The following CL patterns were recognized in isopachous, inclusion-rich, radiaxial calcite cements interpreted as recrystallized HMC.

Uniformly nonluminescent (HM1) - Uniformly nonluminescent zones without identifiable crystal shape and with only traces of luminescent zones (fig. 3-8 a).

Fibrous nonluminescent (HM2a) - Nonluminescent zones with identifiable shapes (fibrous or bladed) surrounded by luminescent or dull films (fig. 3-8 b).

Patchy nonluminescent (HM2b) - Nonluminescent zones with no recognizable shape, with the luminescent and dull zones covering up to 50 % of the surface (fig. 3-8 c, d).

Composite dull (HM3) - Surface dominantly covered by dull zones, generally with no recognizable shape and containing nonluminescent and luminescent microzones (fig. 3-8 e).

Fibrous luminescent (HM4a) - Luminescent zones with fibrous shape or palisade-like fabric and containing nonluminescent patches (fig. 3-8 c, d).

Patchy luminescent (HM4b) - Luminescent zones with no recognizable fabric in which the nonluminescent zones can cover up to 50 % of the surface (fig. 3-8 e).

The following CL pattern was recognized in large calcite crystals that have inclusion-rich and inclusion-free sub-zones (fig. 3-10 a, b). The inclusion-rich portions mimic rhombic crystals (fig. 3-10 a, b) and they are superimposed either over the earlier marine isopachous calcite cements or over the sediments. They are iron-free, generally covered by iron-rich, inclusion-free sub-zones.

Rhombohedral nonluminescent calcite (HMRH) - The rhombohedral sub-crystals are perfectly discernible by CL (compare figs. 3-10 b, 3-13 b with 3-11 a, b). The inclusion-rich portions correspond to precisely defined sub-crystals. The overall crystal shape recalls a rhombohedron. The cross-sections of the crystals show perfect triangles (fig. 3-11 c). The immediate inclusion-free overgrowths on the rhombohedral ghosts are always devoid of microdolomite and they are regularly zoned. In contrast, the inclusion-rich rhombohedral portions themselves can have both, regular and blotchy CL patterns (fig. 3-11 a, b and c) and they always contain abundant microdolomite inclusions.

METEORIC CEMENTS

Equant NL Calcite (MT1) - Equant, anhedral, nonluminescent crystals (10 to 100 micrometres) found within mosaic fabric in fenestral cavities of calcrete or within meniscus fabric in calcitized, texturally disrupted and originally aragonitic oolitic grainstones (fig. 3-11 d, 3-12 a, b). In some cases, these cements bear diagnostive features of meteoric diagenesis such as fine equant size and meniscus (?) fabric.

Equant Zoned Calcite (MT2) - Equant, anhedral crystals (up to 0.6 mm) with multiple nonluminescent/luminescent couplets, having up to 40 zones (fig. 3-12 c, e).

Fibrous Isopachous Calcite (MT3) - Fibres arranged in isopachous layers form a typical calcrete crust.

LATE CEMENTS

Stubby NL Calcite (L1a) - Fine stubby to bladed nonluminescent crystals (10 to 50 micrometres), generally overgrown by a film of brightly luminescent calcite. They can appear directly on cavity walls, or as overgrowth over earlier generations of cements (figs. 3-6 e, f, i; 3-14 b). In terms of abundance, this category is of minor importance.

Stubby Zoned Calcite (L1b) - Fine stubby or bladed crystals (30 to 300 micrometres) showing only one or two alternations of nonluminescent, luminescent and dull calcite layers, and appearing directly on walls of corals (fig. 3-14 a). In terms of abundance, this category is of minor importance.

Xenomorphic Dull Calcite (L2a) - Uniformly dull, coarse calcite crystals that show high frequency of enfacial junctions in a mosaic arrangement. Development of characteristic habits of the rhombohedral system has been prevented by competitive growth and by the lack of space, resulting in poikilotopic (fig. 3-13 a) and xenomorphic (xenotopic; figs. 3-13 c, d; 3-14 a) textures. This is the most abundant category of late cements. In some cases, it is present within microfractures that postdate stylolites, is invariably iron-rich and sometimes contains inclusions of bitumen (3-13 d).

Xenomorphic Zoned Calcite (L2b) - Coarse luminescent/dull calcite crystals appearing as mosaic in the center of cavities (fig. 3-14 b). In microfractures they occasionally postdate stylolitization. In terms of abundance, this category is of minor importance.

Xenomorphic Luminescent Calcite (L2c) - Coarse (up to 0.5 mm) luminescent calcite crystals that appear as a mosaic in the center of cavities or fill microfractures. In microfractures they occasionally postdate stylolitization. In terms of abundance, this category is of minor importance.

SAMPLE	CL Pattern	Mg	Sr	Fe	Mn	$\delta^{18}O$	$\delta^{13}C$	$^{87}Sr/^{86}Sr$	Ba	Ce	Na	Al	Si
		ppm	ppm	ppm	ppm	‰	‰		ppm	ppm	ppm	ppm	ppm
SEQUENCE 1													
Emma Fiord Formation (section 33)													
162431	L2a[1]	2092	478	9516	365				18	50	69	125	111
SEQUENCE 2													
Hare Fiord Formation (section 9.5 "Televak Limestone" - Eastern Area)													
171260	AIR					-0.4	7.9	0.70856					
171258-1	AMY	1792	475	1043	54				n.d.	n.d.	798	198	175
171258-2	AMY	1458	647	342	72				n.d.	n.d.	789	116	178
171259	HM1					-2.3	5.7	0.70857					
171260	Hm2a					-4.4	6.3	0.71013					
171259	HM2a					-1.9	5.7						
171254	HM2b					-1.9	5.3						
171256	HM2b					-2.2	5.3						
171256	HM2b					-1.9	5.4						
171260	HM3					-3.7	6.0						
171260	HM3					-2.7	6.3						
171254	HM4a					-1.4	5.2						
171258-4	L1-FANL[1]	1436	859	87	41				n.d.	n.d.	825	105	189
171258-5	L1-FANL[1]	1164	1037	90	45				12	n.d.	681	181	408
171253	L2a					-11.0	4.0	0.70978					
171255	L2a					-9.1	4.1						
171259	L2a					-8.7	4.5						
171258-6	L2a-Fa[1]	1848	794	51	94				n.d.	n.d.	245	49	89

SAMPLE	CL Pattern	Mg	Sr	Fe	Mn	$\delta^{18}O$	$\delta^{13}C$	$^{87}Sr/^{86}Sr$	Ba	Ce	Na	Al	Si
171260	L2b					-9.6	4.1						
171258-7	L2c-FA[1]	1549	440	149	166				40	n.d.	2063	370	239
171258-7B	L2c-Fa[1]	1599	476	201	200				n.d.	n.d.	378	58	78
Otto Fiord Formation (section 10)													
171262	AIR					-3.0	7.0						
171262	AMY					-4.5	7.0						
171262-1	AMY	4125	410	6700	1630	-3.5	6.9	0.70911	n.d.	n.d.	214	35	39
10681	BRACH					-0.5	7.0						
171262-2	HM4b	1080	367	1779	1021				34	n.d.	277	260	231
171262-4	L2a[1]	1698	103	2662	839	-3.0	7.0		n.d.	n.d.	128	33	119
171262-6	L2a[1]	1021	466	1466	814				n.d.	n.d.	188	105	135
171262-3	L2a-VD[1]	2052	306	3063	614				n.d.	n.d.	431	71	62
171262-5	L2a-VD[1]	2730	131	2098	669				n.d.	n.d.	153	37	69
10681	L2b					-4.3	5.5						
171262-7	L2c[1]	878	1098	511	499	-4.1	4.5	0.70938	n.d.	n.d.	283	46	118
171262-8	L2c[1]	1139	496	833	763				n.d.	n.d.	150	18	46
Hare Fiord Formation (section 11 "Televak Limestones" - Eastern Area)													
171267	AIR					-4.6	6.8						
171287	AIR+MY					-1.5	6.7						
171288	AMY					-3.0	5.7						
171288	AMY					-7.8	7.0						
171318	HM1					-4.4	5.3						
171317	HM1					-6.4	5.5						
171310-2	HM1					-2.6	6.0						
171310	HM1					-3.3	5.8						
171289	HM1					-1.5	6.4						
171289	HM1					-2.2	6.2						

SAMPLE	CL Pattern	Mg	Sr	Fe	Mn	$\delta^{18}O$	$\delta^{13}C$	$^{87}Sr/^{86}Sr$	Ba	Ce	Na	Al	Si
171288	HM1					-2.3	6.2						
171287	HM1					-3.2	6.3						
171284	HM1					-2.2	5.3						
171284	HM1					-2.1	5.8	0.70911					
171282	HM1					-2.2	5.1						
171276	HM1					-2.5	6.4						
ii171310	HM1+2a					-1.5	5.6						
171279	HM1+M4b					-3.2	6.1						
171321	HM2a					-2.0	5.6						
171306	HM2a					-2.8	6.0						
171303-4	HM2a	4729	298	723	92				n.d.	n.d.	505	32	45
171303-3	HM2a	5566	237	518	35				n.d.	n.d.	657	33	46
171300	HM2a					-3.3	5.9						
171296	HM2a					-2.3	5.8						
171294	HM2a					-2.8	6.0						
171288	HM2a					-4.9	6.3						
171287-2	HM2a	3362	446	209	52				n.d.	n.d.	587	47	55
171287-1	HM2a	2648	464	171	66				n.d.	n.d.	209	24	40
171279	HM2a					-3.0	5.5	0.70917					
171279	HM2a					-3.2	5.8						
171271	HM2a					-2.5	5.3						
171270	HM2a					-3.0	5.5						
171270	HM2a					-3.2	5.8						
171319	HM2b					-3.2	5.6						
171311	HM2b					-1.7	5.7						
171310-2	HM2b					-3.7	5.9						
171307	HM2b					-3.4	5.6						
171305	HM2b					-4.2	5.7	0.70997					

SAMPLE	CL Pattern	Mg	Sr	Fe	Mn	$\delta^{18}O$	$\delta^{13}C$	$^{87}Sr/^{86}Sr$	Ba	Ce	Na	Al	Si
171305	HM2b					-3.8	5.9						
171299	HM2b					-3.5	5.8						
171299	HM2b					-2.0	5.8						
171299	HM2b					-2.1	5.1						
171291	HM2b					-4.0	5.7						
171291	HM2b					-2.3	6.0						
171289	HM2b					-2.7	6.5						
171289	HM2b					-3.0	6.3						
171288	HM2b					-4.2	6.3						
171287	HM2b					-3.0	6.3						
171276	HM2b					-1.9	5.9						
171271	HM2b					-2.0	5.6						
32182	HM3					-3.9	9.2						
32173	HM3					-3.0	5.2						
171317	HM3					-7.5	5.3						
171304	HM3					-3.5	5.6						
171303-2	HM3	7290	629	6639	106				13	n.d.	865	109	83
171303-1	HM3	6131	677	238	82	-3.4	5.8		15	n.d.	361	102	79
171302	HM3					-4.8	5.6						
171297	HM3					-3.9	5.5						
171296	HM3					-3.4	5.5						
171296	HM3					-2.4	5.4						
171289	HM3					-2.8	5.8						
171287-4	HM3	2825	481	542	106	-2.6	6.5		n.d.	n.d.	375	26	47
171287-3	HM3	2850	510	670	107				n.d.	n.d.	280	42	47
171271	HM4a					-1.9	5.7						
171321	HM4b					-2.8	5.2						
171320	HM4b					-4.3	5.3						

SAMPLE	CL Pattern	Mg	Sr	Fe	Mn	$\delta^{18}O$	$\delta^{13}C$	$^{87}Sr/^{86}Sr$	Ba	Ce	Na	Al	Si
171319	HM4b					-4.4	5.3						
171318	HM4b					-3.1	5.1						
171310	HM4b					-3.2	5.8						
171299	HM4b					-1.9	5.6						
171267	L1a					-5.2	6.4						
171303-6	L1-NL[1]	7820	192	770	74	-4.0	5.2		n.d.	n.d.	358	48	51
171320	L2a					-13.0	5.2						
171316	L2a					-6.9	5.6						
171307	L2a					-4.0	5.6	0.71059					
171306	L2a					-4.3	5.7						
171303-7	L2a[1]	1263	580	34	94	-3.6	5.9		n.d.	n.d.	389	39	43
171303-5	L2a[1]	7440	315	375	167				n.d.	n.d.	485	42	56
171299	L2a					-3.5	5.6						
171297	L2a					-3.9	5.8	0.71009					
171294	L2a					-2.9	5.6						
171287-6	L2a[1]	1668	553	468	125				n.d.	n.d.	252	135	189
171280	L2a					-2.7	5.9						
171275	L2a					-3.0	6.4						
171267	L2a					-5.2	6.2						
171296	L2aF					-12.0	5.3	0.71098					
171288	L2a+1a(20)					-0.7	6.9						
171304	L2b					-7.6	5.4						
171302	L2bF					-4.7	5.7						
171287-7	L2c[1]	1573	633	37	106				n.d.	n.d.	246	16	37
171287-5	L2c[1]	1556	818	46	69	-4.9	6.2		n.d.	n.d.	112	48	76
171305	L2cF					-9.4	5.5						
171286	L2cF					-3.3	5.9						
171279	L2cF					-9.7	6.1						

SAMPLE	CL Pattern	Mg	Sr	Fe	Mn	$\delta^{18}O$	$\delta^{13}C$	$^{87}Sr/^{86}Sr$	Ba	Ce	Na	Al	Si
171264	L2cF					-8.4	5.3	0.71088					
Nansen Formation (section 37 - Western Area)													
115620-10	AIR[1]	1628	1435	46	15	-7.2	6.7	0.70833	14	n.d.	436	123	395
115620-9	AIR[1]	1182	2336	42	1	-7.2	6.4		n.d.	n.d.	481	124	245
115620-8	AMY	2148	406	72	27				26	n.d.	475	287	372
115615	HM1					-11.0	5.6						
115618	HM1					-5.7	4.0						
115620	HM1pha					-7.2	5.1						
115619	HM2a					-8.9	5.0						
115613-2	HM2b	1363	213	99	58				n.d.	n.d.	1838	336	733
115613-20	HM2b	1373	293	73	20	-9.1	5.0		10	n.d.	2316	100	119
115613-21	HM2b	1691	212	152	14				n.d.	n.d.	739	45	66
115613-22	HM2b	2878	327	177	26	-7.8	5.3		34	n.d.	1639	128	124
115613-23	HM2b	1984	256	127	22	-8.3	5.1		10	n.d.	1970	722	429
115615	HM2b					-11.0	5.7	0.70849					
115617	HM2b					-10.0	4.4						
115618	HM2b					-8.0	4.3	0.70895					
115618	HM2b					-7.8	4.9	0.70843					
115621	HM2b					-8.1	4.6						
115621	HM2b					-10.0	4.8						
115621	HM2b					-8.1	4.6						
115621	HM2b					-8.5	4.7						
115616	HM2b+3					-13.0	4.9						
115616	HM2b+3					-12.0	5.3						
115613-1	HM3	1262	200	55	33				n.d.	n.d.	931	84	97
115613-15	HM3	2778	220	97	19				n.d.	n.d.	1278	109	105
115613-19	HM3	1754	242	100	17				15	n.d.	1336	132	124

SAMPLE	CL Pattern	Mg	Sr	Fe	Mn	$\delta^{18}O$	$\delta^{13}C$	$^{87}Sr/^{86}Sr$	Ba	Ce	Na	Al	Si
115615	HM3					-15.0	4.8						
115620-6	HM3	1213	278	94	28				24	n.d.	3960	228	467
115620-6B	HM3	1227	262	126	26	-6.3	5.5		41	n.d.	721	571	1333
115620-7	HM3	1836	237	79	28	-13.0	4.8	0.70915	19	n.d.	3391	140	250
115615	HM3By					-15.0	5.1	0.70903					
115475	L1-NLF					-15.0	4.4						
115616	L2a					-7.1	5.0						
115618	L2a					-7.3	4.7						
115620-B-1	L2a[1]	1252	173	62	44	-7.1	4.8	0.70833	n.d.	n.d.	1683	146	427
115621	L2a					-7.6	4.7	0.70901					
115360	L2aF					-29.0	0.0						
115620-B-3	L2b[1]	1222	263	29	20				n.d.	n.d.	632	31	64
115620-B-4	L2b[1]	1066	435	23	17				n.d.	n.d.	1066	78	585
115613-10	L2b-X	1124	255	85	23				n.d.	n.d.	1161	192	197
115613-11	L2b-X	916	320	127	18				n.d.	n.d.	1313	227	205
115613-12	L2b-X	962	203	75	34				n.d.	n.d.	1130	82	125
115613-13	L2b-X	1367	176	41	24	-6.8	6.9		n.d.	n.d.	640	57	82
115613-14	L2b-X	1189	242	71	23				n.d.	n.d.	943	140	151
115613-3	L2b-X	1234	164	59	31				n.d.	n.d.	3037	126	163
115613-4	L2b-X	1188	150	56	29				n.d.	n.d.	582	118	95
115613-5	L2b-X	1120	135	39	28				n.d.	n.d.	885	108	93
115613-6	L2b-X	745	184	41	27				n.d.	n.d.	612	46	60
115613-7	L2b-X	1220	157	60	43				n.d.	n.d.	698	81	82
115613-8	L2b-X	1686	194	76	23				n.d.	n.d.	739	152	158
115613-9	L2b-X	1584	290	88	25				n.d.	n.d.	956	212	208
115620-B-2	L2b-X	1596	179	31	29				n.d.	n.d.	1075	31	71
115617	L2c					-22.0	3.1						
115613-16	MT2-X	2853	186	149	13				n.d.	n.d.	1480	163	144

SAMPLE	CL Pattern	Mg	Sr	Fe	Mn	$\delta^{18}O$	$\delta^{13}C$	$^{87}Sr/^{86}Sr$	Ba	Ce	Na	Al	Si
115613-17	MT2-X	615	58	50	21				n.d.	n.d.	671	73	100
115613-18	MT2-X	648	77	69	19				n.d.	n.d.	854	105	109
115613-24	MT2-X	5563	181	129	9				11	n.d.	1312	232	187
Canyon Fiord Formation (section 40 - Calcrete)													
170126-1	MT1b[1]	1397	133	34	634				n.d.	n.d.	231	11	37
170126-2	MT1-XL	270	744	42	132				n.d.	20	343	47	70
170126-6	MT1-X	467	514	51	588				n.d.	n.d.	103	77	107
170127-1	MT1-NL[1]	611	58	59	2	-7.6	-4.0		n.d.	n.d.	313	275	243
170126-5	MT1-XL	1353	238	69	806				n.d.	n.d.	182	131	239
170127-2	MT1-NL[1]	393	172	38	1				n.d.	n.d.	146	146	181
170126-7	MT1b[1]	382	473	41	705	-8.6	-3.0	0.71017	25	n.d.	245	51	72
170126-4	MT1-XN	924	331	138	65				71	n.d.	4864	705	400
170121	MT1a-NL					-7.8	-4.0	0.71131					
170126-3	MT1-XN	227	546	50	10	-8.3	-4.0		n.d.	n.d.	1080	210	161
SEQUENCE 3													
Nansen Formation (section 2)													
119424-3	AOO-NL[1]	1507	3123	199	19				n.d.	n.d.	1135	345	4433
119424-3B	AOO-NL[1]	1800	3347	448	33				n.d.	n.d.	1682	1360	1720
119424-6	AOO-NL[1]	2345	827	738	47				n.d.	n.d.	483	354	200
119424-7	AOO-NL[1]	2306	912	481	35				n.d.	n.d.	1084	488	81
123200-B-5	Crin	2854	297	135	19				n.d.	n.d.	3241	115	117
123192	HM1					-2.6	6.2	0.70847					
123236-4	HM1[1]	1996	178	104	14				n.d.	n.d.	683	91	60
123236-5	HM1[1]	2454	189	66	100	-2.8	5.4		n.d.	n.d.	967	88	67
123154-2	HM2a	1791	324	338	20				66	n.d.	250	28	41
123154-3	HM2a	1530	257	233	19				12	n.d.	263	39	38

SAMPLE	CL Pattern	Mg	Sr	Fe	Mn	$\delta^{18}O$	$\delta^{13}C$	$^{87}Sr/^{86}Sr$	Ba	Ce	Na	Al	Si
123154-4	HM2a	1463	267	98	24				n.d.	n.d.	159	12	36
123154-5	HM2a	1492	209	137	18				n.d.	n.d.	169	15	38
123191	HM2a					-2.5	6.8						
123154-1	HM2b	2418	356	135	18	-3.9	6.3	0.70864	22	n.d.	228	24	39
123200-A-4	HM2b	1692	151	230	164				n.d.	n.d.	257	38	83
123200-A-5	HM2b	4745	350	117	8				17	n.d.	378	132	122
123226	HM2b					-4.6	6.4						
123226-A-1	HM2b	2478	197	73	60	-5.8	5.4		n.d.	n.d.	321	100	83
123226-A-2	HM2b	2458	234	57	52				n.d.	n.d.	366	135	85
123236-3	HM4b	1619	179	75	192				n.d.	n.d.	687	71	59
123200B-3B	L1[1]	2906	126	323	30				n.d.	n.d.	2922	184	79
123200-B-4	L1[1]	2766	137	138	33				12	n.d.	3627	104	42
123226-A-3	L1	2195	218	652	63				n.d.	n.d.	196	315	270
123226-A-4	L1	2232	155	144	85				n.d.	n.d.	110	85	86
123226-A-5	L1	2652	140	90	303				n.d.	n.d.	132	52	56
123191-2	L1a-NL[1]	3434	117	155	219				n.d.	n.d.	573	101	76
123191-3	L1a-NL[1]	3577	89	205	102				38	n.d.	795	196	120
123191-4	L1a-NL[1]	2133	241	276	43				n.d.	n.d.	1017	128	129
123200A-3B	L1b[1]	1421	167	193	107				13	n.d.	285	76	120
123154-6	L1b-NL[1]	1951	660	958	56				14	n.d.	280	17	39
123200-A-3	L1-x	2123	104	161	63				n.d.	n.d.	310	55	87
119409-2	L1-X	3938	808	1352	51				76	n.d.	4119	558	595
119409-3	L2a[1]	3138	236	1974	71				20	n.d.	4790	206	176
123001	L2a					-6.7	4.3						
123056	L2a					-8.0	4.0						
123087-5	L2a[1]	3053	588	405	53				n.d.	n.d.	1304	344	2175
123115	L2a					-6.9	5.0						
123119	L2a					-6.6	4.2						

SAMPLE	CL Pattern	Mg	Sr	Fe	Mn	$\delta^{18}O$	$\delta^{13}C$	$^{87}Sr/^{86}Sr$	Ba	Ce	Na	Al	Si
123134	L2a					-11.0	5.5						
123135	L2a					-7.9	5.6						
123147-4	L2a[1]	1008	230	32	21				n.d.	n.d.	287	74	64
123148	L2a					-7.1	5.8						
123154-7	L2a[1]	1793	1224	712	40				n.d.	n.d.	88	18	37
123154-8	L2a[1]	2192	687	821	49				n.d.	n.d.	146	24	48
123154-9	L2a[1]	2221	673	1015	58	-8.9	5.2	0.70893	n.d.	n.d.	114	7	33
123191-1	L2a[1]	2577	268	197	58	-9.9	4.9		n.d.	n.d.	428	162	83
123192	L2a					-11.0	4.7						
123196	L2a					-9.0	6.1						
123200-2	L2a[1]	1560	334	5473	535	-8.7	5.4		45	25	91	7053	6670
123200-A-1	L2a[1]	1420	157	179	150				n.d.	n.d.	115	30	51
123200-A-2	L2a[1]	1308	221	188	153				n.d.	n.d.	246	62	94
123200-B-1	L2a[1]	2509	347	231	45				34	n.d.	2472	72	34
123200-B-2	L2a[1]	3077	225	314	70				11	n.d.	4245	89	39
123200-C-B	L2a[1]	1910	522	1018	33				n.d.	n.d.	1172	324	576
123206	L2a					-11.0	5.3	0.70858					
123223	L2a					-10.0	4.8						
123236-1	L2a[1]	1930	1159	296	94	-8.2	5.7		n.d.	n.d.	809	60	60
123236-2	L2a[1]	1564	669	1056	188				n.d.	n.d.	801	71	65
123206	L2aF					-8.2	4.1						
119424-1A	L2a-MET[1]	3088	295	2666	75				23	n.d.	303	727	772
119424-8	L2a-MET[1]	2551	380	1404	45				n.d.	n.d.	312	101	80
199424-1B	L2a-MET[1]	3007	262	3818	113				n.d.	n.d.	144	58	151
123087-6	L2a-VD[1]	2242	692	868	92				n.d.	n.d.	1463	204	160
123087-2	L2b	2376	871	1081	112	-11.0	4.6	0.70934	n.d.	n.d.	282	97	83
123147-2	L2b[1]	2213	266	484	61				n.d.	n.d.	405	142	56
123149	L2bF2					-24.0	3.3						

SAMPLE	CL Pattern	Mg	Sr	Fe	Mn	$\delta^{18}O$	$\delta^{13}C$	$^{87}Sr/^{86}Sr$	Ba	Ce	Na	Al	Si
123087-1	L2c[1]	2813	658	1358	127				n.d.	n.d.	218	796	598
123147-1	L2c[1]	3012	76	229	71	-11.0	4.8		n.d.	n.d.	254	48	44
123148	L2c					-6.1	5.9						
123226-B	L2c[1]	1859	1117	756	106				n.d.	34	52	5	32
119424	L2cF					-10.0	4.7						
119433	L2cF					-8.3	1.8						
123147-5	L2c+L2a	1113	201	58	47				n.d.	n.d.	398	306	202
119433	LabF					-10.0	1.6	0.70869					
123001-56	Lum MCC[1]	6024	5362	194	56				10	n.d.	940	41	60
119424-5	MT1-NL[1]	1562	3052	87	11				n.d.	n.d.	1003	189	183
119424-9	MT1-NL[1]	3252	1081	1205	49				n.d.	n.d.	1092	10771	6234
123001-7	NL MCC[1]	8465	13529	30	3				16	n.d.	867	33	120
123001-8	NL MCC[1]	4280	10083	42	2				15	n.d.	1006	31	52
123001-8	NL MCC[1]	4192	4462	54	2				n.d.	n.d.	2349	130	88
Nansen Formation (section 3)													
162162	HM1					-3.9	6.1						
162180	HM1					-3.2	6.5						
162166	HM3					-3.4	6.5	0.70852					
162150	L2a					-4.3	8.6						
162162	L2a					-5.4	6.1						
162167	L2a					-6.6	6.4						
162175-11	L2a[1]	1588	489	55	22	-5.3	6.0		n.d.	n.d.	368	158	218
162175-12	L2a[1]	1358	875	76	18				n.d.	n.d.	214	146	195
162175-13	L2a[1]	1592	484	134	19				n.d.	n.d.	2396	387	545
162180	L2a					-6.6	5.9						
162183	L2a					-6.1	5.9						
162184	L2a					-4.7	6.0	0.70910					

SAMPLE	CL Pattern	Mg	Sr	Fe	Mn	$\delta^{18}O$	$\delta^{13}C$	$^{87}Sr/^{86}Sr$	Ba	Ce	Na	Al	Si
162187	L2a					-6.2	4.0						
162190	L2a					-8.1	5.1						
162194	L2a					-8.0	5.2						
162198	L2c					-7.5	4.9	0.70872					
162177-3	MT2-D[1]	2431	198	127	55				n.d.	n.d.	177	14	38
162177-B	MT2F	3150	767	202	18				n.d.	n.d.	653	89	70
162175-1	MT2-L[1]	3094	162	260	52				n.d.	n.d.	424	258	336
162175-2	MT2-L[1]	2331	449	261	44				n.d.	n.d.	1406	407	440
162175-3	MT2-L[1]	1320	464	210	21				n.d.	n.d.	1138	247	381
162175-6	MT2-L[1]	1074	786	100	29				n.d.	n.d.	611	121	200
162177-1	MT2-NL[1]	3862	363	166	32				n.d.	n.d.	356	13	38
162177-2	MT2-NL[1]	1837	142	184	30				n.d.	n.d.	1298	46	61
162175-14	MT2-X	3265	83	84	16				n.d.	n.d.	1262	296	429
162175-15	MT2-X	2265	277	271	29				n.d.	n.d.	2134	623	888
162175-16	MT2-X	3742	131	84	17				n.d.	n.d.	1613	239	353
162175-17	MT2-X	2407	154	115	20				n.d.	n.d.	360	257	234
162175-18	MT2-X	2223	223	639	32				n.d.	n.d.	1864	480	831
162175-19	MT2-X	3033	236	363	50				n.d.	n.d.	989	420	491
162175-20	MT2-X	1693	320	182	30				n.d.	n.d.	792	296	464
162175-21	MT2-X	1640	199	174	68				n.d.	n.d.	1147	253	359
162177-5	MT2-XN	4335	86	39	61	-4.5	5.2	0.70859	n.d.	n.d.	204	27	38
162177-6	MT2-XN	3708	156	118	66				n.d.	n.d.	300	60	65
Nansen Formation (section 4)													
119104-1	L2a[1]	1318	636	43	22				n.d.	n.d.	339	44	65
119068	MT2					-6.1	5.1						
119103	MT2					-6.1	4.9						
119104-2	MT2-NL[1]	2426	294	45	14				n.d.	n.d.	324	46	67

SAMPLE	CL Pattern	Mg	Sr	Fe	Mn	$\delta^{18}O$	$\delta^{13}C$	$^{87}Sr/^{86}Sr$	Ba	Ce	Na	Al	Si
119104-3	MT2-X	3750	132	69	13				n.d.	n.d.	402	92	101
119104-4	MT2-X	2426	73	153	42	-7.9	5.2	0.70884	n.d.	n.d.	287	61	75
119104-5	MT2-X	3111	108	36	25				n.d.	n.d.	283	43	56
Nansen Formation (section 6)													
119229-1	L1a[1]	2994	467	390	40	-7.7	4.5		n.d.	n.d.	1043	115	162
119229-2	L2a[1]	2627	138	694	60	-7.7	4.5		n.d.	n.d.	1641	160	172
119229-3	L2b-X	2324	79	935	68				n.d.	n.d.	1076	79	78
Canyon Fiord Formation (section 9)													
132049-2	L1-X	2487	184	1238	57				n.d.	n.d.	303	232	239
131817-5	L2a[1]	2686	235	2726	257	-14.0	2.4	0.70883	n.d.	n.d.	1635	89	81
132020	L2a					-6.2	4.5						
132033	L2a					-8.0	3.6						
132049-5	L2a[1]	2908	149	150	33	-5.7	5.0	0.70846	n.d.	n.d.	359	43	75
132087	L2a					-11.0	4.6						
132049-1	L2c[1]	2939	237	172	61				n.d.	n.d.	346	147	163
171258-7	L2c-FA	1549	440	149	166	-3.4	5.4		40	n.d.	2063	370	239
131817-1	MT1-L[1]	3664	297	419	260	-6.8	3.8	0.70852	n.d.	n.d.	509	409	337
131817-4	MT1-L[1]	2874	273	211	244				n.d.	n.d.	299	35	52
131817-2	MT1-X	1847	284	1670	197				n.d.	n.d.	2753	92	108
131817-3	MT1-X	2359	280	1052	223				n.d.	n.d.	716	126	64
Canyon Fiord Formation (section 28)													
162353	BRACH					-4.0	5.1						
162362-2	L1b-X	2991	766	1453	195	-7.2	4.6	0.70812	n.d.	n.d.	2463	244	294
162386-1	L1L+FCOR	4797	1075	1014	189				n.d.	n.d.	1083	199	215
162362-3B	L2a[1]	3135	128	2189	284				n.d.	n.d.	1213	169	91
162367	L2a					-7.0	4.3						

SAMPLE	CL Pattern	Mg	Sr	Fe	Mn	$\delta^{18}O$	$\delta^{13}C$	$^{87}Sr/^{86}Sr$	Ba	Ce	Na	Al	Si
162370	L2a					-7.4	3.6						
162371	L2a[1]	3041	271	2888	434	-8.9	3.5		n.d.	18	248	274	159
162372	L2a					-7.3	3.6						
162375	L2a					-7.1	3.8						
162377	L2a					-6.6	3.5	0.70806					
162378	L2a					-7.4	4.0						
162382	L2a					-6.9	3.9						
162385	L2a					-8.4	4.4	0.70816					
162386-3	L2a[1]	3349	316	4221	320	-6.5	3.5		n.d.	14	286	77	172
162391-1	L2a[1]	3406	153	3438	364				n.d.	n.d.	295	55	62
162391-3	L2a[1]	1736	506	2091	303				n.d.	11	339	107	103
162392	L2a[1]	1966	1384	1017	54	-5.5	4.9		n.d.	n.d.	78	40	41
162396	L2a					-7.7	5.2						
162369	L2b					-8.5	3.5						
162368	L2c					-7.3	3.6						
162386-2	L2c[1]	4705	488	923	181				n.d.	n.d.	608	85	62
Nansen Formation (section 35)													
119251-2	HM2a80	1622	168	95	55				n.d.	n.d.	335	96	79
119251-1	HM2b	1016	176	121	29				n.d.	n.d.	464	273	269
115251-1	HM2b+L1a	1604	108	146	38				n.d.	n.d.	99	11	53
119250	MT2					-11.3	4.9						
119250	L2a					-9.3	3.8						
115251-8	L2a[1]	1439	387	76	28				n.d.	n.d.	771	72	76
119250	MT2					-10.8	5.6	0.71085					
119251-3	MT2-NL[1]	2249	67	52	26				n.d.	n.d.	376	67	63
115251-4	MT2-D[1]	1022	160	42	14				n.d.	n.d.	137	55	66
115251-2	MT2-VD[1]	1886	110	60	22				n.d.	n.d.	72	9	44

SAMPLE	CL Pattern	Mg	Sr	Fe	Mn	$\delta^{18}O$	$\delta^{13}C$	$^{87}Sr/^{86}Sr$	Ba	Ce	Na	Al	Si
115251-5	MT2-X	829	92	237	55				n.d.	n.d.	195	187	132
115251-6	MT2-X	2692	194	90	46	-11.5	3.6	0.71030	n.d.	n.d.	222	139	167
115251-7	MT2-X	1586	384	68	50				n.d.	n.d.	1015	112	117
SEQUENCE 4													
Great Bear Cape Formation (section 17)													
131740	HM1					-2.4	5.6						
131741	HM1					-2.7	5.8						
131740-1	HM3	2084	226	92	17				n.d.	n.d.	562	73	73
131740-4	HM4a	2149	191	81	102				n.d.	n.d.	813	139	102
131740-3	HM4a	1584	259	68	215				n.d.	n.d.	602	70	81
131741	HM4a					-3.1	5.7						
131740-2	HM4a	2211	240	100	43	-3.4	5.6	0.70787	82	n.d.	747	72	72
131740-5	L2a[1]	1706	258	101	109	-6.8	5.4		n.d.	n.d.	461	102	79
131741	L2a					-6.1	5.5						
Great Bear Cape Formation (section 18)													
131796-3	HM4b	1639	204	130	84				n.d.	n.d.	472	75	7591
131758	HM1					-2.2	6.8						
131750	HM2b					-3.3	6.1						
131761-1	HM2b	2048	257	52	16	-2.9	5.3		n.d.	n.d.	255	34	50
131761-2	HM2b	2098	234	88	15				n.d.	n.d.	747	31	55
131761-3	HM2b	1713	223	135	24				n.d.	n.d.	248	20	44
131796-5	HM2b	1579	238	137	137			0.70788	n.d.	n.d.	436	49	48
131758	HM3					-3.2	5.6						
131761-4	HM3	1882	295	65	62	-3.2	5.3		n.d.	n.d.	231	25	42
131750	HM4a					-3.0	5.6						
131750	HM4a					-3.1	5.5						

SAMPLE	CL Pattern	Mg	Sr	Fe	Mn	$\delta^{18}O$	$\delta^{13}C$	$^{87}Sr/^{86}Sr$	Ba	Ce	Na	Al	Si
131756	HM4a					-3.0	5.4						
131761-5	HM4b	1666	263	105	255				n.d.	n.d.	336	53	71
131761-6	HM4b	1810	323	334	491				n.d.	n.d.	300	35	61
131796-4	HM4b	2188	156	80	81	-1.4	7.5		n.d.	n.d.	603	124	164
131750	L2a					-6.0	5.8						
131756	L2a					-3.3	5.8						
131756	L2a					-6.6	5.7						
131761-7	L2a[1]	1230	362	33	76				n.d.	n.d.	130	11	32
131796-1	L2a[1]	972	255	371	143	-6.8	5.5	0.70848	n.d.	n.d.	241	31	55
131805	L2a					-6.5	6.6						
Great Bear Cape Formation (section 27)													
161579-1	HM1[1]	1565	346	296	43				n.d.	n.d.	250	43	108
161578-2	L1a-NL[1]	1419	297	323	77				n.d.	n.d.	177	662	341
161578-4	L1-X	2366	159	370	614				n.d.	n.d.	137	76	42
161578-5	L2a[1]	2603	196	587	114	-13.0	3.7	0.70851	n.d.	n.d.	164	83	35
161579-4	L2a[1]	644	308	384	82	-4.2	5.3	0.70842	n.d.	n.d.	248	81	80
161584	L2a					-7.2	4.7	0.70837					
161588	L2a					-5.3	4.5	0.70835					
161579-3	L2b-X	1461	229	295	73				n.d.	n.d.	204	24	54
Raanes Formation (section 29)													
162403	BRACH					-1.8	4.1						
Great Bear Cape Formation (section 30)													
162420	BRACH					-2.6	4.7						
162423	BRACH					-3.9	1.0						
162423	BRACH					-2.1	5.8						

SAMPLE	CL Pattern	Mg	Sr	Fe	Mn	$\delta^{18}O$	$\delta^{13}C$	$^{87}Sr/^{86}Sr$	Ba	Ce	Na	Al	Si
Canyon Fiord Formation (section 42)													
171323-7	MT1-F	397	113	145	76				n.d.	n.d.	162	35	52
171323-13B	MT3 (L)	807	387	60	138				n.d.	n.d.	123	34	44
171323-4	MT3 (L)	1140	547	89	131				n.d.	n.d.	221	30	49
171323-6	MT3(NL)	1583	473	79	96				n.d.	n d.	195	361	203
171323-10	MT3 (L)	1730	440	180	64				10	n.d.	139	62	52
171323-11	MT3 (L)	995	471	72	106				n.d.	n.d.	243	214	138
171323-12	MT3 (L)	1248	336	64	90				n.d.	n.d.	108	48	46
171323-13	MT3 (L)	1517	296	48	48				n.d.	n.d.	185	73	64
171323-14	MT3 (L)	1429	275	62	88				10	n.d.	96	18	33
171323-14b	MT3 (L)	1327	248	88	146				11	n.d.	433	44	61
171323-15	MT3 (L)	899	265	211	133	-9.6	-6.0	0.70877	13	n.d.	182	38	56
171323-8	MT3 (L)	1484	385	85	80				n.d.	n.d.	160	37	42
171323-9	MT3 (L)	1346	244	212	91				11	n.d.	182	45	54
171323-1	L2a[1]	1008	172	3020	202	-22.0	5.4	0.70884	n.d.	n.d.	123	32	60
171323-5	L2b	237	92	74	206				n.d.	31	144	50	58
171323-2	L2c[1]	183	29	257	162				n.d.	10	122	18	44
171323-3	L2c[1]	548	60	115	324				n.d.	n.d.	129	24	48